

ผลของสภาวะการสังเคราะห์ของอลูมินาขนาดนาโนโดยวิธีการตกตะกอน
ต่อความโปร่งใสของชิ้นงานอลูมินา



นายศาสตร์ ปิ่นแก้ว

วิทยานิพนธ์นี้เป็นส่วนหนึ่งของการศึกษาตามหลักสูตรปริญญาวิศวกรรมศาสตรมหาบัณฑิต

สาขาวิชาวิศวกรรมเคมี ภาควิชาวิศวกรรมเคมี

คณะวิศวกรรมศาสตร์ จุฬาลงกรณ์มหาวิทยาลัย

ปีการศึกษา 2549

ลิขสิทธิ์ของจุฬาลงกรณ์มหาวิทยาลัย

EFFECT OF SYNTHESIS CONDITION OF NANOSIZED ALUMINA BY
PRECIPITATION METHOD ON TRANSPARENCY OF ALUMINA SPECIMEN



Mr. Sart Pinkaew

สถาบันวิทยบริการ
จุฬาลงกรณ์มหาวิทยาลัย

A Thesis Submitted in Partial Fulfillment of the Requirements
for the Degree of Master of Engineering Program in Chemical Engineering
Department of Chemical Engineering

Faculty of Engineering
Chulalongkorn University

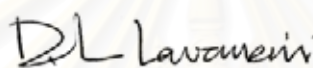
Academic Year 2006

Copyright of Chulalongkorn University

Thesis Title EFFECT OF SYNTHESIS CONDITION OF NANOSIZED ALUMINA BY PRECIPITATION METHOD ON TRANSPARENCY OF ALUMINA SPECIMEN


By Mr. Sart Pinkaew
Field of Study Chemical Engineering
Thesis Advisor Assistant Professor Varong Pavarajarn, Ph.D.
Thesis Co-advisor Thanakorn Wasanapiarnpong, Ph.D.

Accepted by the Faculty of Engineering, Chulalongkorn University in Partial Fulfillment of the Requirements for the Master's Degree



..... Dean of the Faculty of Engineering
(Professor Direk Lavansiri, Ph.D.)

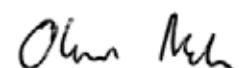
THESIS COMMITTEE


..... Chairman
(Associate Professor Tawatchai Charinpanitkul, Ph.D.)


..... Thesis Advisor
(Assistant Professor Varong Pavarajarn, Ph.D.)


..... Thesis Co-advisor
(Thanakorn Wasanapiarnpong, Ph.D.)


..... Member
(Akawat Sirisuk, Ph.D.)


..... Member
(Assistant Professor Okorn Mekasuwandumrong, D.Eng.)

ศาสตราจารย์ ปิ่นแก้ว : ผลของสภาวะการสังเคราะห์ของอลูมินาขนาดนาโนโดยวิธีการตกตะกอนต่อความโปร่งใสของชิ้นงานอลูมินา (EFFECT OF SYNTHESIS CONDITION OF NANOSIZED ALUMINA BY PRECIPITATION METHOD ON TRANSPARENCY OF ALUMINA SPECIMEN) อ.ที่ปรึกษา: ผศ.ดร. วงศ์ ปวรจารย์, อ.ที่ปรึกษาร่วม: ดร. ธนากร วาสนาเพียรพงศ์ , 93 หน้า.

ผงอลูมินาที่มีขนาดผลึกในระดับนาโนเมตรสามารถสังเคราะห์ได้จากการเผาผงอลูมิเนียมแอมโมเนียมคาร์บอนเนตไฮดรอกไซด์ซึ่งสังเคราะห์จากวิธีตกตะกอน โดยได้ทำการศึกษาปัจจัยของเวลาที่ใช้ในการเผาผงอลูมิเนียมแอมโมเนียมคาร์บอนเนตไฮดรอกไซด์ เวลาที่ใช้ในการบดผงอลูมิเนียมแอมโมเนียมคาร์บอนเนตไฮดรอกไซด์ ผลของการใช้คลื่นเหนือเสียงในระหว่างการสังเคราะห์ผงอลูมิเนียมแอมโมเนียมคาร์บอนเนตไฮดรอกไซด์ และการปรับเปลี่ยนพื้นผิวของผงอลูมิเนียมแอมโมเนียมคาร์บอนเนตไฮดรอกไซด์ด้วยสารลดแรงตึงผิว พบว่าการเผาผงอลูมิเนียมแอมโมเนียมคาร์บอนเนตไฮดรอกไซด์ที่อุณหภูมิ 1200 องศาเซลเซียสเป็นเวลา 1 ชั่วโมง ทำให้ได้ผงอลูมินาในเฟสแอลฟาทั้งหมดแต่เกิดการเกาะติดกันของอนุภาคในปริมาณน้อย โดยที่การเผาผงอลูมิเนียมแอมโมเนียมคาร์บอนเนตไฮดรอกไซด์ที่อุณหภูมิสูงในทันทีที่สามารถลดการเกิดการเกาะติดกันของอนุภาคได้เมื่อเทียบกับการเผาโดยเพิ่มอุณหภูมิขึ้นอย่างช้าๆจากอุณหภูมิห้อง ในขณะที่การบดอลูมิเนียมแอมโมเนียมคาร์บอนเนตไฮดรอกไซด์และการใช้คลื่นเหนือเสียงระหว่างการสังเคราะห์ผงอลูมิเนียมแอมโมเนียมคาร์บอนเนตไฮดรอกไซด์ ช่วยให้อนุภาคของผงอลูมินาที่ได้มีการเกาะกันน้อยลง แต่การปรับเปลี่ยนพื้นผิวของผงอลูมิเนียมแอมโมเนียมคาร์บอนเนตไฮดรอกไซด์โดยการเติมสารลดแรงตึงผิวก่อนนำไปเผาไม่สามารถช่วยลดการเกาะกันของอนุภาคได้ ผงอลูมินาที่สังเคราะห์ได้จะถูกนำไปขึ้นรูปโดยเครื่องอัด และทำการอัดความดันทุกทิศทางแบบเย็น จากนั้นจะถูกเผาผนึกในอากาศที่อุณหภูมิ 1350 องศาเซลเซียส และเผาผนึกซ้ำอีกครั้งที่อุณหภูมิ 1500 องศาเซลเซียส เป็นเวลา 2 ชั่วโมงพบว่า และนำไปอัดความดันทุกทิศทางแบบร้อน พบว่าค่าความหนาแน่นสัมพัทธ์ของชิ้นงานอลูมินาที่เตรียมมาจากตัวอย่างต่าง ๆ มีค่าอยู่ในช่วงร้อยละ 62-99 ของความหนาแน่นทางทฤษฎี โดยมีขนาดเกรนอยู่ในช่วง 0.5-1.7 ไมโครเมตร และชิ้นงานที่ได้มีค่าการผ่านของแสงที่ความยาวคลื่น 700 นาโนเมตร อยู่ในช่วงประมาณร้อยละ 30-60

สถาบันวิทยบริการ จุฬาลงกรณ์มหาวิทยาลัย

ภาควิชา.....วิศวกรรมเคมี.....
สาขาวิชา.....วิศวกรรมเคมี.....
ปีการศึกษา.....2549.....

ลายมือชื่อนิสิต.....ศาสตราจารย์ ปิ่นแก้ว.....
ลายมือชื่ออาจารย์ที่ปรึกษา.....
ลายมือชื่ออาจารย์ที่ปรึกษาร่วม.....

4870484421: MAJOR CHEMICAL ENGINEERING

KEYWORDS: PRECIPITATION, ALUMINA, AGGLOMERATE,
TRANSPARENT

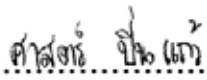
SART PINKAEW: EFFECT OF SYNTHESIS CONDITION OF NANOSIZED ALUMINA BY PRECIPITATION METHOD ON TRANSPARENCY OF ALUMINA SPECIMEN. THESIS ADVISOR: ASSISTANT PROFESSOR VARONG PAVARAJARN, Ph.D., THESIS CO-ADVISOR: THANAKORN WASANAPIARNPONG, Ph.D., 93 pp.


Nanosized alumina powder was obtained from the calcination of ammonium aluminum carbonate hydroxide (AACH) which was synthesized by precipitation method. Effects of calcination time, milling of AACH, the use of ultrasonic during synthesis of AACH and surface modification of AACH by surfactant were investigated. It was found that AACH which was calcined 1 h at 1200°C would become α -Al₂O₃ completely, but it contained small degree of agglomeration. When AACH was suddenly calcined at high temperature without long heating up period, it would be able to reduce hard agglomeration in alumina particle. Furthermore, AACH milling and using of ultrasonic during AACH synthesis would also reduce hard agglomerates in the alumina particle. However, modification of AACH surface before calcination could not reduce the agglomeration. The synthesized alumina powder was fabricated into compacted bodies by biaxial press and cold isostatic press, respectively. The compacted bodies were then sintered at 1350°C for 2 h, sintered at 1550°C for 2 h in air and hot-isostatic pressed, repeatedly. The relative density of the sintered specimens prepared from various samples was in the range of 62-99% of theoretical density, whereas grain size was in the range of 0.5 – 1.7 μ m. The transmittance of the specimens was in the range of 30-60% at wave length 700 nm.

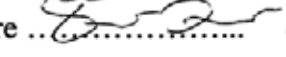
DepartmentChemical Engineering.....

Field of Study ..Chemical.Engineering.....

Academic year 2006.....

Student's signature 

Advisor's signature 

Co-advisor's signature 

ACKNOWLEDGEMENTS

The author would like to express his sincere gratitude and appreciation to his advisor, Assistant Professor Dr. Varong Pavarajarn and his co-advisor, Dr. Thanakorn Wasanapiarnpong for his invaluable suggestions, stimulating, useful discussions throughout this research and devotion to revise this thesis otherwise it can not be completed.

The author is similarly grateful to Mr. Nirut Wangmuklang for their kind suggestion throughout this work. In addition, the author would also be grateful to Associate Professor Dr. Tawatchai Charinpanitkul, as the chairman, and Associate Professor Dr. Okorn Mekasuwandumrong and Dr. Akawat Sirisuk, as the members of the thesis committee.

The author would like to acknowledge to Thailand Research Fundd (TRF), Thailand Japan Technology Transfer Project (TJTTP), Graduate School of Chulalongkorn University and National Nano-Technology Center (NANOTEC) for their financial support.

The author wishes to thank the members of the Center of Excellence on Catalysis and Catalytic Reaction Engineering, Department of Chemical Engineering, Faculty of Engineering, Chulalongkorn University for their assistance.

Finally, the author would like to express his highest gratitude to his parents who always pay attention to his all the times for suggestions and have provided his support and encouragement. The most success of graduation is devoted to his parents.

CONTENTS

	PAGE
ABSTRACT (IN THAI).....	iv
ABSTRACT (IN ENGLISH).....	v
ACKNOWLEDGMENTS.....	vi
CONTENTS.....	vii
LIST OF TABLES.....	x
LIST OF FIGURES.....	xi
CHAPTER	
I INTRODUCTION.....	1
II THEORY AND LITERATURE REVIEWS.....	3
2.1 Alumina (Al ₂ O ₃).....	3
2.2 Crystal Structure of Alumina	3
2.3 Phase Transformation of Alumina.....	4
2.4 Preparation of Alumina Powder by Precipitation Method	6
2.5 Method for Shape Forming.....	8
2.6 Sintering.....	12
2.7 Transparency of Specimen.....	15
2.7.1 Sources of light scattering.....	16
2.7.2. Grain-boundary reflection.....	17
2.7.3 Grain boundary refraction.....	18
2.7.4 Effect of grain size and transmittance.....	18
2.8 Surfactant.....	19
2.8.1) Adsorption of surfactants onto solid particles.....	20
2.8.2) Surfactant Modified Alumina.....	21
2.9 Development of a modified alumina powder synthesis	22
Method.....	
2.10 Influence of impurities on the properties and microstructure	23
changes in the alumina sintered body.....	

	PAGE
III EXPERIMENTAL.....	25
3.2.1 Synthesis of alumina powder.....	25
3.2.2 Fabrication of alumina specimens.....	32
3.3 Characterizations	33
3.3.1 Characterization of Synthesized Powder.....	33
3.3.2 Characterization of Green Specimens.....	34
3.3.3 Characterization of Sintered Specimens.....	35
IV RESULTS AND DISCUSSION	36
4.1 Characterization of commercial alumina powder (TMDA) compared with synthesized alumina.....	36
4.1.1 Characterization of commercial alumina powder (TMDA).....	37
4.1.2 Characteristic of products synthesized by normal routine.....	41
4.2 Effect of calcination time and initial calcination temperature on properties of alumina particles and specimens.....	43
4.3 Effect of AACH milling on synthesized alumina	60
4.4 AACH Surface Modification.....	69
4.5 Precipitation Assisted by Ultrasonic.....	73
V CONCLUSIONS AND RECOMMENDATIONS.....	77
5.1 Conclusions.....	77
5.2 Recommendations.....	77

	PAGE
REFERENCES.....	78
APPENDICES.....	80
APPENDIX A: Calculation of concentration of both reactants in precipitation method.....	81
APPENDIX B: Calculation of The crystallite size.....	82
APPENDIX C: Density.....	85
APPENDIX D: Condition for ball mill and dispersion of powder.....	88
APPENDIX E: Effect of milled alumina powder mass on mass of splite alumina ball	89
Vitae	93


สถาบันวิทยบริการ
จุฬาลงกรณ์มหาวิทยาลัย

LIST OF TABLES

TABLE		PAGE
4.1	Properties of TMDA alumina powder, alumina powder synthesized by normal routine and synthesized ammonium aluminium carbonate hydroxide (AACH) powder.	41
4.2	Density of the specimen fabricated from alumina powder synthesized with AACH surface modification.	73
4.3	Density of the specimen fabricated from alumina powder synthesized with assistance of ultrasonic wave comparing with the product fabricated by conventional method.	75



สถาบันวิทยบริการ
จุฬาลงกรณ์มหาวิทยาลัย

LIST OF FIGURES

FIGURE		PAGE
2.1	Illustration of Al and O atoms packing in the basal plane.....	4
2.2	Transformation sequences of aluminum hydroxides.....	5
2.3	Parameters affecting property of the precipitate.....	7
2.4	Correlation between green bulk density, final density, and forming pressure of high-purity alumina ceramics.....	9
2.5	Steps of dry pressing operation.....	10
2.6	Formation of a neck during the sintering of two fine particles.....	12
2.7	Changes in pore shape do not necessarily require shrinkage.....	12
2.8	Density as a function of sintering temperature for reactive alumina powder showing the stages of sintering.....	13
2.9	Development of the ceramic microstructure during sintering: (a) loose powder particles, (b) initial stage, (c) intermediate stage and (d) final stage.....	14
2.10	Various interactions between radiation and solid.....	15
2.11	Illustration of the most important light-scattering mechanisms in polycrystalline alumina.....	17
2.12	The real in-line transmittance (RIT) of alumina ceramic measured at wavelength 645 nm as a function of the mean grain size: experimental data points.....	19
2.13	Molecular structure of surfactant.....	19
2.14	Model for hydrophobic coagulation and peptization of negatively charged sol by surfactants.....	21
2.15	Adsorption isotherm of SDS on alumina.....	21
3.1	Diagram of α -alumina powder preparation by normal route.....	26
3.2	Diagram of α -alumina powder preparation by ultrasonic.....	27
3.3	Diagram of α -alumina powder preparation with an addition of AACH milling.....	28
3.4	Diagram of α -alumina powder preparation with a stg of AACH surface modification by acetic acid or oleic.....	30
3.5	Diagram of α -alumina powder preparation with a step of AACH surface modification by PVA.....	31

FIGURE	PAGE
4.1 Particle size distributions of TMDA alumina powder, alumina synthesized via normal routine and ammonium aluminium carbonate hydroxide (AACH) powder synthesized.....	38
4.2 SEM micrographs of TMDA alumina powder (a), alumina powder synthesized via normal routine (b), synthesized AACH powder(c).....	39
4.3 TEM micrographs of TMDA alumina powder (a), alumina powder synthesized via normal routine (b), synthesized AACH powder(c).....	40
4.4 XRD patterns of product calcined at various time.....	42
4.5 SEM micrographs of the specimen fabricated from: (a) TMDA powder (b) α -alumina powder synthesized by normal precipitation procedure...	44
4.6 UV/Visible spectrophotometry micrographs of the specimen fabricated from: TMDA powder and α -alumina powder synthesized by normal precipitation procedure.....	45
4.7 TEM micrographs of AACH powders of which was calcined at various conditions: (a) pre-calcined AACH, (b) AACH calcined at 1300 °C for 0.5 minutes (boehmite), (c) AACH calcined at 1200 °C for 5 minutes (α , γ -alumina), (d) AACH calcined at 1200 °C for 20 minutes (α -alumina), (e) AACH calcined at 1200 °C for 60 minutes (α -alumina)...	47
4.8 XRD patterns of products from calcination of AACH at 1200°C for various holding times: (a) The samples are heated up from room temperature, (b) The samples are put into a furnace at temperature is around 1100°C.....	49
4.9 Particle size distributions of products from calcination of AACH at 1200°C for various holding time: (a) The samples are heated up from room temperature, (b) The samples are put into a furnace at temperature is around 1100°C.....	51
4.10 SEM micrographs of products obtain from calcination of AACH by different approaches: (a) The samples were put into a furnace at high temperature, (b)The samples were calcined starting from room temperature.....	52
4.11 Correlation between tapped density of AACH after calcination and holding time at 1200°C.....	53

FIGURE	PAGE	
4.12	Correlation between green body density after biaxial pressing at 20 MPa and holding time at 1200°C for AACH calcination.....	54
4.13	Correlation between green body density after CIP at 300 MPa and holding time at 1200°C for AACH calcination.....	54
4.14	Correlation between density of specimen after sintering at 1350°C and holding time at 1200°C for AACH calcination.....	55
4.15	Correlation between density of specimen after sintering at 1500°C and holding time at 1200°C for AACH calcination.....	55
4.16	Correlation between density of specimen after HIP at 1350°C and 300 MPa for 1h and holding time at 1200°C for AACH calcination.....	56
4.17	Progress of density change for specimens fabricated from powder calcined by putting AACH into the furnace at 1100°C and held at 1200°C for various periods of time.....	57
4.18	Progress of density change for specimens fabricated from powder calcined with temperature ramping up and held at 1200°C for various periods of time.....	57
4.19	SEM micrographs of the specimen fabricated from: (a) No ramping & held at 1,200°C for 60 min , Average grain size= 0.54µm, (b) Ramping & held at 1,200°C for 30 min , Average grain size= 1.46µm, (c) Ramping & held at 1,200°C for 30 min (Normal routine), Average grain size= 1.67µm.....	59
4.20	UV/Visible spectrophotometry micrographs of the specimen fabricated from: TMDA powder ,α-alumina powder synthesized by normal precipitation procedure and α-alumina powder varied AACH calcination time.	60
4.21	Particle size distributions of AACH powder after milling for various period of time. particle size distribution(a), cumulative particle size distribution(b).....	61
4.22	SEM image of AACH powder which varied time of milling: (a)AACH with out balls milling, (b)AACH milled for 8 h and (c) AACH milled for 72 h.....	62

FIGURE	PAGE
4.23 Particle size distributions of alumina powder obtained from AACH That was milled for various periods of time: (a) particle size distribution (b) cumulative particle size distribution.....	64
4.24 SEM images of alumina powder obtained from AACH that was milled for various periods of time: (a) Alumina obtained from unmilled AACH (b) Alumina obtained from AACH milled for 8h, (c) Alumina obtained from AACH milled for 48h.....	65
4.25 Correlation between tapped density of AACH before and after calcination, and milling time for AACH powder.....	66
4.26 Correlation between densities of specimens after biaxial pressing and cold isostatic pressing and milling time for AACH powder.....	66
4.27 Correlation between density of specimens after sintering and hot isostatic pressing and milling time for AACH powder.....	67
4.28 SEM micrographs of the specimen fabricated from: (a) Unmilled AACH (Normal routine), Average grain size= 1.67 μ m, (b) AACH milled for 24 h, Average grain size= 1.46 μ m.....	68
4.29 UV/Visible spectrophotometry micrographs of the specimen fabricated from: TMDA powder , α -alumina powder synthesized by normal precipitation procedure and α -alumina powder varied AACH milling time.....	68
4.30 SEM micrographs of AACH modified with PVA(a) and oleic acid(b)..	70
4.31 SEM micrographs of alumina powder obtained from calcination of: (a) PVA modified AACH, (b) Oleic acid modified AACH, (c) Acetic acid modified AACH.....	71
4.32 TG-DTA curves of (a) PVA and (b) Oleic acid.....	72
4.33 Particle size distribution comparison for AACH (a) and α -alumina (b) synthesized by conventional stirring and by assistant of ultrasonic wave.....	74
4.34 UV/Visible spectrophotometry micrographs of the specimen fabricated from: TMDA powder , α -alumina powder synthesized by precipitation assisted by ultrasonic and α -alumina powder synthesized by precipitation assisted by convensional stirring.....	76

FIGURE	PAGE
B.1 The observation peak of α -alumina for calculating the crystallite size.....	85
B.2 The graph indicating that value of the line broadening attribute to the experimental equipment from the α -alumina standard.....	86
E.1 SEM images of the pieces of split alumina balls was blended with alumina powder after milled by ball milling.....	91
E.2 Correlation between mass of the pieces of split alumina balls and mass of the put alumina powder.....	92
E.3 SEM images of the specimen after sintering at 1500°C.....	92



สถาบันวิทยบริการ
จุฬาลงกรณ์มหาวิทยาลัย

CHAPTER I

INTRODUCTION

Alumina is an important material in many fields because of its excellent and wide range properties. It has high electrical resistance, good thermal conductivity, high melting point, excellent chemical resistance, high hardness and high mechanical strength. Therefore, alumina ceramics have been widely used as an integrated circuit (IC) substrate, the insulator for spark plug, a media ball, crucibles, and the envelope of high pressure sodium lamp.

Alumina ceramics are usually poly-crystalline and not transparent. Transparent alumina ceramic can be synthesized either in single crystal (SCA) or polycrystalline forms (PCA). SCA (single crystal alumina) is used as highly transparent material for many industrial and military applications, such as optical windows for laser, armor part, IR-dome for infrared missile guidance system and jewelry. PCA (polycrystalline alumina) has been available for optical application since early 1962 when Coble (Ryshkewitch 1960) invented translucent alumina, which was composed of micrometer-sized grains and not transparent, but translucent. Recently, it has been reported that transparent alumina with nano-meter sized grain can be made (Hayashi et al. 1991).

Alumina is white when it is chemically pure. However, the color changes to pink or red when small amount of Cr-ion are added and blue when Fe-ion is contaminated. If beautiful colors could be added to PCA, it would become a kind of jewelry. The advantage of such invented ceramic is that its size and shape can be formed artificially. If technology for doping color into such transparent ceramic can be developed, it would be possible to produce the statue of Buddha, the statue of liberty or any other complicated figures in various colors. The development of PCA would actuate a new world of artificial precious stones, which could be differentiated from that of natural jewelry and in turn could help increase the nation's benefits. Compared to SCA, the cost to manufacture PCA is much lower, and it is easier to produce in large size and complicated shape.

From the background above mentioned, it is interested in the development of technology to synthesize a transparent polycrystalline alumina ceramic.

Normally, light transmission of PCA is relatively small in contrast to SCA, which shows a complete transparency. The translucent of PCA is caused by scattering of light at grain boundaries and residual pores. Thus, transparency of PCA can be increased by complete eliminating of the residual porosity, and reducing the grain size to submicron or nanometer level. Key factors to obtain this characteristic are using high purity, fine particle size alumina powder (submicrometer or nanometer level), low pores in particle and low accumulation of particle.

In this research, alumina nanoparticles are synthesized by precipitation method, using ammonium aluminium sulfate and ammonium hydrogen carbonate as precursors. The main concern for this research is the improvement of the synthesized alumina powder to have low porosity and low degree of agglomeration. In consequence, find technology to disperse alumina particles via surface modification of particles by using adsorption of surfactants onto alumina particles was investigated. Moreover, reductions of pores by optimize calcination time, and particle size reduction by AACH milling was investigated also.

สถาบันวิทยบริการ
จุฬาลงกรณ์มหาวิทยาลัย

CHAPTER II

THEORY AND LITERATURE SURVEY

2.1) Alumina (Al_2O_3)

Aluminium oxide or alumina is a chemical compound of aluminium and oxygen with the chemical formula Al_2O_3 . Alumina is an important material in many fields because of its excellent and wide range properties. It has high electrical resistance, good thermal conductivity, high melting point (2054°C), excellent chemical resistance, very high hardness and high mechanical strength, high surface area with fine particle size and good catalytic activity. Alumina powder can be produced cheaply in massive quantities. Therefore, it has been considered as one of the most promising advanced materials for varieties of application, such as being catalyst, catalyst support, wear-resistance materials, ceramics, abrasives, insulators for spark plug, media balls, crucibles, medicinal material, and adsorbent.

Alumina is also an important material in field of catalytic technology because its properties are also desirable for catalyst support. For catalytic applications, alumina can be used in three functions: as catalyst, co-catalyst and support. For example, alumina is used as catalyst in the steam reforming process at high temperature. Alumina is used as co-catalyst in the catalytic reforming of gasoline and as support in many cases, such as in catalytic converter and in membrane technology.

2.2) Crystal Structure of Alumina

The extensive crystallographic researches on various phases of alumina have been conducted by many researchers. For instance, very detailed crystallographic description of sapphire single crystals was given by Kronberg et al. (1957). The structure of α -alumina consists of close packed planes of large oxygen ions stacking in A-B-A-B sequence, thus forming hexagonal close packed array of anions. Aluminium cations are located at octahedral sites of this basal array and form another

type of close packed planes between the oxygen layers. To maintain neutral charge, however, only two third of the available octahedral sites are filled with cations. Figure 2.1 illustrates the packing of Al and O atoms in the basal plane. Since the vacant octahedral sites also form regular hexagonal array, three different types of cation layer can be defined, namely a, b, and c layer, depending on the position of the vacant cation site within the layer. These layer are stacked in a-b-c-a-b-c sequence in the structure of alumina.

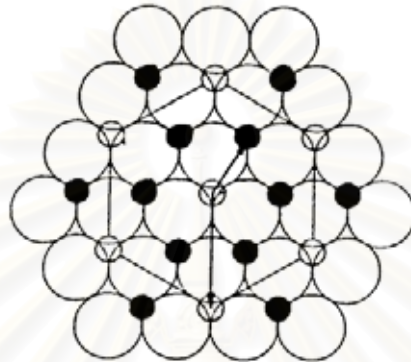


Figure 2.1 Illustration of Al and O atoms packing in the basal plane (Kronberg 1957).

2.3) Phase Transformation of Alumina

Alumina can exist in many metastable phases before transforming to the stable α -alumina (corundum form). There are six principal metastable phases of alumina designated by the Greek letters chi (χ), kappa (κ), eta (η), theta (θ), delta (δ), and gamma (γ), respectively. Many industrial solid catalysts are made up from active centers anchored on transition alumina supports. This is a consequence of prominent characteristics of such transition aluminas, such as high porosity, high surface area, good mechanical strength and high thermal stability. Although the range of temperature at which each transition phase is thermodynamically stable has been reported by many researchers, it depends on amount of impurities in the starting materials and thermal history of samples. Most of the studies on phase transformation of alumina was conducted by calcination of alumina precursor. It was found that difference in the phase transformation sequence was resulted from the difference in the precursor structure. Moreover, the transformation sequence is irreversible as shown in Figure 2.2 The nature of the product obtained by calcination depends on the

starting hydroxide and on the calcination condition. The phase transformation sequences, from metastable Al_2O_3 structures to the final stable α -alumina phase, reported in the literature are also approximates.

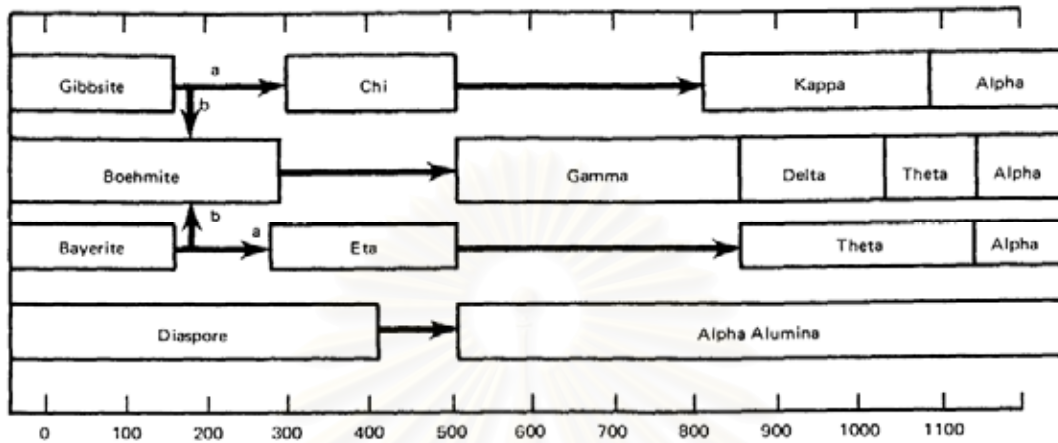


Figure 2.2 Transformation sequences of aluminum hydroxides (W.H. 1970).

The phase transformation sequence normally starts with aluminum hydroxide ($\text{Al}(\text{OH})_3$ and AlOOH) transforming to low-temperature phase of alumina (η and χ) at temperature around $150\text{--}500^\circ\text{C}$, and subsequently to high temperature phase (δ , θ , κ) at temperature around $650\text{--}1000^\circ\text{C}$. Finally, the thermodynamically stable phase, α -alumina, is formed at temperature around $1100\text{--}1200^\circ\text{C}$. It is generally believed that α -phase transformation takes place through the nucleation and growth mechanism.

Transition aluminas start to lose their surface area even at temperature below 800°C due to the elimination of micro-pores. However, drastic loss occurs at temperature higher than 1000°C when the crystallization to the thermodynamically stable α -alumina occurs (Dynys and Halloran 1982).

Several studies have been carried out on the direct phase transformation of alumina. The mechanism of direct phase transformation from γ -alumina to α -alumina involves the conversion of the cubic close packing of oxygen ions into a stable hexagonal close packing (Levin and Brandon 1998; Simpson et al. 1998). Morinaga et al. (2000) studied the phase transformation that occurred during the thermal

decomposition of ammonium aluminum carbonate hydroxide into α -alumina. Amorphous, γ -, θ -alumina were identified as intermediate products. They have found that the atmosphere affects the grain size distribution of the final α -alumina particles.

2.4) Preparation of Al₂O₃ Powder by Precipitation Method

There are many methods which have already been used to prepare alumina powder, such as precipitation from solution (Hen and Chen 1993), sol-gel synthesis (Brinker 1990), hydrothermal synthesis (Kaya et al. 2002), microwave synthesis (Deng 1997), emulsion evaporation (Sarıkaya, et al. 2001) and solvothermal synthesis (Inoue, et al. 1988). In this research precipitation method is investigated.

Precipitation method involves growth of crystals from solvent of different composition. The reactants may or may not be in the same phase before the precipitation takes place. If the reactants are in the same phase, the precipitation is homogeneous, otherwise, it is heterogeneous. The homogeneous precipitation is often preferred because its behavior is more controllable (Chen 1993). Homogeneous precipitation of alumina precursor can be carried out by heating aqueous solution containing excess urea and aluminum salt approximately up to its boiling temperature (Nagai et al. 1991; Nagai et al. 1993)

Basically, all process parameters influence quality of the final product of the precipitation. It is usually desired to get the precipitates with specific properties. These properties may involve physical properties of particle such the nature of the phase formed, chemical composition, purity, particle size, surface area, pore size, pore volumes, and separability from the mother liquor. On the other hand, it may include the demands which are imposed by the requirement of downstream processes, such as drying, palletizing or calcinations. It is therefore necessary to optimize the parameters in order to produce the desired material. Figure 2.3 summarizes the parameters which can be adjusted in precipitation processes and the properties which are mainly influenced by these parameters.

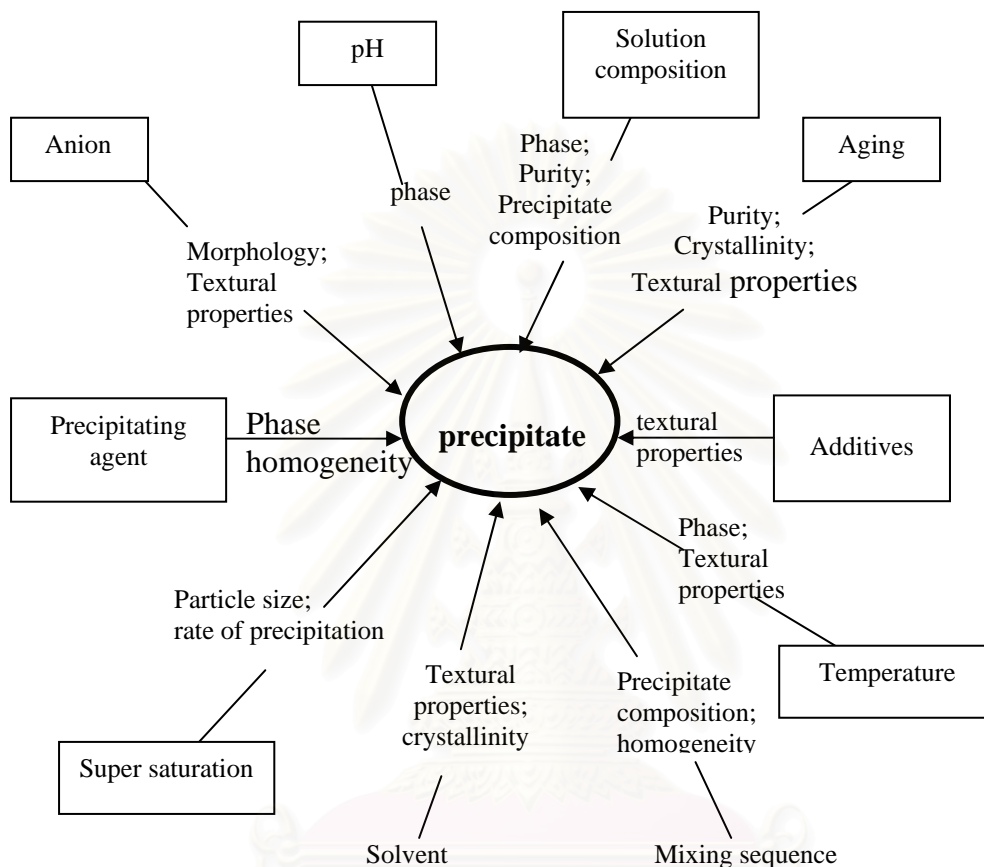
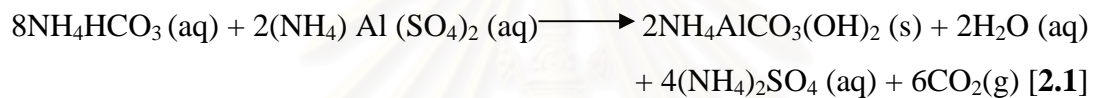


Figure 2.3 Parameters affecting property of the precipitate (ERTL, KNOZINGER and WEITKAMP).

As stated above, precursors, which can be easily decomposed to volatile products, are usually chosen. There are preferably the nitrates of metal precursors and ammonia or sodium carbonate as the precipitating agent. Since nucleation rate is extremely sensitive to temperature change, precipitation temperature is a decisive factor in controlling properties of the precipitate such as primary crystallite size, surface area, and phase. However, it is very difficult to state how the precipitation temperature should be adjusted to achieve a product with specific properties. The optimum precipitation temperature is usually a parameter which has to be determined experimentally. In general, most precipitation process is carried out above room

temperature, often close to 100°C. Furthermore, pH directly controls the degree of super saturation, at least in case that hydroxides are precipitated. Therefore, it is one of the crucial factors in precipitation process. As for many other parameters, the influence of pH is not straight forward and it has to be investigated experimentally for a specific system.

Alumina powder has been prepared from ammonium aluminum carbonate hydroxide via the precipitation method as reported by Kato et al. Ammonium aluminum carbonate hydroxide is firstly produced from the reaction between a solution of ammonium hydrogencarbonate and aluminum salt solution, according to the following equation 2.1(Shuzo et al. 1975).



After allowing the mixed solution to age for a prescribed period of time to permit growth of crystals, the precipitate is then separated by filtration and drying. The ammonium aluminum carbonate hydroxide obtained is subsequently decomposed at temperature in a range of 1200 to 1300°C to form α -alumina.

The main advantages of precipitation method are the potential to create very pure material and the flexibility of the process with respect to quality of final product

2.5) Method for Shape Forming

There are many forming techniques to make ceramics from ceramic powder, for instance, dry pressing, hydrostatic molding, extrusion, injection molding, and hot pressing. The choice of the forming process depends on dimension and shape of parts to be fabricated, quantity of parts, and requirements of the final product. The forming pressure to be applied should be approximately 100 MN/m², but it is usually adaptable in each type of the forming process. Bulk density of the green compacted body is as well as density of the final product after sintering, increases with increasing in forming pressure (Figure 2.4). If the forming pressure is too low, the final product

will not achieve the full density. On the contrary, excessive pressure, which has the same effect as insufficient plasticization or inhomogeneous distribution of the plasticizer, can lead to defects such as flaws and cracks in the compacted bodies.

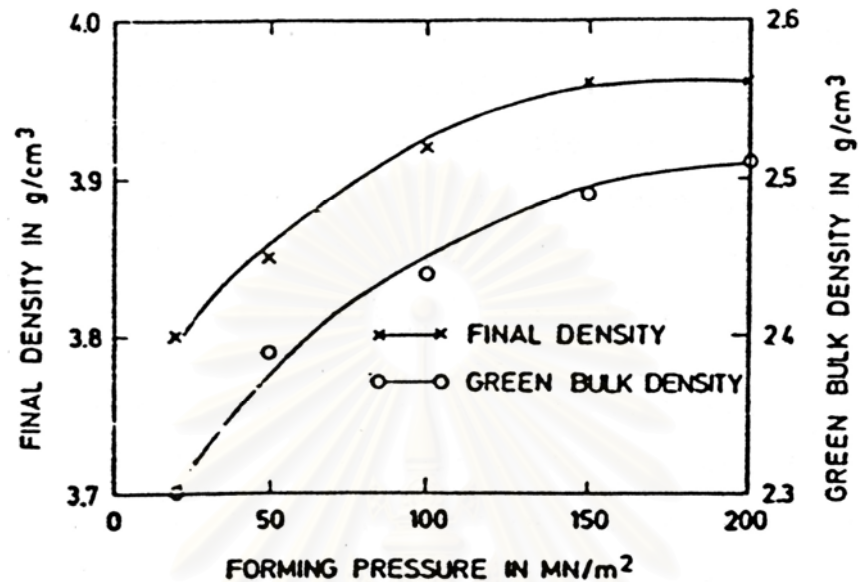


Figure 2.4 Correlation between green bulk density, final density, and forming pressure of high-purity alumina ceramics (Dorre and Hubner 1984).

The dry press technique which has advantage in simplicity and low operation cost could provide a green body of ceramic with sufficient physical strength if its morphology is not so complicated. The method is not suitable to form complicated figure parts. It is restricted, however, to parts with simple shape and to wall thickness greater than 1 mm. Dry pressing is unidirectional. Figure 2.5 illustrates the dry pressing operation using a simple ring, as well as a ring with a flange, under a pressure of 150 MN/m². The procedure is carried out in three basic steps. In order to development of internal stresses, the following requirements should be met.

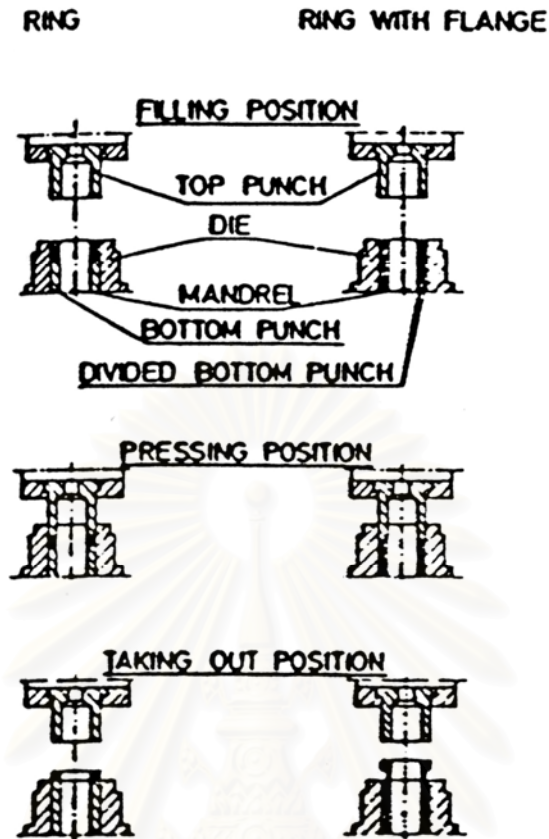


Figure 2.5 Steps of dry pressing operation (Dorre and Hubner 1984).

1. It is important to get homogeneous distribution of the powder when the die is filled. This can be achieved by using suitably prepared free-flowing alumina powder and by filling the die evenly, for example, by means of a fill shoe.
2. In the pressing position, a homogeneous compaction of the powder within the desired shape should be ensured.
3. Removal of the part from the die should be simple, without any risk of damage.

Due to the substantial tool wear caused by the extremely abrasive alumina powder, all parts of the die which are exposed to wear, such as mandrels and punches, are preferably made of cemented carbides.

The isostatic pressing is a process to form ceramic components from dry powder by uniform pressing from all directions. It is also used for other materials,

such as metals, plastics, graphite, and carbon. The process is accomplished by enclosing the powder in a deformable mold and then collapsing the mold by using a hydrostatic pressure exerted from fluid medium. For cold isostatic pressing (CIP), the process carried out at or near room temperature.

On the other hand, hot isostatic pressing (HIP) is performed at elevated temperature. Full densification of Al_2O_3 by sintering and then hot-pressing is only possible when the open pores are completely eliminated during sintering. If the open pores are eliminated, sintering at low temperature appears to be favorable, since the closed pores should remain between the grains in order to be eliminated by subsequent hot isostatic pressing (Won and Kim, 1987)

The general advantages of cold isostatic (CIP) pressing are:

- Very few size or dimensional limitations, because the uniform application of pressure associated with this process obviates the size limitations of many other processes, particularly the length-to-diameter problems of dry pressing.
- Very uniform pressed compacts, due to the uniform application of pressure, which leads to very consistent density and shrinkage resulting in a reproducible process.
- Generally moderate tooling costs particularly in case of prototype and low-volume production, where the tooling can be quite simple.
- Short overall process time, which do not require long binder burnout or drying period.

On the other hand, the general advantages of hot isostatic pressing (HIP) are:

- Void, particularly large ones, in most materials can be efficiently reduced in size and frequency.
- Ceramics can be densified at relatively low temperature.
- Ceramics that are extremely difficult to sinter can be fully densified, for example high-purity silicon-nitride powders.

- The reduced sintering temperature means that grain growth and undesirable reactions can be controlled or avoided.
- A very high uniformity in properties, i.e. density, can be obtained.

2.6) Sintering

Sintering is a process by which small particles of material are bonded together by solid-state diffusion during thermal treatment. In the sintering process, particles are coalesced by solid-state diffusion at very high temperatures yet lower than melting point of the compound being sintered. Atomic diffusion takes place between the contacting surfaces of the particles so that they become chemically bonded together. These results are obtained during firing by the transfer of material from one part of the structure to the other; as shown in Figure 2.6 (Kingery et al.1976). In ceramic manufacturing, this thermal treatment results in changes in grain size and shape, changes in pore shape, and changes in pore size, compact into a dense, coherent product. The kind of change that may occur are shown in Figure 2.7. As the process proceeds, larger particles are form at the expense of the smaller ones, while the porosity of the compacts decreases. Finally, at the end of the process, an "equilibrium grain size" is attained.

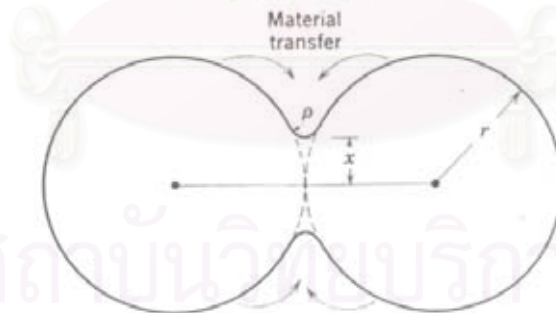


Figure 2.6 Formation of a neck during the sintering of two fine particles (Kingery et al. 1976).

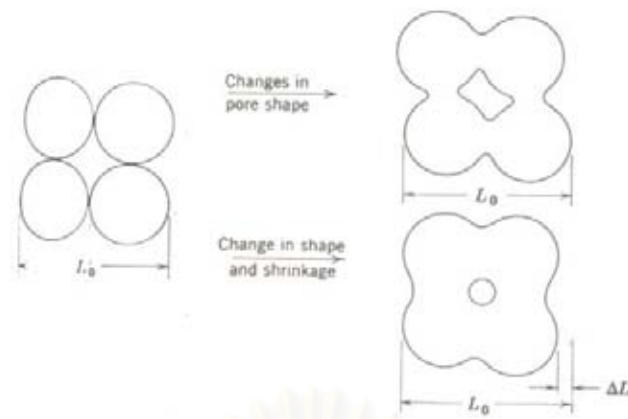


Figure 2.7 Changes in pore shape do not necessarily require shrinkage(Kingery et al. 1976).

Densification, recrystallization, and grain growth occur in the same temperature range. Therefore, strict control of the sintering process as well as small addition of grain growth inhibitor, e.g. MgO, to the alumina powders is essential to achieve a fully dense sintered body with fine-grained microstructure. In the course of sintering, the density increases with the logarithm of time, and the grain size increases with the one-third power of time.

The shrinkage upon sintering a ceramic component can be monitored by measuring sample size or density as a function of firing temperature and time. A plot of density as a function of time is typically as shown in Figure 2.8.

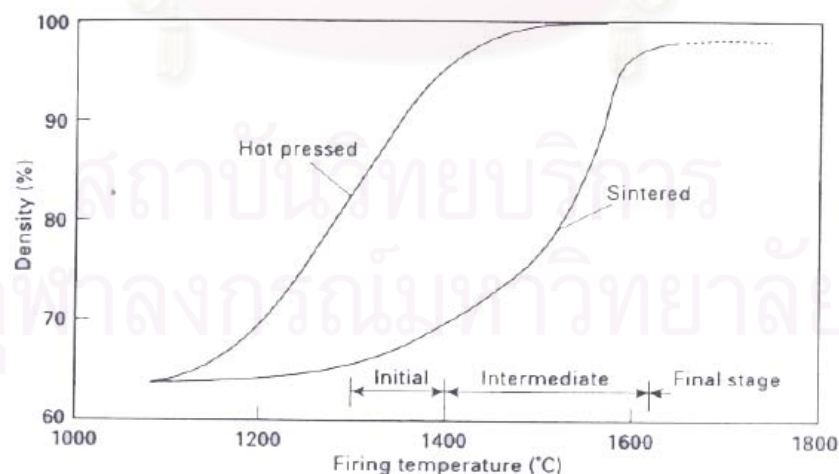


Figure 2.8 Density as a function of sintering temperature for reactive alumina powder showing the stages of sintering (after Reed, 1988).

1. Initial sintering involves rearrangement of the powder particles and formation of a strong bond or neck (Figure. 2.9(b)) at the contact points between particles. Relative density of the compact may increase from 0.5 to 0.6 due mostly to the increased packing of the particles.

2. Intermediate sintering is where the size of the necks grows, the amount of porosity decreases substantially and particles move closer (Figure. 2.9(c)) leading to shrinkage of the component. Grain boundaries (and grains) are formed and move so that some grains grow at the expense of others. This stage continues while the pore channels are connected (open porosity) but is considered over when the pores are isolated (closed porosity). The majority of the shrinkage of the ceramic component occurs during intermediate sintering and relative density at the end of this stage may be about 0.9.

3. In final stage of sintering, the pores become closed and are slowly eliminated generally by diffusion of vacancies from the pores along grain boundaries with only a little densification of the component. The grain boundaries are regions of more open crystal structure than the grains themselves so that diffusion along them is more rapid. Grain size increases during this stage (Figure. 2.9(d)).

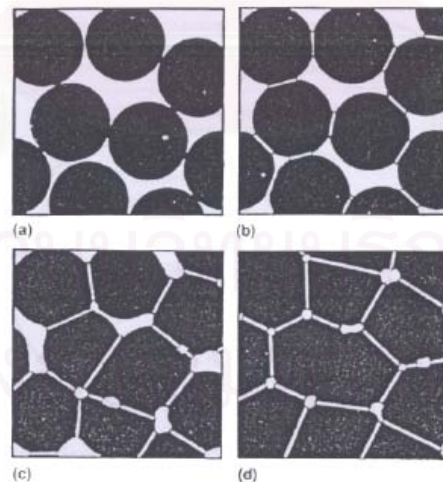


Figure. 2.9 Development of the ceramic microstructure during sintering: (a) loose powder particles, (b) initial stage, (c) intermediate stage and (d) final stage.(William et al. 1994)

The nature of the sintering atmosphere may influence the rate of sintering and the residual porosity. Many additives besides temporary binders have been used in sintering process for several purposes, such as crystal growth repression, crystal growth acceleration, acceleration of sintering or shrinkage rate, reduction in maturing temperature, porosity alteration, changes in physical or chemical properties, and removal of impurities. Many researchers have studied the effects of sintering additives on the sintering process in order to improve properties of material obtained. The choice of sintering temperature, which is usually between 1600 and 1800°C, depends on surface energy, grain size distribution, and the additives of the alumina powder. The sintering time and particularly the heating rate should be adapted to the size and the wall thickness of the body to be sintered. Larger parts require a longer sintering time and a slower rate of heating-up. Smaller parts can be heated up more quickly, allowing a much shorter sintering time.

2.7) Transparency of Specimen

When beam of light or electromagnetic (EM) radiation impinges on the solid (Figure. 2.10), several things happen. Some of light radiation may be transmitted through the medium, some will be absorbed, and some will be reflected at the interface between the two media. The intensities of the incident beam (I_0) to the surface of the solid medium must equal to the sum of the intensity of the transmitted, absorbed, and reflected beams, denoted as I_T , I_R , and I_A , respectively,

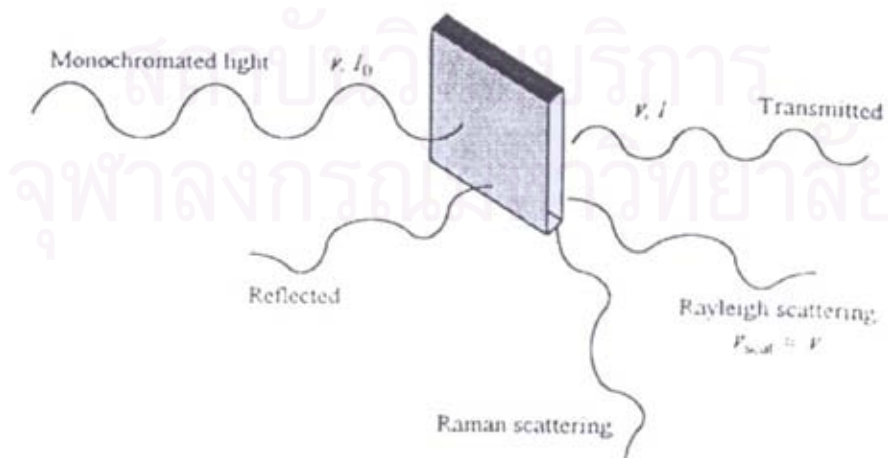


Figure 2.10 Various interactions between radiation and solid (Barsoum 1997).

$$I_0 = I_R + I_T + I_A \dots\dots\dots (2.2)$$

An alternate form of Equation 2.2 is

$$1 = T + R + A \dots\dots\dots (2.3)$$

where T, R and A represent the transmissivity (I/I_0), reflectivity (I_R/I_0) and absorptivity (I_A/I_0), which are the fractions of incident light that are transmitted, absorbed, and reflected by a material respectively.

Materials that are capable of transmitting light with relatively little absorption and reflection are transparent. One can see through them. Translucent materials are those that light transmit diffusely through the interior; that is, light is scattered within the interior to the degree that objects are not clearly distinguishable when viewed through a specimen of the material. Materials that are impervious to the transmission of visible light are termed opaque.

There are many possible factors affecting the transparency of PCA and can be found in the literatures (Grimm et al. 1971). In these papers, sources of light scattering such as grain boundary reflection, refraction in Al_2O_3 grain and effect of grain size on transparency are to be described.

2.7.1 Sources of light scattering

The major important origins of light scattering in high-purity PCA are rough surfaces, pores, and grain boundaries. The light scattering mechanism is schematically illustrated in Figure. 2.11. Light scattering at the surfaces of the second phases (inclusions) can be neglected in high-purity PCA. For MgO-doped PCA, it has no significant effect of MgO on the optical properties of PCA up to MgO content of 300 ppm. Absorption of light by high-purity PCA is generally low when it is sintered to full density, and it also can be neglected. When sample surfaces are smooth, the scattering of light at the surfaces can also be neglected. Only the specular reflection at

the surfaces has to be taken into account. Therefore, grain boundaries and pores remain as the most important factors for the light scattering of high-purity PCA.

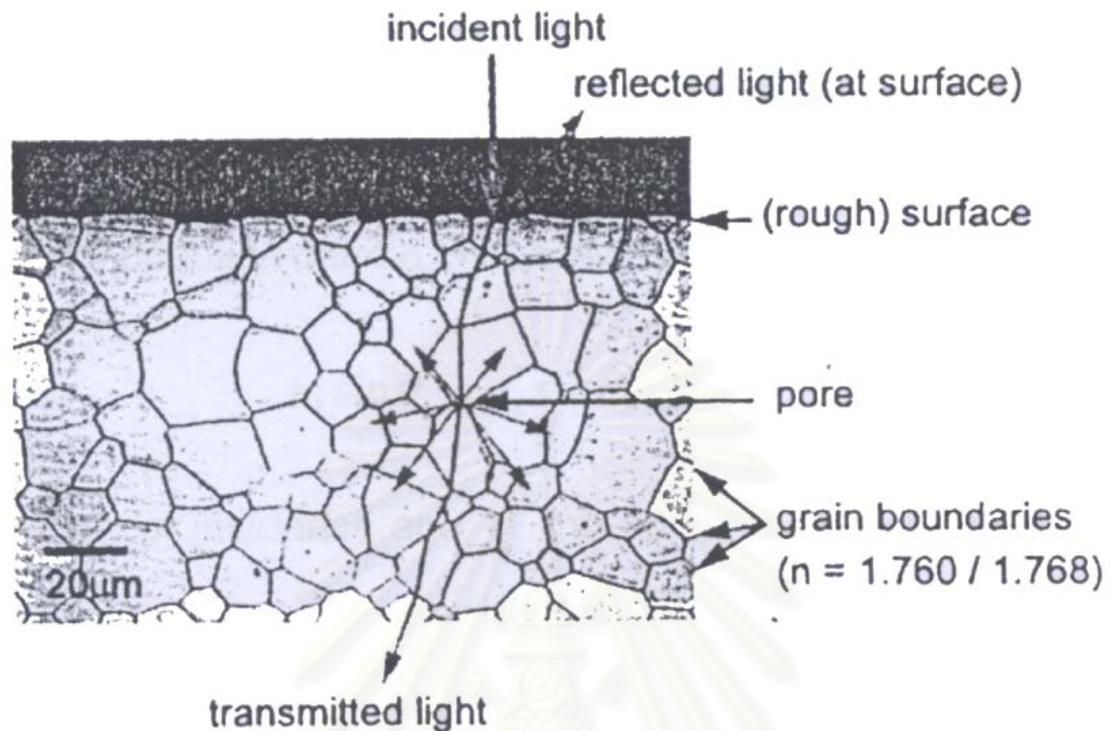


Figure 2.11 Illustration of the most important light-scattering mechanisms in polycrystalline alumina (Apetz and Broggen 2003).

The real in-line transmittance (*RIT*) decreases exponentially with the sample thickness *d*:

$$RIT = (1 - R_s) \exp(-\gamma d) \dots\dots\dots (2.4)$$

R_s describes the reflection losses at two sample surfaces at normal incidence. γ is the total scattering coefficient, which is the sum of grain-boundaries and pores. So, the *RIT* is affected by material variables (via γ and R_s) as well as the sample thickness.

2.7.2. Grain-boundary reflection

Because the crystal structure of $\alpha\text{-Al}_2\text{O}_3$ (corundum) is hexagonal, it shows birefringence. This means that the refractive index is not the same in all crystallographic directions. For example, at wavelength of 600 nm, the refractive

index of Al_2O_3 is 1.768 for the ordinary ray (polarization perpendicular to the c-axis) and 1.760 for the extraordinary ray (polarization parallel to the c-axis)(Thomas et al.). The refractive index different of 0.008 is virtually independent of temperature and wavelength. The birefringence leads to a discontinuity of the refractive index (Δn) at the grain boundaries, if the crystallographic orientations of the neighboring grains are not the same. As in normal PCA, the grains are randomly oriented, and Δn at a given grain boundary should range from zero to maximum of 0.008. Therefore, on average, the light is refracted as well as reflected at a grain boundary. However, the reflectivity of the grain boundaries is extremely low because of small Δn .

2.7.3 Grain boundary refraction

In contrast to the reflection, the refraction of light at the grain boundaries cannot be neglected in PCA. This is first shown qualitatively for large grains by simple geometrical optics. Geometrical optics can be applied when the grains are much larger than the wavelength of the light. (More exactly, the condition where $G\Delta n > 2\pi\lambda_m$. Here λ_m , is the wavelength in the medium and G is the average grain size). The deviation of light beam from its original direction can be calculated using Snell's law (Born and Wolf 1975).

$$n_1 \sin \theta_1 = n_2 \sin \theta_2 \dots\dots\dots(2.5)$$

where θ_1 , is the angle of incidence and θ_2 , the angle of the refracted ray of light. Both angles *refer* to the normal of the grain boundary surface. For $\theta = 45^\circ$ and $\Delta n = 0.008$, the deflection ($\theta_1 - \theta_2$) of the light beam from its original direction is 0.28° . This rough calculation shows that the refraction (deflection) of light at the grain boundaries can not be neglected, especially when it is taken into account that the light beam has pass tens or hundreds of grain boundaries in a typical PCA sample, depending on grain size and sample thickness.

2.7.4 Effect of grain size and transmittance

Generally, when light passes through a transparent ceramic, the in-line transmittance, *RIT*, follows the relation in Figure (2.12). From this equation the scattering terms depend on grain size of the specimen, wavelength, and sample thickness and it is applicable to all birefringent polycrystalline materials as long as the restrictions bound to the derivation of the Rayleigh-Gans-Debye theory.

In 2003, Apezt et al. early studied the effect of grain size of alumina on transmittance. *RIT* values of various samples with a thickness of 0.80 mm were measured, using a red laser with a wavelength of 645 nm. It was found that the in-line transmittance depended on grain size and on the amount and size distribution of pores. The in-line transmittance rapidly increased when grain size decreased to sub-micrometer or nano-meter level as shown in Figure. 2.12.

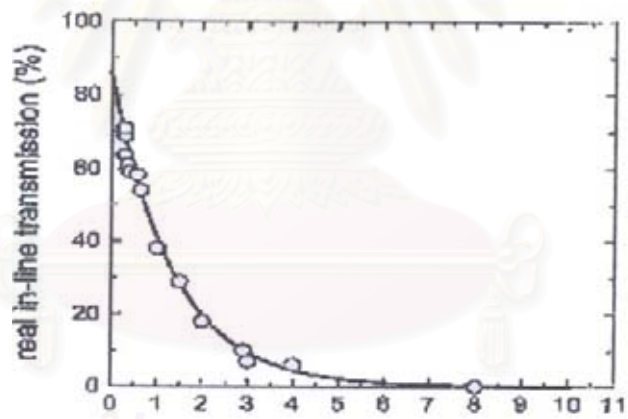


Figure 2.12. The real in-line transmittance (RIT) of alumina ceramic measured at wavelength 645 nm as a function of the mean grain size: experimental data points.

2.8) Surfactant

Surface active agents (usually referred to as surfactants) are amphipathic molecules consisting of nonpolar hydrophobic portion, which is usually the equivalent of an 8 to 18 carbon hydrocarbon atoms attaching to a polar or ionic portion (hydrophilic). The hydrophilic portion can therefore be nonionic, ionic.

A particular type of molecular structure performs as a surfactant. This molecule is made up of a water soluble (hydrophilic) and a water insoluble (hydrophobic) component (Figure 2.13).

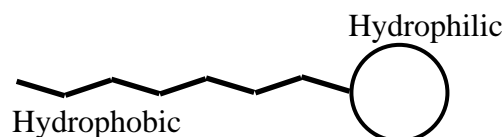


Figure 2.13 Molecular structure of surfactant.

2.8.1 Adsorption of surfactants onto solid particles

Adsorption of surfactants on solids in contact with aqueous solutions is important for controlling a variety of interfacial processes such as detergency, cleansing action of personal care products, flocculation and dispersion, enhanced oil recovery, mineral flotation and other solid liquid separations.

Adsorption of surfactants onto solid particles controls many interfacial processes, such as stabilization of solid dispersions, selective flotation of minerals, detergency, protection of metal surfaces, and lubrication. Surfactant adsorption at the solid–liquid interface is a major event in which the surfactant molecules can interact with the solid surface. When ionic surfactants adsorb onto metal oxide particles, the stability of dispersed particles is often altered by the surfactant concentration; a high dispersion stability without surfactants decreases by addition of low concentrations of surfactants, but at high surfactant concentration the dispersion stability becomes high. This process is called “dispersion–flocculation–redispersion” and is very useful for fundamental study of aqueous dispersion of particles by surfactants (Esumi 2001).

The model for hydrophobic coagulation and peptization is shown in Figure 2.14. When an oppositely charged surfactant is added to a sol, the sol is coagulated (see the middle of Figure. 2.14). Then, the coagulated sol is peptized by further addition of the same surfactant as the first one, a surfactant charged oppositely to the first one, or a nonionic surfactant (right side of Figure. 2.14). From the experimental

evidence in several adsorption systems, it has been found that ionic surfactants adsorb in appreciable amounts onto oppositely charged solids and the zeta potential of solids converts from positive to negative or vice versa. In addition, the dispersion state of solids after addition of surfactants can be correlated with the formation of a surfactant monolayer or bilayer.

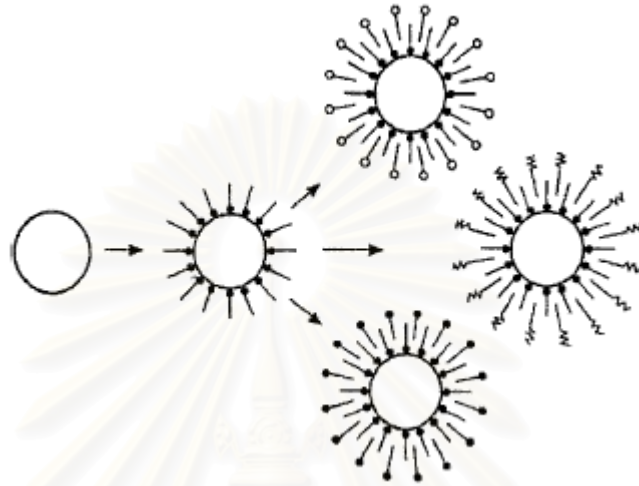


Figure 2.14 Model for hydrophobic coagulation and peptization of negatively charged sol by surfactants: (—●) cationic surfactant: (—○) anionic surfactant: (— ω) nonionic surfactant.

2.8.2 Surfactant modified alumina

Sodium dodecyl sulfate (SDS), an anionic surfactant (AS) was used for the surface modification of neutral alumina. Micelle-like structures are formed on the surface of alumina. The adsorption isotherm was drawn to understand the nature of the equilibrium distribution on the surface of alumina. The initial concentration was varied from 0 to 40,000 ppm. The adsorbent dose was kept fixed at 100 g/l (Figure 2.15) (Adak, et al. 2005).

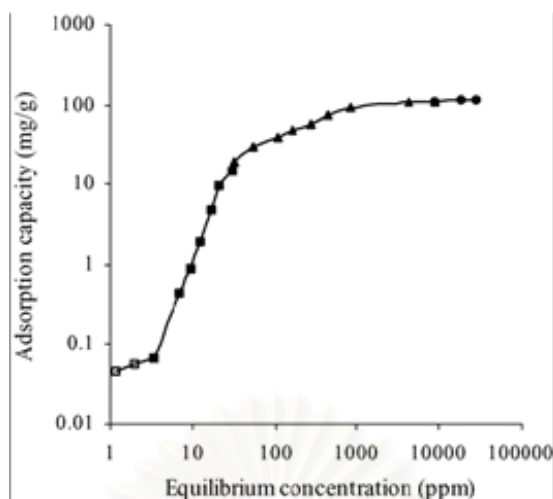


Figure 2.15. Adsorption isotherm of SDS on alumina.

2.9) Development of a Modified Alumina Powder Synthesis Method

This subject is devoted for review of some previous representative reports about a modified alumina powder synthesis method by using precipitation technique for preparing transparent poly-crystal alumina

Alumina in the form of α -alumina can be produced using transient aluminas (such as γ -, α -, θ -, ξ -, δ - alumina) that have such as aluminum hydroxide, boehmite, aluminum sulfate, and prepared but nanosized α -alumina powder can hardly be prepared in an agglomerate-free state because the α -alumina transformation occurs at a temperature of $\sim 1200^\circ\text{C}$, where sintering also occurs (Himanshu, 1989)

Himanshu Jain, Om Parkash and M. Y. Xu in 1989 proved that surface area, linear shrinkage, and compressive strength measurements, with the help of neutron irradiation, sintering of high-purity alumina can be initiated at temperatures lower than $1,200^\circ\text{C}$.

Upon the calcination at low temperature (600°C), AACH is decomposed and transformed to amorphous form. At calcination temperature of 700°C , $\gamma\text{-Al}_2\text{O}_3$ is formed, as detected by the XRD analysis. It should be noted that the diffraction peaks corresponding to $\gamma\text{-Al}_2\text{O}_3$ are weak in intensity, which indicates that it is under transition from amorphous phase. The crystallinity of $\gamma\text{-Al}_2\text{O}_3$ phase is improved as

the calcination temperature is increased to 800°C. Phase transformation from γ - to α - Al_2O_3 takes place at temperature lower than 1000°C, as evidenced from the fact that the powder calcined at 1000°C is mixture of α - and γ -phase. However, trace amount of θ - Al_2O_3 detected from the sample calcined at this temperature suggests that γ - to θ -phase transformation also takes place. At temperature higher than 1000°C, the phase transformation is completed and only peaks corresponding to α - Al_2O_3 are observed. Sharpness and high-intensity of α - Al_2O_3 XRD peaks suggest the growth of crystallite grains upon the completion of phase transition (Muangsombut et al,2005).

Many research has continued in regard to control of the morphology and particle-size distribution of α -alumina powder by means of reducing the phase-transformation temperature for the $\theta \rightarrow \alpha$ phase transformation, via the introduction of seeds or the use of controlled precipitation from an aluminum salt or alkoxidehydrothermal processing, or mechanochemical processing(Hen et al., 1993)

A method is introduced to prepare almost-spherical submicrometer-sized α -alumina via surface modification of γ -alumina with an alumina sol. Milled γ -alumina, in the presence of 3 wt% of α -alumina with a median particle size(d_{50}) of 0.32 μm (AKP-30) produced irregularly shaped α -alumina with $d_{50} \sim 0.3 \mu\text{m}$ after heat treatment at 1100 °C for 1 h. γ -alumina that had been surface-modified by milling in the presence of 3 wt% of the alumina sol resulted in almost monosized, spherical α -alumina $\sim 0.3 \mu\text{m}$ in size after heat treatment at 1100 °C for 1 h. Furthermore, almost-spherical α -alumina 0.1-0.2 μm in size was obtained by milling γ -alumina with 3 wt% of AKP-30 alumina in the presence of 3 wt% of the alumina sol, followed by heat treatment at 1100°C for 1 h. The alumina sol that has been introduced in this work seems to act as a dispersant, in addition to helping to form a spherical shape.

2.10) Influence of Impurities on the Properties and Microstructure Changes in the Alumina Sintered Body

For obtaining the green body with highest density, the impurities of specimen must be significantly emphasized. This section of report focused on what kinds of and how impurities that take the bad effect to specimens after final stage sintering.

N. Louet et al. (2005) investigated the effects of the relative amounts of the impurities such as Na_2O and SiO_2 that normally encountered in commercial powder obtained by Bayer process. They found that an increase in Na_2O content significantly slows down the densification and slightly slows down the grain growth. In contrast, the addition of SiO_2 does not affect significantly the final density but leads to abnormal grain growth and increases the aspect ratio of grains.

S. H. Hong et al. (2001) investigated the microstructure evolution of alumina ceramic prepared by adding small amounts of CaO and TiO_2 that become a liquid phase during sintering. They found that a duplex microstructure of a few abnormal grains and fine matrix grains were observed when the $\text{CaO} + \text{TiO}_2$ content was small (≤ 0.04 wt%). Meanwhile, adding of relatively high $\text{CaO} + \text{TiO}_2$ (≥ 0.1 wt%) provided many growth of grains that impinged upon each other.

S. J. Cho et al. (2001) examined the effect of the coarse-powder portion on the abnormal grain growth occurrence in commercial-purity alumina. They found that adding of coarse alumina powder which has high impurity in MgO-doped high purity alumina significantly leads to extensive abnormal grain growth occurrence.

CHAPTER III

EXPERIMENTAL

This chapter describes experimental system and procedures for alumina synthesis and fabrication of alumina specimen. It is divided into three parts, i.e. used chemicals, preparation of samples and characterization of the obtained products, respectively.

3.1) Chemicals

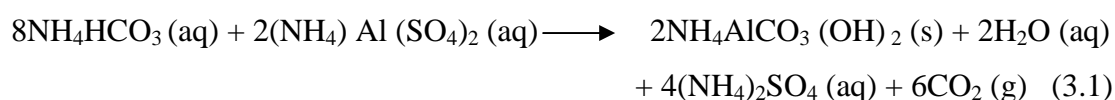
All chemicals used in this work are listed as following:

1. Ammonium aluminum sulfate (99 %+) ($\text{NH}_4\text{Al}(\text{SO}_4)_2 \cdot 12\text{H}_2\text{O}$) available from Merck Co., Ltd., Germany.
2. Ammonium hydrogencarbonate (98%) (NH_4HCO_3) available from Unilab.
3. Acetic acid (99%+)(CH_3COOH) available from CARLO ERBA REAGENT.
4. Oleic acid (99%) available from PRS Panreac.
5. Polyvinyl alcohol, MW ~ 72,000 (99%) available from Fluka.
6. Ethanol (99%+) available from MERCK.
7. Alumina powder (TMDA)(>99.99%) available from Taimei Chemical Co.Ltd., Japan.
8. Magnesium Oxide(>99.98%) available from Ube Material Industries, Ltd.

3.2) Experimental Procedures

3.2.1 Synthesis of Alumina Powder

The method as shown in Figure 3.1 to produce alumina powder from ammonium aluminum carbonate hydroxide, $\text{NH}_4\text{AlCO}_3(\text{OH})_2$, has been invented by Shuzo et al. since 1975. Ammonium aluminum carbonate hydroxide (AACH) is synthesized from a reaction between solution of ammonium hydrogencarbonate and aluminum salt solution, according to the following equation (3.1):



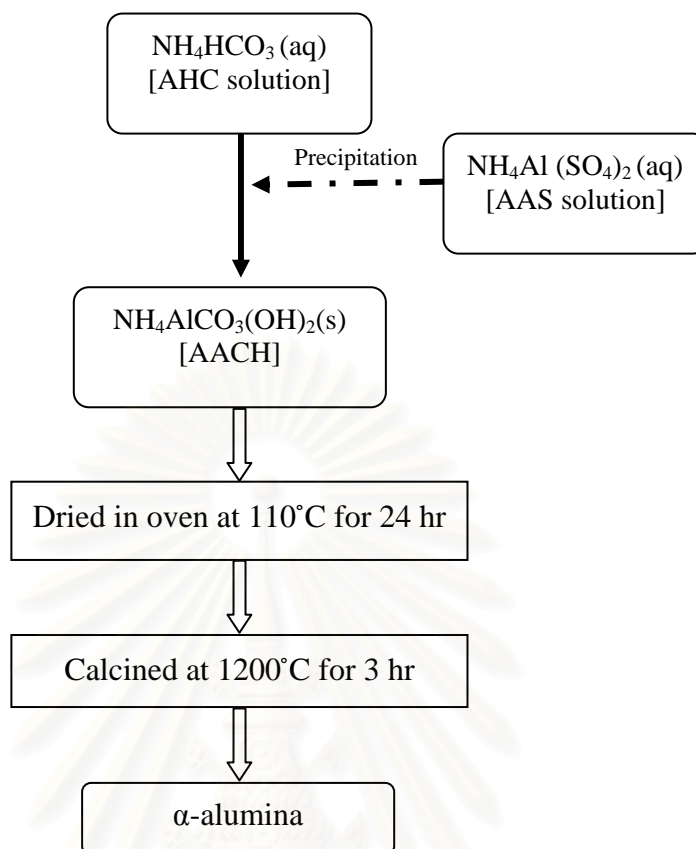


Figure 3.1 Diagram of α -alumina powder preparation by normal route.

In this work, ammonium aluminium sulfate (AAS) solution 500 ml was gradually added to ammonium hydrogencarbonate aqueous (AHC) solution 500 ml with concentration ratio of AAS to AHC of 0.5:2.0 mol/l at the temperature in a range of $40\text{--}45^\circ\text{C}$. The addition rate of AAS solution to AHC solution is 3 ml/min. The mixture was constantly stirred using magnetic stirrer rotating at 450 rpm. The pH of the mixture during the reaction was found to be constant at 9. After the reaction, the mixed solution was aged for 15 minutes to allow complete reaction. Then, the white precipitates formed were separated from the solution by centrifugation, repeatedly washed with methanol and dried in the oven at 110°C overnight.

The dried precipitate was calcined in air in a box furnace. The precipitate had been heated at a rate of $10^\circ\text{C}/\text{min}$ to the desired temperature, 1200°C and held at that temperature for 2 h. The obtained powder was found to be alumina in α -phase.

The procedures described above are considered as the standard synthesis route. Several modifications were made on this set of procedures, in order to investigate effects of various factors on particle size of the obtained powder as well as properties of the sintered articles. Such modifications are listed as followed.

3.2.1.1 Precipitation Assisted by Ultrasonic

This modification is almost the same procedure as the standard synthesis, but ultrasonic both were employed to assist the mixing, instead of magnetic stirrer. The schematic diagram of the synthesis procedure is shown in Figure 3.2.

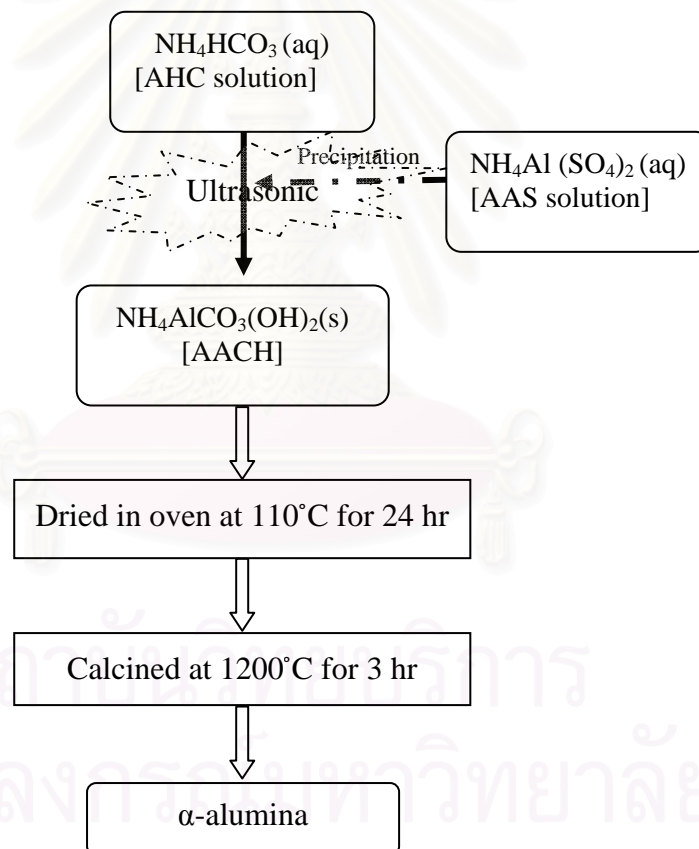


Figure 3.2 Diagram of α -alumina powder preparation by ultrasonic.

3.2.1.2 Milling of AACH

In the attempt to reduce size of the α -alumina aggregates, the intermediate compound, i.e. AACH, was milled before subjected to the calcination. The schematic diagram of this modified synthesis approach is shown in Figure 3.3. AACH obtained according to the normal synthesis was milled by ball milling. High purity alumina ball 100 g, AACH powder 40 g, and ethanol solution 50 cc was placed into the polypropylene bottle which has volume 125 cc. this bottle was rotated with rotating speed 150 rpm. The milling time was varied from 8 h, 24 h, 48 h and 72 h respectively.

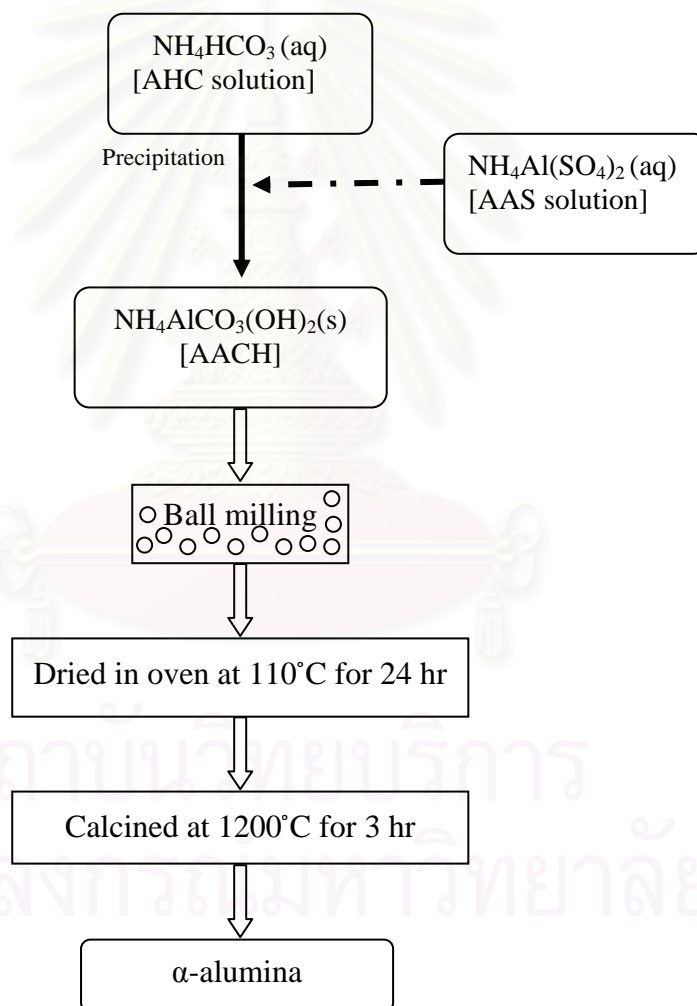


Figure 3.3 Diagram of α -alumina powder preparation with an addition of AACH milling.

3.2.1.3 Surface Modification of AACH

Surface modification is another approach used in the attempt to prevent aggregation of AACH, which subsequently results in heavily agglomerated α -alumina powder. In this work, surface of AACH particles was modified with compounds such as acetic acid, oleic acid and polyvinyl alcohol (PVA), in order to employ steric effect and electrostatic repulsion from such compounds. Details of procedures for such modification are shown in the following sections.

3.2.1.3.1 Modification of AACH by Acetic Acid and Oleic Acid

The procedure of this modified synthesis is shown in Figure 3.4. AACH obtained according to the synthesis route was mixed with the solution of acetic acid or oleic acid in methanol for 24 h. Concentration and PH of the solution was varied. Acetic acid solution was prepared by using various concentrations which is 99.9%, 16.7% and 0.33% by volume and Oleic acid solution was prepared by using various concentrations 10% and 0.5% by volume. It should be noted that the acid was added to the mixture after the precipitation was completed, in order to avoid the change in pH of the precipitation system.

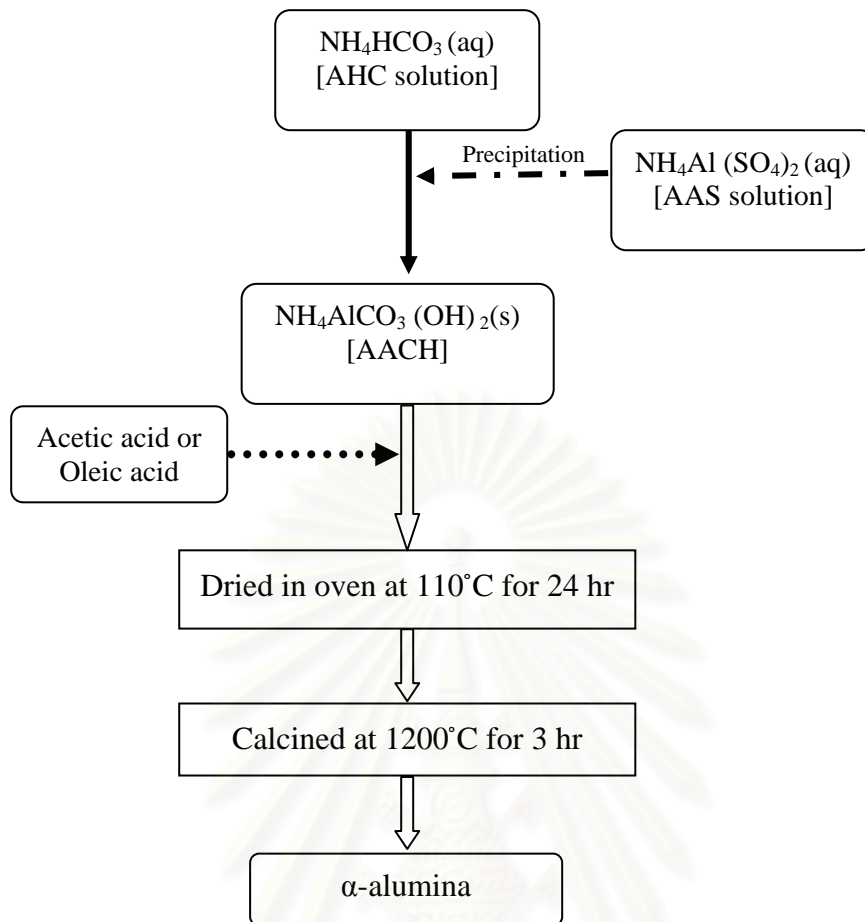


Figure 3.4 Diagram of α -alumina powder preparation with a stg of AACH surface modification by acetic acid or oleic.

3.2.1.3.2 Polyvinyl alcohol (PVA) modified AACH

For the surface modification with polyvinyl alcohol (PVA), PVA solution was added into the AHC solution before synthesis of AACH for 0.5 wt% and 10 wt% of PVA in the mixing solution. The synthesis procedure afterward was done in the manner as the normal synthesis route. The schematic diagram for this modification is shown in Figure 3.5.

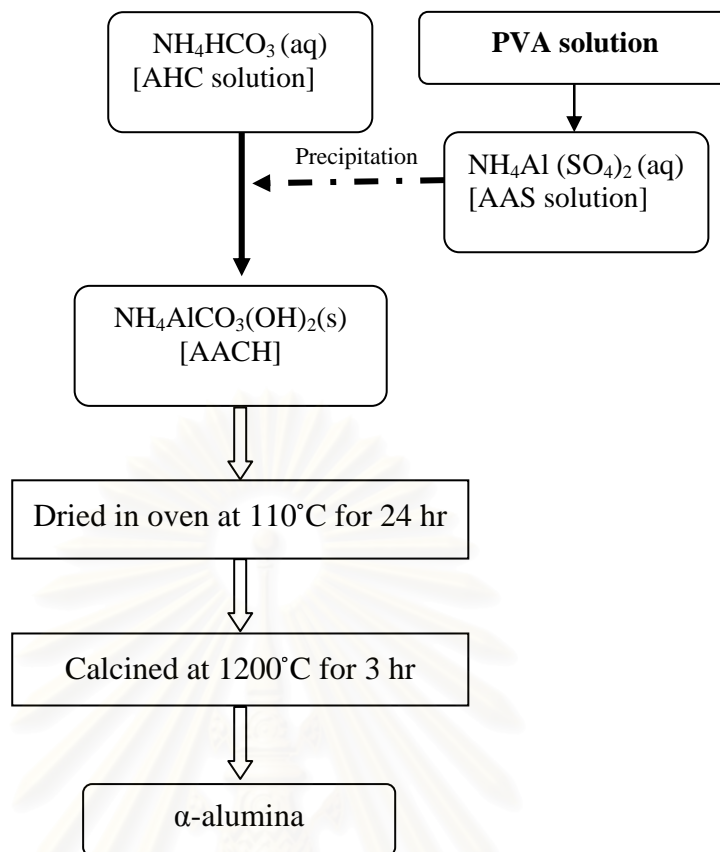


Figure 3.5 Diagram of α -alumina powder preparation with a step of AACH surface modification by PVA.

3.2.1.4 Variation in Calcination Time

The AACH powders synthesized according to the normal synthesis procedure were calcined at 1200⁰C, using different method and holding time. For the first method, the AACH powder was heated up from room temperature to 1200⁰C at rate of 10⁰C /min, and was held at 1200⁰C for various holding time, i.e. 5, 10,20,30,60 and 120 minute respectively. For the second method, the AACH powder was put into the oven when oven temperature was around 1140⁰C. The system was further heated up to 1200⁰C and held at that temperature for 5, 10,20,30,60 and 120 minute respectively.

3.2.2 Fabrication of Alumina Specimens

3.2.2.1 *Ball Milling*

The synthesized alumina powder was mixed with $\text{Mg}(\text{NO}_3)_2 \cdot 6\text{H}_2\text{O}$ in the content of 0.03 wt.% (on the basis of MgO after decomposition) in polypropylene bottle (125 ml), using ethanol as solvent. Alumina balls were used as grinding media. The powder was milled for 24 h (see Appendix x) and subsequently dried in an oven at 110°C for 24 h to eliminate residual ethanol and moisture.

3.2.2.2 *Biaxial Hydraulic Press and Cold Isostatic Press*

The milled powder was pressed into a pallet of 13 mm in diameter by biaxial hydraulic press with pressure of 20 MPa and followed by cold isostatic press under the pressure of 300 MPa. The green compact was dried in the oven at 105°C for 2 h.

3.2.2.3 *Pressureless Sintering*

The dried green bodies were sintered at 1350°C for 2 h in air under atmospheric pressure. After cooled down and measure their density, the samples were sintered again at 1500°C for 2 h in the same atmospheric conditions.

3.2.2.4 *Hot Isostatic Press*

Further densification was enforced by using Hot Isostatic Press (Dr.HIP, KOBELCO) at 1350 to 1400°C for 0.5 to 1 hr with heating rate of $10^\circ\text{C}/\text{min}$ and the pressure of 150 MPa in Ar atmosphere. Only the sintered specimens with relative density $>95\%$ of the theoretical density, were selected for applying HIP.

3.3) Characterizations

3.3.1 *Characterization of Synthesized Powder*

3.3.1.1 *X-Ray Diffraction (XRD)*

The X-ray diffraction (XRD) analysis of powder was performed by a SIEMENS D5000 X-ray diffractometer, using Ni-filtered CuK α radiation. The scan was performed over the 2θ range from 20° to 80° , using step size of 0.020° .

The crystallite size of the powder was estimated from the XRD line broadening according to the Scherrer equation. The value of shape factor, K , was taken to be 0.9 and α -alumina was used as an external standard.

3.3.1.2 *Surface Area Measurement*

Specific surface area of the powder was calculated based on nitrogen uptake at liquid-nitrogen temperature, using the Brunauer-Emmett-Teller (BET) equation by the single point method.

3.3.1.3 *Particle Size Distribution Analysis (PSD)*

The particle size and particle size distribution were analyzed by using laser scattering particle size distribution analyzer (Mastersizer S model) at the Scientific and Technological Research Equipment Centre, Chulalongkorn University.

3.3.1.4 *Thermogravimetric Analysis (TGA)*

The powder samples were subjected to a differential thermal analysis (Diamond Thermogravimetric and Differential Thermal Analyzer, STA 4094) to determine the temperature of possible decomposition and phase change in the range of 20 - 1300°C . The analysis was performed at a heating rate of $10^\circ\text{C}/\text{min}$ in $50\text{ ml}/\text{min}$ flow of air.

3.3.1.5 Scanning Electron Microscopy (SEM)

Morphology the samples were observed on JSM-5410LV scanning electron microscope. The SEM was operated using the secondary electron mode at 15 kV at the Research Equipment Center, Faculty of Science, Chulalongkorn University.

3.3.1.6 Transmission Electron Microscopy (TEM)

Morphology and size of primary particles of the samples were observed by transmission electron microscope (TEM) model JEM-100SX at the Scientific and Technological Research Equipment Center, Chulalongkorn University (STREC)

3.3.2 Characterization of Green Specimens

The diameter and thickness of green specimens were measured using vernier caliper and the bulk density was calculated by the equation (3.1).

$$\text{Bulk density } (\rho) = \frac{M}{V} \quad (3.1)$$

Where M is the mass of green pellet and V is the volume of green pellet.

3.3.3 Characterization of Sintered Specimens

3.3.3.1 Density of the Sintered specimens

The sintered densities were measured by the Archimedes method (see Appendix C), using water as an immersion medium. The relative densities were calculated with respect to the theoretical density of $\alpha\text{-Al}_2\text{O}_3$ (3.98 g/cm^3).

3.3.3.2 UV/Visible Spectrophotometry (UV/Vis)

The absorption range, as well as the transparency, of sample was determined by using UV/Visible spectrometer (Perkin Elmer Lambda 650), operated at wavelength 350-650 nm using step size of 1 nm.



สถาบันวิทยบริการ
จุฬาลงกรณ์มหาวิทยาลัย

CHAPTER IV

RESULTS AND DISCUSSION

This research has set its purpose to develop a modified alumina powder synthesis method by using precipitation technique suitable for preparing transparent polycrystalline alumina specimen. Effect of the starting synthesized powder and process variables on the properties of powder and specimen obtained in each preparation stage will be thoroughly reported and discussed in this chapter.

In this chapter, the experimental results and discussion are described. The chapter can be divided into 4 sections as follows:

Section 4.1 describes characteristic of synthesized alumina compared with commercial alumina powder (TMDA).

Section 4.2 describes effect of calcination time and initial calcination temperature on sintering of alumina particles and the obtained specimens.

Section 4.3 describes effect of milled AACH milling on synthesized alumina.

Section 4.4 describes effect of AACH surface modification.

Section 4.5 describes precipitation assisted by ultrasonic.

4.1) Characteristic of Synthesized Alumina Compared with Commercial Alumina Powder (TMDA).

In order to get transparent alumina sintered body with grain size in nanometer to submicrometer scale, the starting raw material must be smaller than the target grain size, otherwise growth of grains (or particles) during the sintering process will hinder light transmission by multilevel scattering inside the specimen (Apetz et al., 2003). Therefore, the particle size distribution (PSD) of the starting alumina powder was taken into account as the first factor.

Tap density and particle morphology are also important because about high powder density, low degree of powder agglomeration and non-porous particles would be able to bring about high density and non-porous specimen, which are main requirements for transparency of materials (Apetz et al., 2003).

4.1.1 Characteristic of commercial alumina powder (TMDA)

In this work, commercially available TMDA alumina powder (Taimei Chemical Co.Ltd., Japan) was used as comparing raw material. It is ultra-fine and agglomerate-free powders with high purity of >99.99%. This powder can be made into a specimen, which has density near theoretical density at temperature lower than 1300 °C. The specimen has fine and homogeneous microstructure (Tansungnoen 2005).

The TMDA alumina powder was ball milled by using alumina balls. The sample was dispersed in water and ultrasonicated before measurement by the dynamic light-scattering technique, in order to give the well-dispersed suspension. The suspension was characterized to get particle size distribution (PSD). The result is shown in Figure 4.1. From the result, it is found that TMDA alumina powder has very narrow range of size distribution, in which a median size is around 120 nm. Its morphology, which could be also observed from typical SEM image and TEM image, is spherical and non-agglomerated, as shown in Figure 4.2(a) and Figure 4.3(a) respectively.

Others physical properties are shown in Table 4.1. The TM-DA alumina powder; according to the X-ray diffraction (XRD) analysis, is in alpha phase. The crystallite size, which is calculated from the half-height width of the diffraction peak of XRD pattern using the Scherrer equation (Appendix B), is around 100 nm. B.E.T. specific surface area is 13.5 m²/g. Tap powder density is 0.97 g/cm³. When the powder was processed into a specimen, the density of the specimen after biaxial pressing, after cold isostatic pressing, after sintering at 1350⁰C for 2 h, after sintering at 1500⁰C for 2 h, and after hot isostatic pressing at 1400⁰C at 1,500 MPa for 1h is 1.95, 2.19, 3.90, 3.95 and 3.96 g/cm³ respectively.

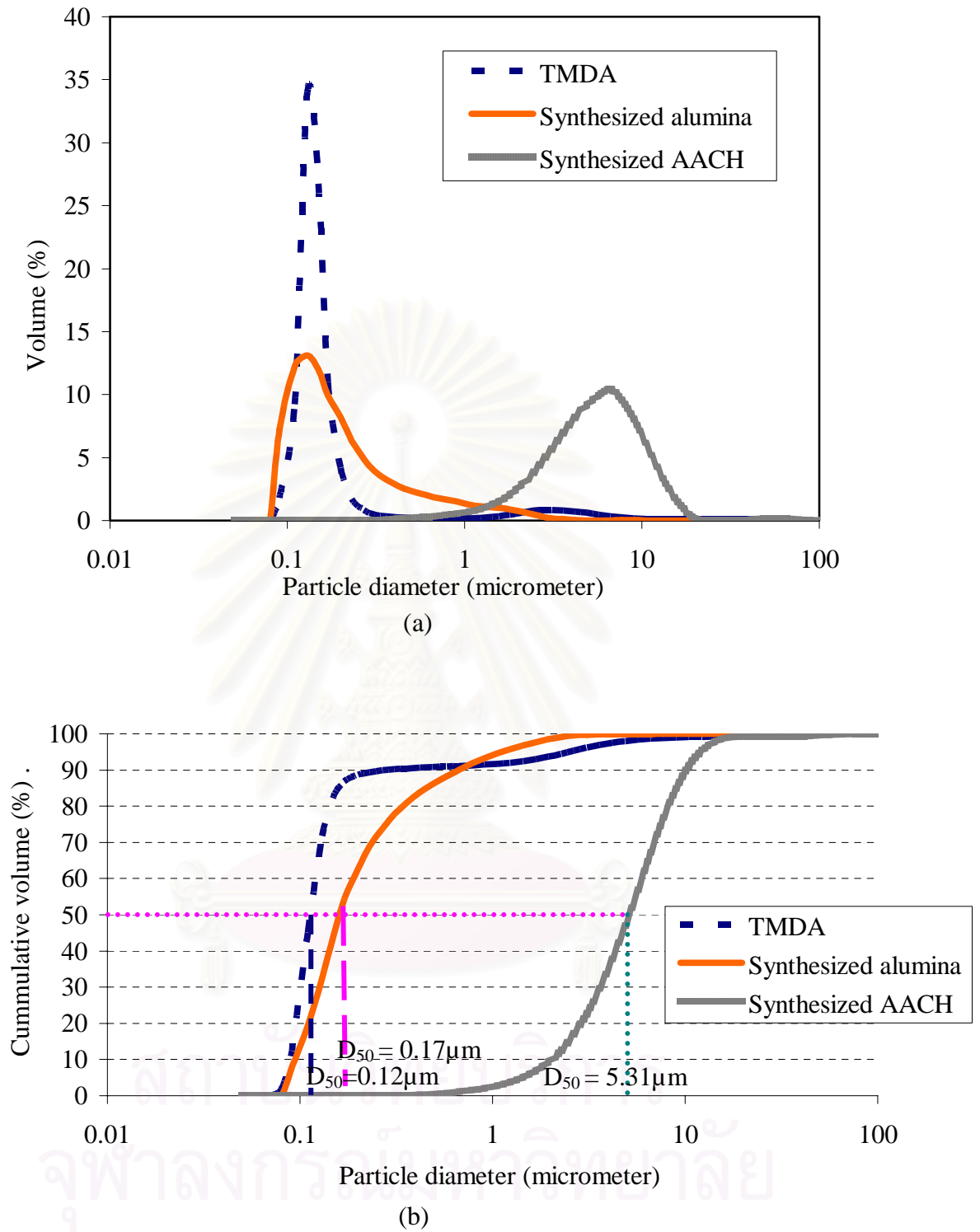
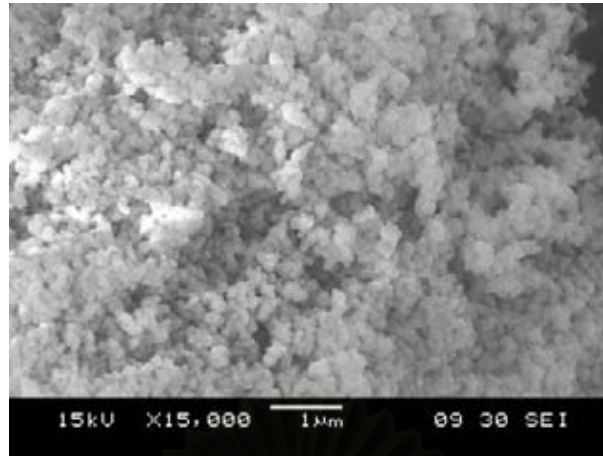


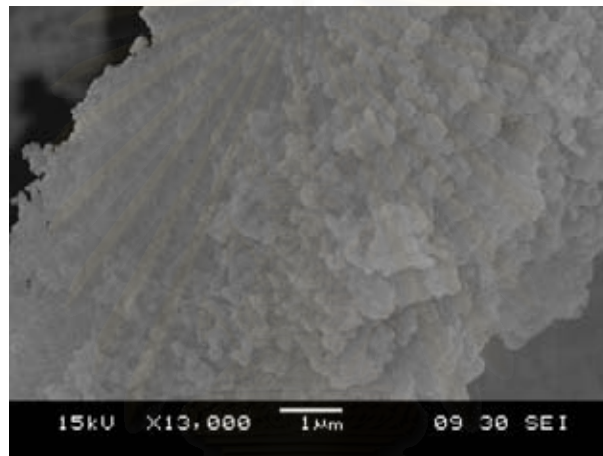
Figure 4.1 Particle size distributions of TMDA alumina powder, alumina synthesized via normal routine and ammonium aluminium carbonate hydroxide (AACH) powder synthesized:

(a) particle size distribution

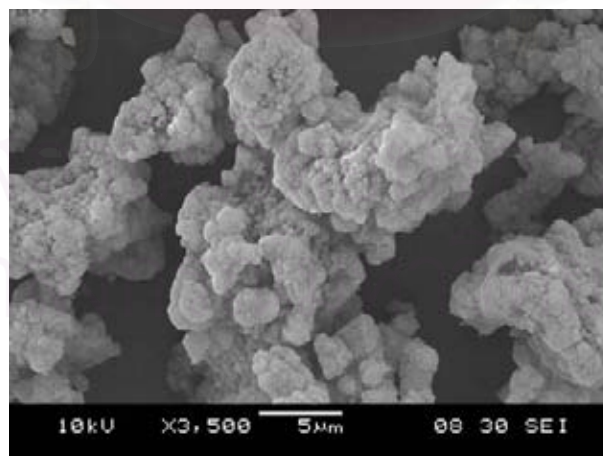
(b) cumulative particle size distribution



(a)

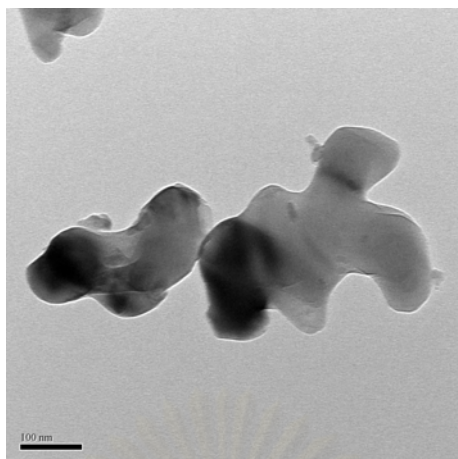


(b)

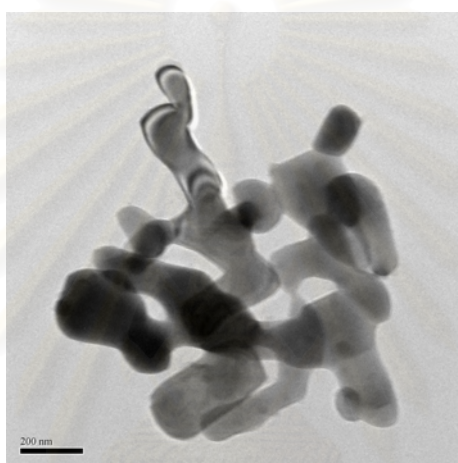


(c)

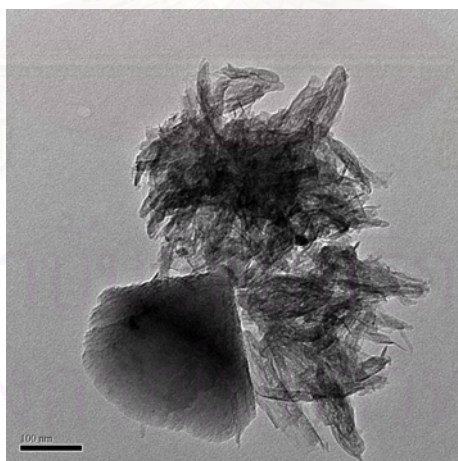
Figure 4.2 SEM micrographs of TMDA alumina powder (a), alumina powder synthesized via normal routine (b), synthesized AACH powder(c).



(a)



(b)



(c)

Figure 4.3 TEM micrographs of TMDA alumina powder (a), alumina powder synthesized via normal routine (b), synthesized AACH powder(c).

Table 4.1 Properties of TMDA alumina powder, alumina powder synthesized by normal routine and synthesized ammonium aluminium carbonate hydroxide (AACH) powder.

Categories	TMDA	Normal synthesized alumina	Normal synthesized AACH
Crystalline form	alpha phase	alpha phase	AACH
Crystallite size (nm)	100	49	3
Median particle size (μm)	0.12	0.17	5.3
B.E.T. specific surface area (m^2/g)	13.5	12.2	131.1
Tap powder density (g/cm^3)	0.97	0.62	0.46
Biaxial pressed density at 20MPa(g/cm^3)	1.95	1.87	-
Density of specimen after cold isostatic pressing density at 250MPa (g/cm^3)	2.19	1.89	-
Density of specimen after Sintering at 1350°C for 2Hr. (g/cm^3)	3.90	2.94	-
Sintered density at 1500°C for 2Hr, repeatedly. (g/cm^3)	3.95	3.81	-
Density of specimen after Hot isostatic pressing at 1400°C 1500MPa (g/cm^3)	3.96	3.88	-

4.1.2 Characteristic of products synthesized by normal routine

The XRD analysis of normal synthesis sample, as shown in Figure 4.4, reveals that the XRD pattern of the product from the reaction between AAS and AHC does not match any polymorph of alumina. It is in fact corresponding to the reflection of ammonium aluminium carbonate hydroxide (AACH). The diffraction peaks are broad, indicating that the crystals are very small and imperfect, which agrees with the previous findings in (Prasitwuttisak et al, 2004).

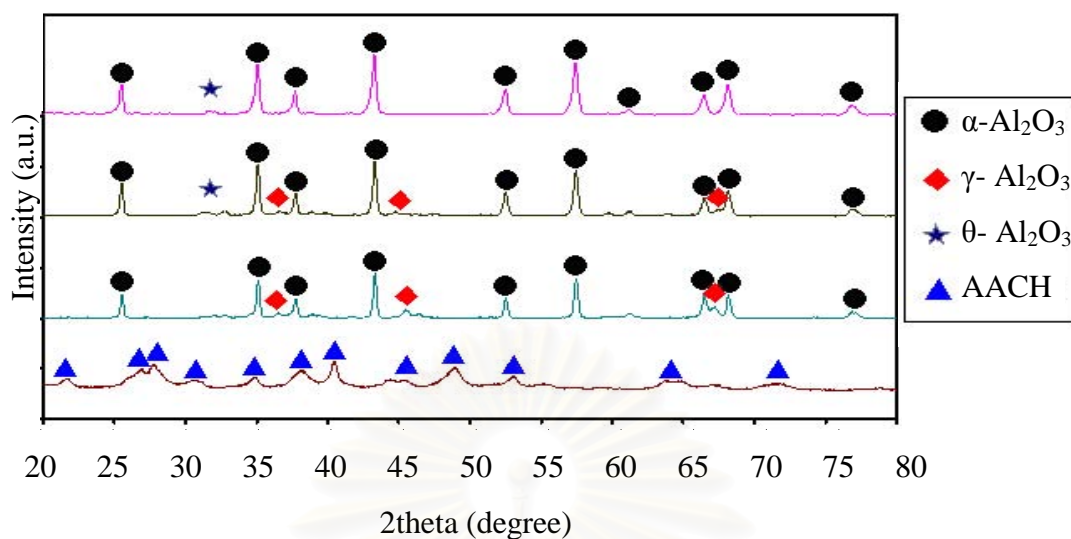


Figure 4.4 XRD patterns of product calcined at various time.

Upon the calcinations, AACH decomposes and forms into alumina structure. As the calcination temperature is increased, alumina undergoes phase transformation from amorphous to α -alumina and α -alumina, respectively. At temperature around 1200°C , the phase transformation is completed and only peaks corresponding to α - Al_2O_3 are observed. Sharpness and high-intensity of the XRD peaks suggest the growth of crystallite grains upon the completion of phase transition (Youn, 1999).

In this section α - Al_2O_3 and AACH powder were sampled in the same manner as previously described for TMDA alumina powder and characterized to find the particle size distribution (PSD). The results are shown in Figure 4.1. From PSD the results, it can be seen that AACH powder and the α -alumina powder synthesized by the normal routine have average size around 530 nm and 170 nm respectively.

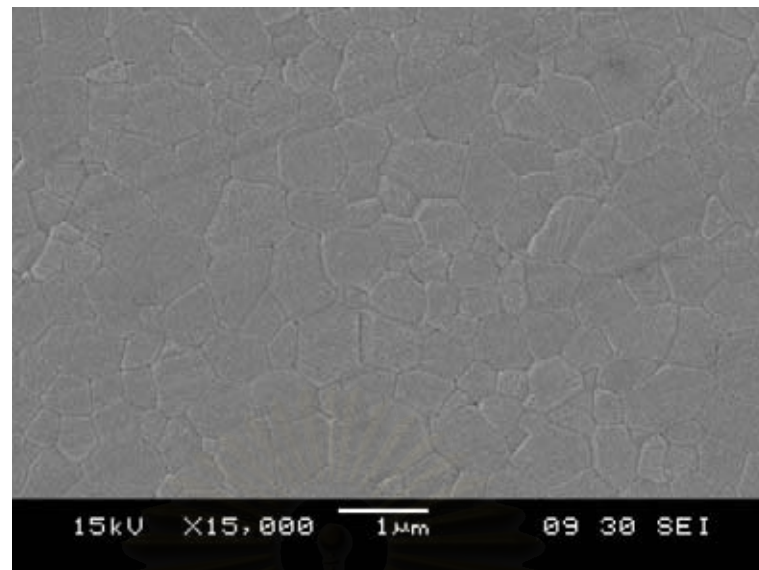
Crystallite size of the AACH powder, which was calculated from the half-height width of the diffraction peak of XRD pattern using the Scherrer equation (Appendix B), is much smaller than the crystallite size of the synthesized alumina. The B.E.T. specific surface area of the AACH powder ($131 \text{ m}^2/\text{g}$) is much larger than that of the synthesized alumina ($12 \text{ m}^2/\text{g}$). However, the particle size distribution results show that size of the AACH powder is larger than the synthesized alumina. From these results, it is suggested that the AACH powder is agglomerated and has a lot of

pore within its large secondary particle. This characteristic makes tap density of the AACH powder lower than the synthesized alumina as shown in Table 4.1.

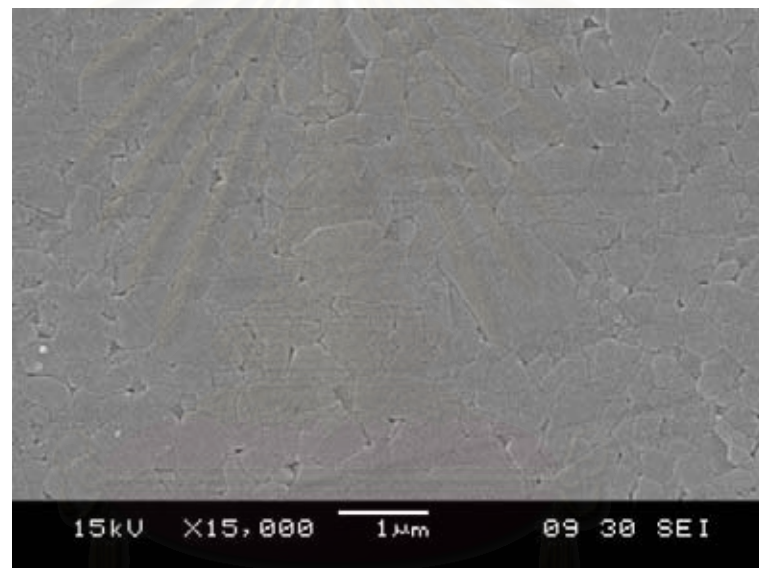
According to Table 4.1, although crystallite size of the synthesized alumina is smaller than the TMDA powder, B.E.T. specific surface area of the synthesized alumina is only slightly less than that of the TMDA powder because of the agglomeration within the synthesized alumina particle, as shown in the TEM image in Figure 4.3(b).

Figure 4.1 shows not only that the range of size distribution of TMDA powder is more narrow than that of the synthesized alumina powder, but also shows that the median size of TMDA powder is smaller than the median size of the synthesized alumina powder. These results confirm that TMDA powder is not significantly agglomerated, while the synthesized alumina powder contains a lot of hard agglomerates, which results in large secondary with particles many pores.

SEM and TEM micrographs of the synthesized alumina and the TMDA powder clearly show that the synthesized alumina particles are heavily agglomerated, while the TMDA powder is less agglomerated. Even though crystallite size of the synthesized alumina is smaller than that of the TMDA powder, the primary particles of the synthesized alumina agglomerate and become big particles. This is due to the fact that smaller particles have higher surface energy than the bigger ones and the reduction in the surface energy is a driving force for the agglomeration (Cao,1998)



(a)



(b)

Figure 4.5 SEM micrographs of the specimen fabricated from:

- (a) TMDA powder
- (b) α -alumina powder synthesized by normal precipitation procedure.

SEM images in Figure 4.5 show that the specimen, which was fabricated from TMDA, has smaller fraction of pore inside the specimen and more uniform grain than the specimen fabricated from α -alumina powder synthesized by normal precipitation procedure which contains lots of pore inside the specimen and shows non-uniform grains.

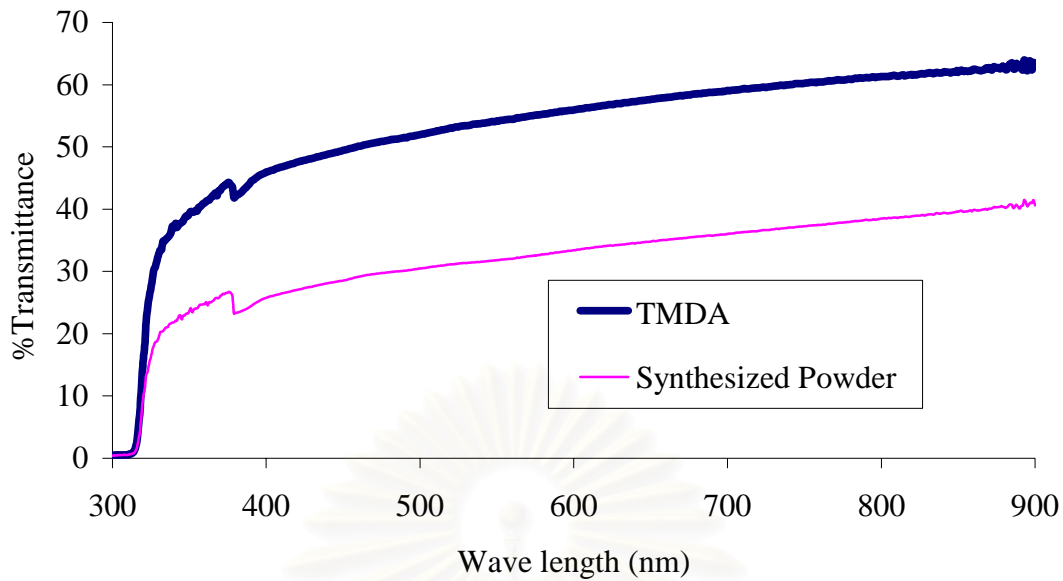


Figure 4.6 UV/Visible spectrophotometry results of the specimen fabricated from: TMDA powder and α -alumina powder synthesized by normal precipitation procedure

UV/Visible spectrophotometry micrographs in Figure 4.6 which compare specimen which was fabricated from TMDA powder and α -alumina powder synthesized by normal precipitation procedure, it is shown that the specimen, which was fabricated from TMDA, has higher transmittance of light in wave length between 400 to 800 nm which is the length of visible light.

Because the agglomerates in the synthesized alumina particle contain a lot of pore within its secondary particles, it results in low tap density and low pressed density (see Table 4.1). The low pressed density would bring not only low specimen density but also many pores in the specimen, which makes the specimen non-transparent (Apetz et al, 2003). Therefore, the method to reduce the agglomerates in the synthesized alumina particles was concerned.

4.2) Effect of Calcination Time and Initial Calcination Temperature on Properties of Alumina Particles and Specimens.

Nanosized α -alumina powder can hardly be prepared in an agglomerate-free state because phase transformation into α -alumina occurs at temperature around 1200°C, where sintering has already occurred. (Jain et al, 1989) proved that with the help of neutron irradiation, sintering of high-purity alumina can be initiated at temperatures lower than 1,200°C.

Therefore, many researches have continued to control of the morphology and particle-size distribution of α -alumina α -alumina powder by means of reducing the phase-transformation temperature, via the introduction of seeds or the use of controlled precipitation from an aluminum salt or alkoxidehydrothermal processing, or mechanochemical processing (Kumagai et al, 1985).

For this research, the sintering behavior of alumina particles at high temperature (i.e. 1200 and 1300°C) was monitored by TEM image. Figure 4.7 shows AACH powder, boehmite powder obtained from calcination of AACH for 0.5 minutes at 1300 °C, alumina obtained from calcination of AACH at 1200 °C for 5 minutes, 20 minute and 2 h, respectively. It should be noted that the sample calcined for 0.5 minutes (Figure 4.7(b)) was obtained by flowing the AACH powder through a heated tube, using air as the carrier gas. For other samples, they were heated in a box furnace. From the TEM images, it is shown that a large secondary α -alumina particle is produced from a lot of small primary particles via sintering, which is hard agglomerates. The sintering increases upon the calcination time. Furthermore, it can be observed that size of the primary particles of alumina increases by grain growth, while size of the secondary particles also increases size by sintering. Figure 4.7(e) also clearly shows pores remaining in the secondary particles after sintering of the primary particles.

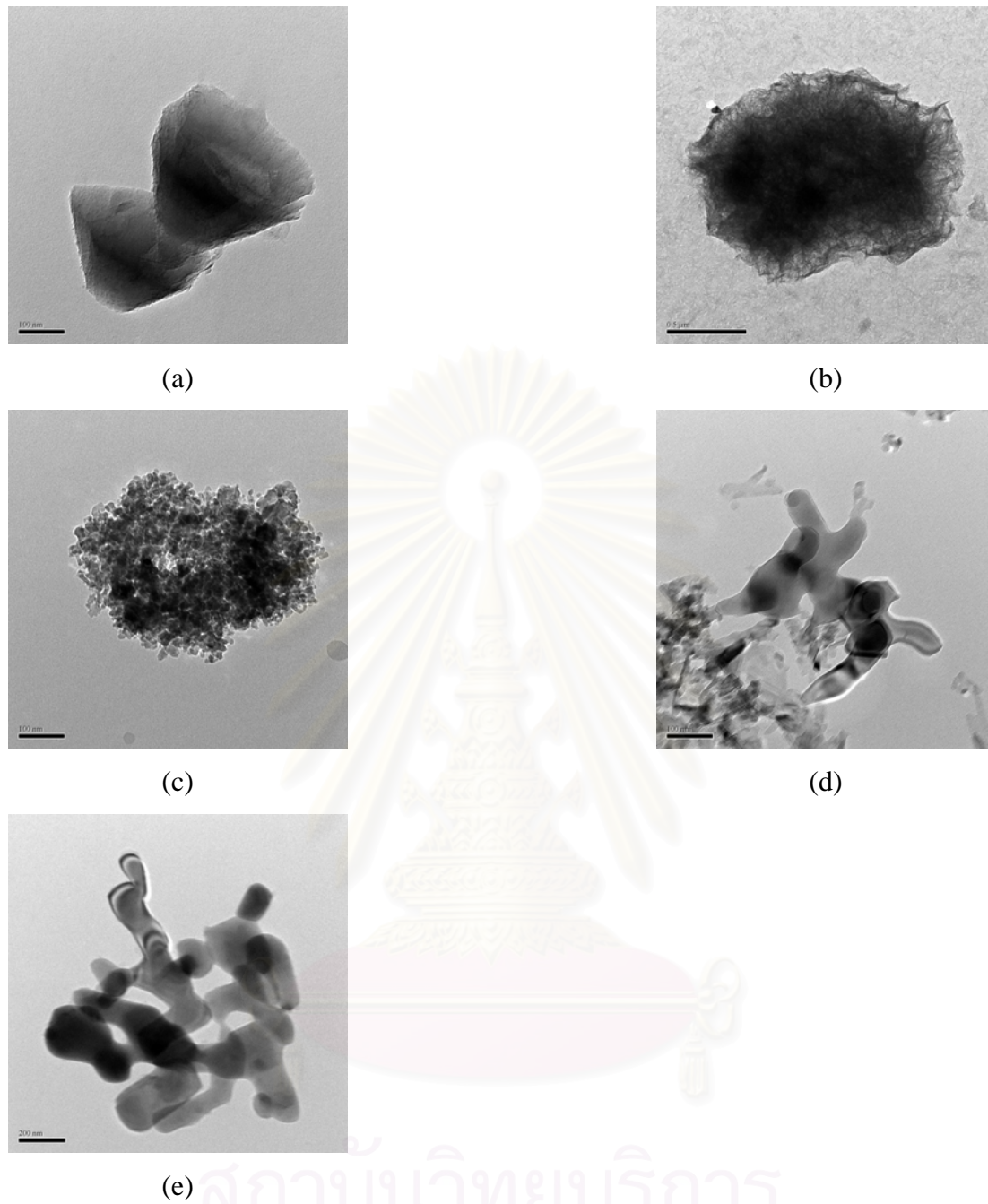


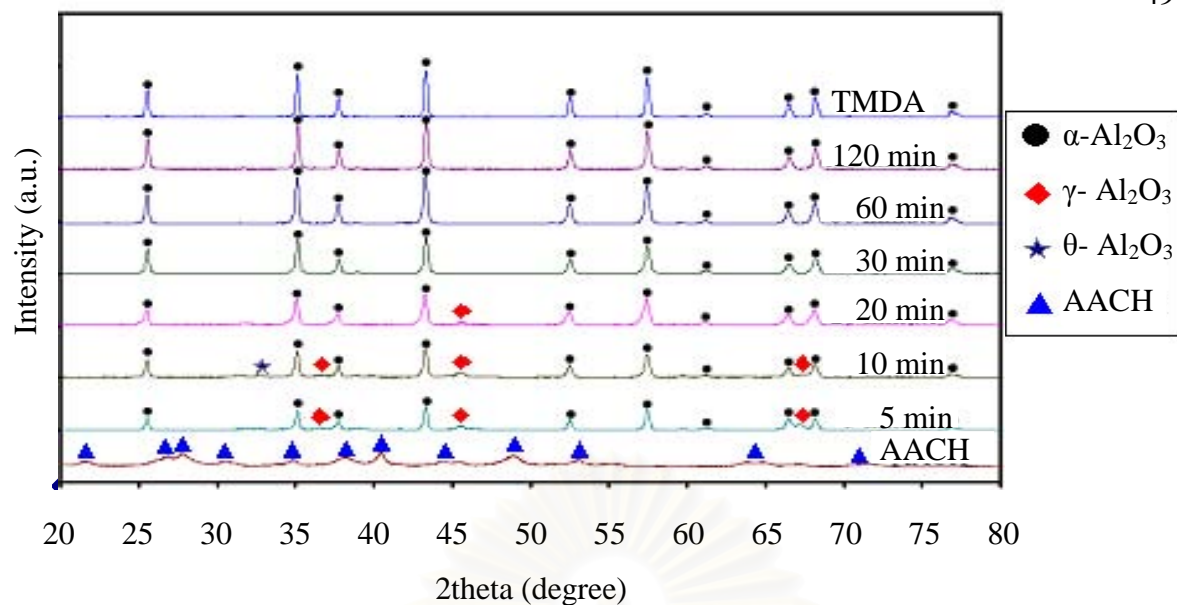
Figure 4.7 TEM micrographs of AACH powders of which was calcined at various conditions:

- (a) pre-calcined AACH.
- (b) AACH calcined at 1300 °C for 0.5 minutes (boehmite).
- (c) AACH calcined at 1200 °C for 5 minutes (α , γ -alumina).
- (d) AACH calcined at 1200 °C for 20 minutes (α -alumina).
- (e) AACH calcined at 1200 °C for 120 minutes (α -alumina).

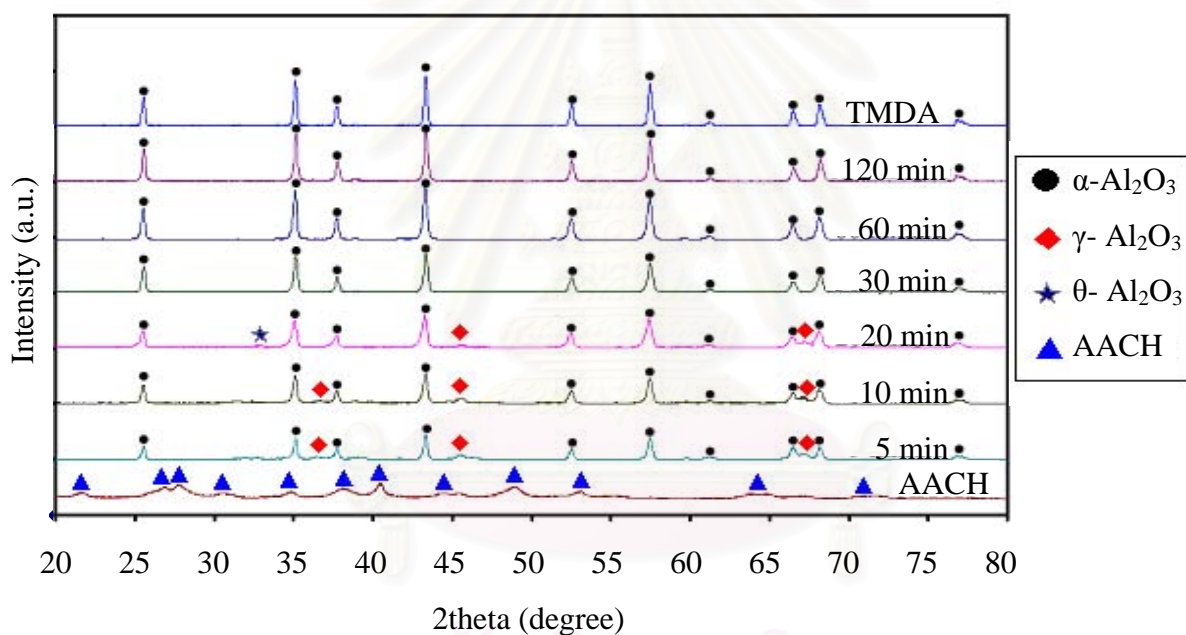
In this research, α -alumina was prepared by calcination of AACH in 2 ways. The first approach of calcination was done by ramping temperature slowly (around

10°C/min) from room temperature to 1200°C. The system was held at 1200°C for a desired period of time. The other method is calcination by avoiding sintering of particles during the long period of heating up. In the second calcinations approach, AACH powder was put into a furnace when the temperature of the furnace is around 1100°C. After the desired period of time at 1200°C, the powder was brought out of the furnace and cooled down to room temperature as fast as possible.

XRD patterns of AACH powder calcined at various time in Figure 4.8 clearly show progress of phase transformation. AACH powder that is calcined by heating from room temperature and held at 1200°C for 5, 10 and 20 minutes is a mixed phase of γ , θ and α alumina. It has been reported earlier in the literature that γ -alumina is formed from decomposed AACH at temperature around 800°C. Phase transformation from γ - to α -alumina then occurs at around 1000°C. (Muangsombut 2005) Nevertheless, according to the results shown in Figure 4.8(a), the formation of α -phase takes place rather quickly. Sign of α -alumina was observed even in the sample held at 1200°C for only 5 minutes. The AACH powder can be completely transformed to α -alumina at 1200°C by using holding time for the calcination of only 30 minutes. On the other hand, for AACH calcined by putting the sample into the furnace at 1100°C, the results are similar to that previously described. The product after calcination at 1200°C for 5, 10 and 20 minutes is alumina in mixed phase. The transformation into α -phase is complete after the calcinations for only 30 minutes.



(a)

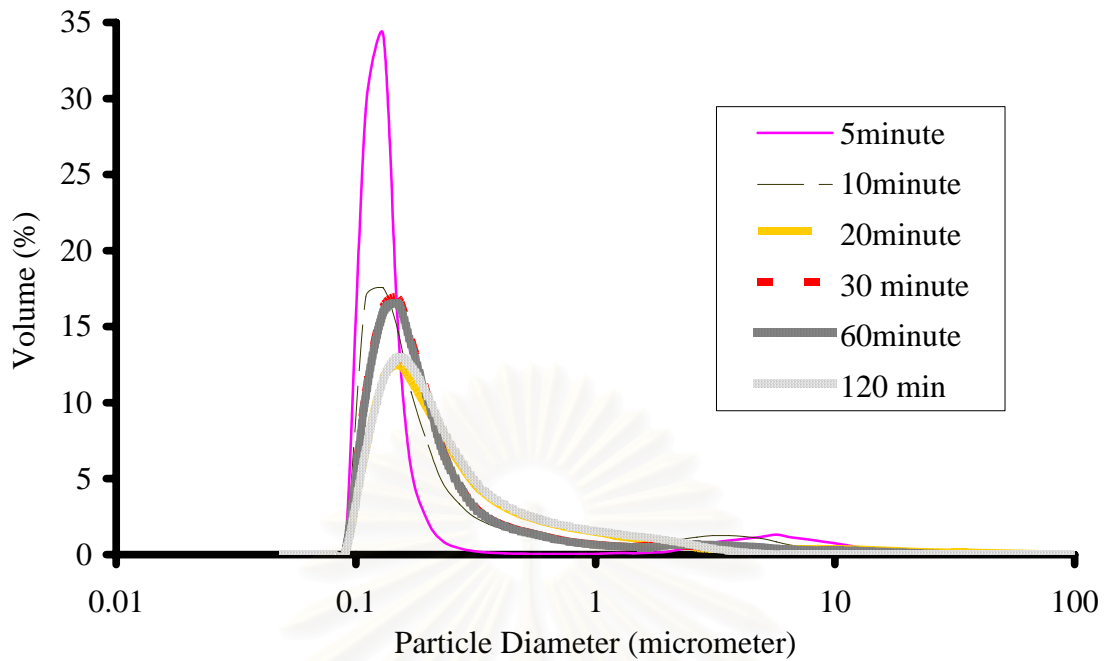


(b)

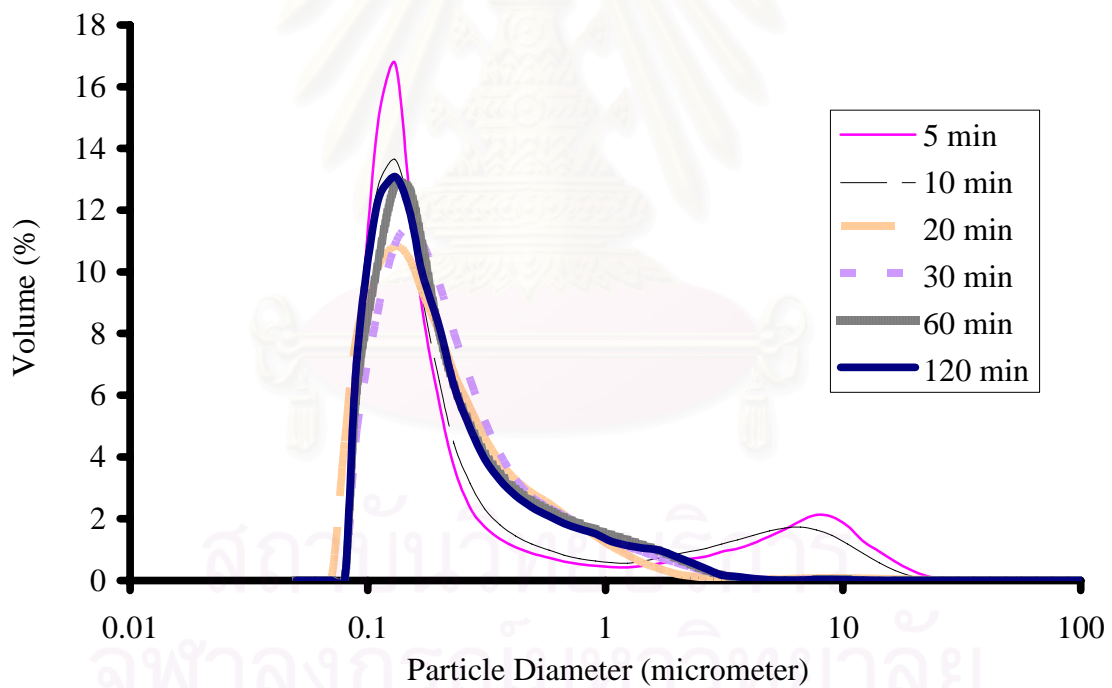
Figure 4.8 XRD patterns of products from calcination of AACH at 1200°C for various holding times:

- (a) The samples are heated up from room temperature.
- (b) The samples are put into a furnace at temperature is around 1100°C .

According to the particle size distribution of the calcined products shown in Figure 4.9, it can be observed that AACH which was calcined differently would have different particle size distribution pattern. Because calcination for only 5 or 10 minutes can not result in full transformation to α -alumina, size distribution in these cases is bimodal. The small particles are expected to be γ - and α -alumina, which has not been agglomerated, while the large particles are expected to be a compound, which has not been decomposed completely. On the other hand, AACH powder which was calcined for long time (e.g. 2h) contains large α -alumina particles. This result suggests that the sintering process progresses steadily, but slowly. Furthermore, by comparing the products obtained from the calcinations starting at room temperature to those put into the furnace at high temperature, it is found that particle size of the former is larger than the latter. The results confirm that the significant sintering takes place during long period of heating up. SEM images in Figure 4.10 show that morphology of the powder obtained from these two calcination approaches are quite different. Hard agglomerate by sintering can be seen from the calcination starting from room temperature, while calcination with sudden increase in temperature results in less sintering.



(a)

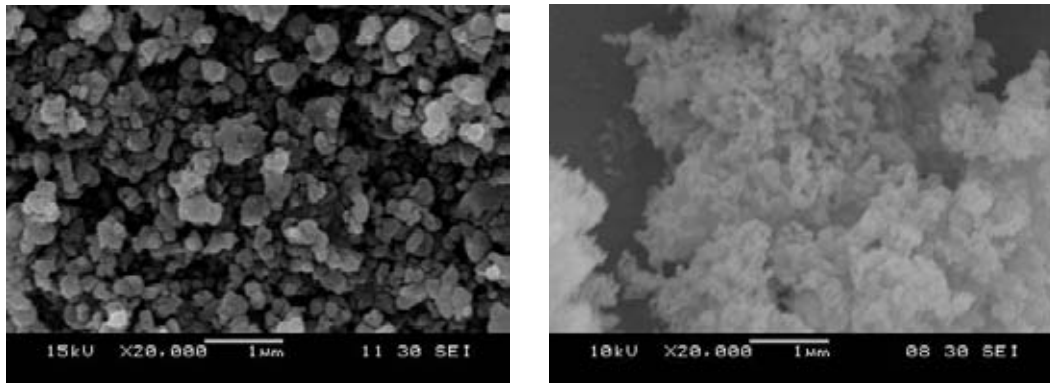


(b)

Figure 4.9 Particle size distributions of products from calcination of AACH at 1200°C for various holding time:

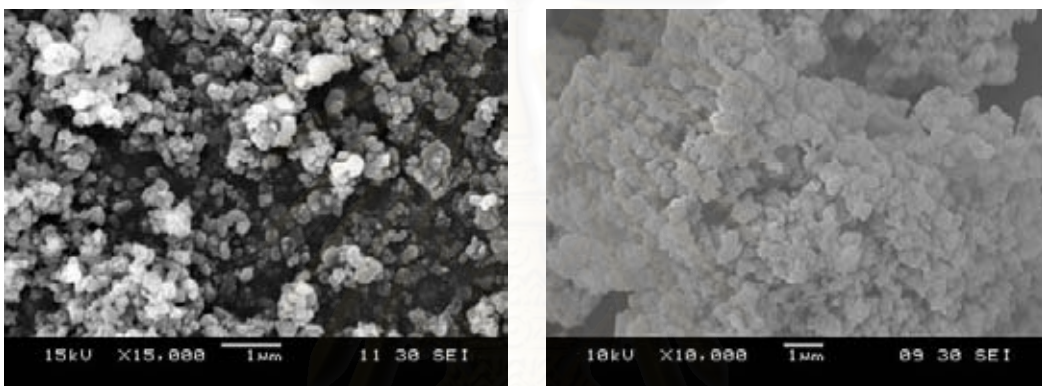
(a) The samples are heated up from room temperature.

(b) The samples are put into a furnace at temperature is around 1100°C.



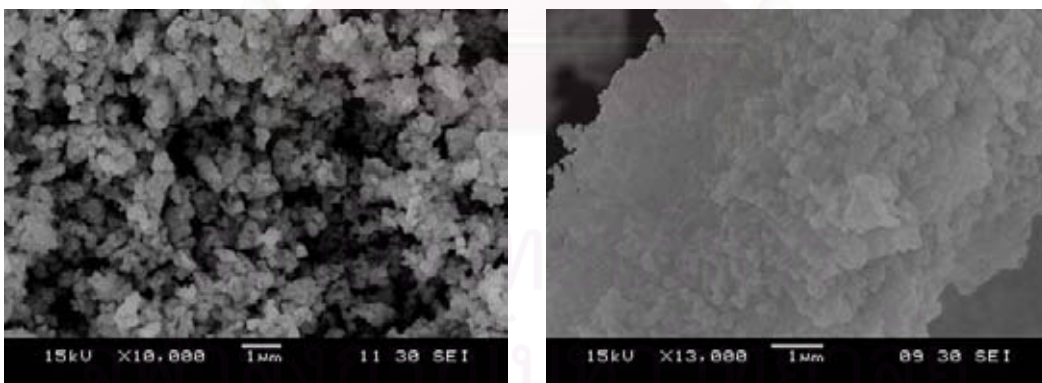
(a)

(b)

held at 1200⁰C for 10 min

(a)

(b)

held at 1200⁰C for 30 min

(a)

(b)

held at 1200⁰C for 2h.

Figure 4.10 SEM micrographs of products obtain from calcination of AACH by different approaches:

- (a) The samples were put into a furnace at high temperature.
- (b) The samples were calcined starting from room temperature.

Next, the calcined powder was fabricated into specimens, according to the procedures described in the previous chapter. Density of the powder and the specimen was measured in every step along the process and shown in Figure 4.11-4.16.

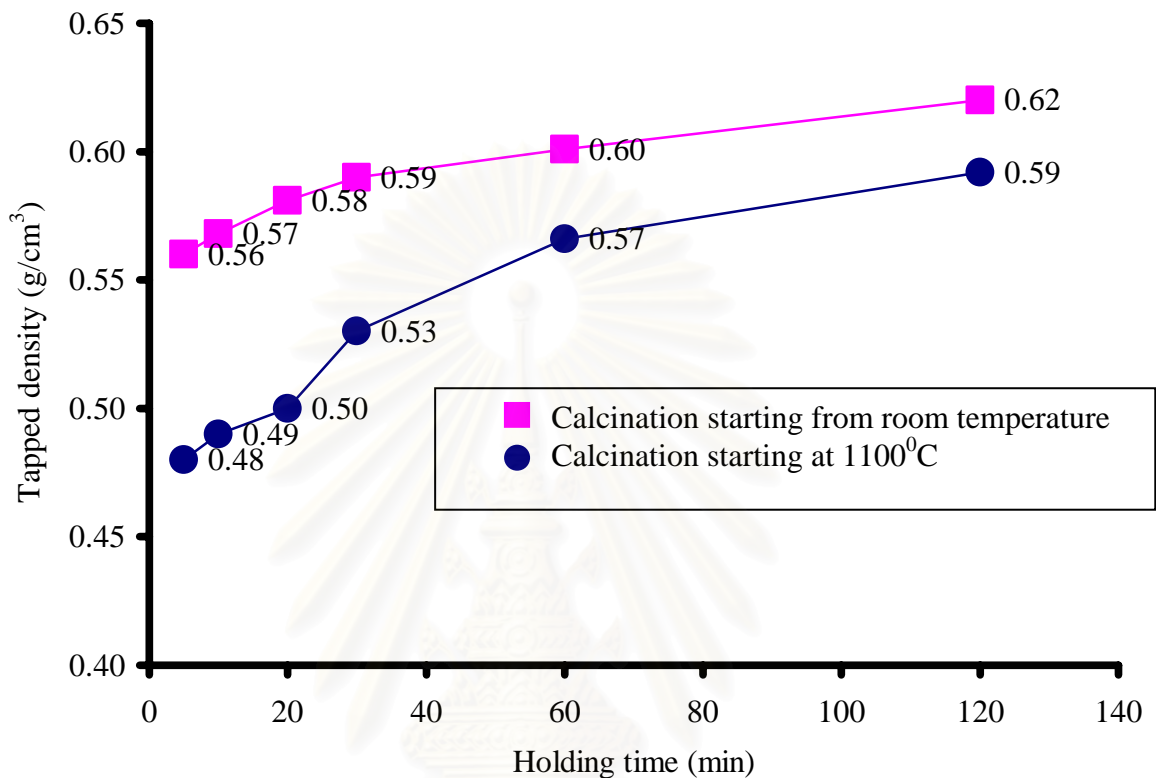


Figure 4.11 Correlation between tapped density of AACH after calcination and holding time at 1200°C.

In Figure 4.11, it can be described that tapped density of powder would increase when holding time of the calcination is prolonged. AACH will have enough time to complete the transformation to α -alumina, which has high density, and grain growth also helps increasing density (Levin et al., 1998). Moreover, it is found that long period of time for ramping up the temperature to phase transformation temperature (1200°C) would help increasing the tapped density of the powder. Although using long time to calcine AACH causes pores in the secondary particles, as already shown by TEM images in Figure 4.7, the increase in grain size has more effect toward the increase in tapped density. After the powder was pressed by biaxial pressing, it can be observed from Figure 4.12 that according to holding time, which is too long, does not help increasing green bodies. According to Figure 4.12 and 4.13, it can be described that pores remaining in the secondary particles of the

calcined powder, has effect after pressing pressure on the powder to form the green bodies. It should be noted that the green body fabricated from the powder calcined at 1200 °C for only 20 minutes, has the lowest density because it has not been completely transformed to α -alumina, as previously shown in XRD pattern in Figure 4.7.

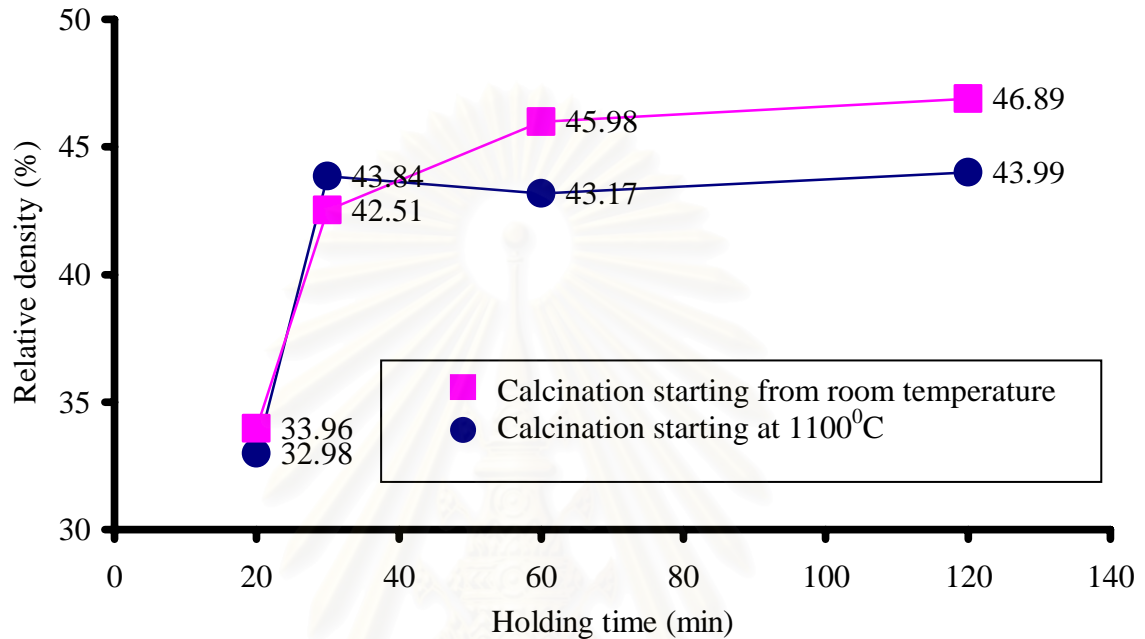


Figure 4.12 Correlation between green body density after biaxial pressing at 20 MPa and holding time at 1200°C for AACH calcination.

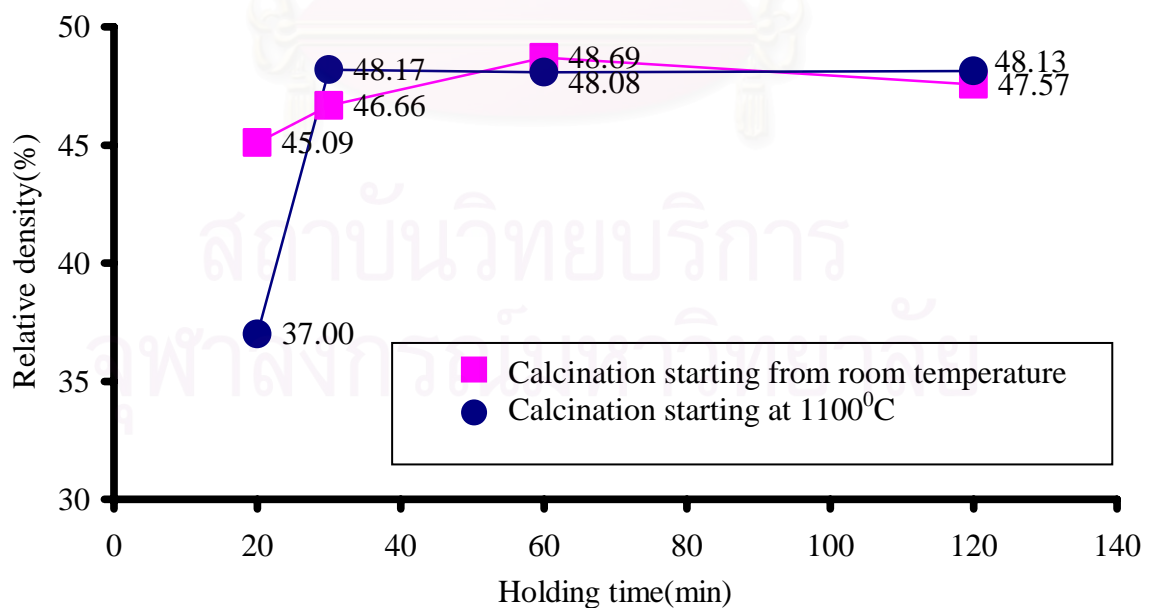


Figure 4.13 Correlation between green body density after CIP at 300 MPa and holding time at 1200°C for AACH calcination.

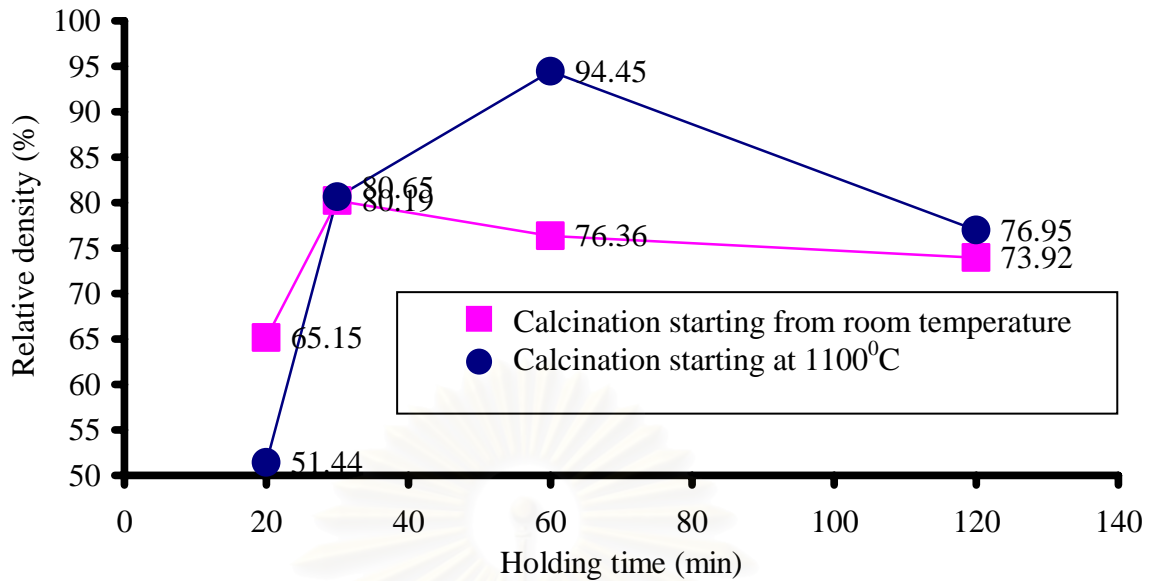


Figure 4.14 Correlation between density of specimen after sintering at 1350°C and holding time at 1200°C for AACH calcination.

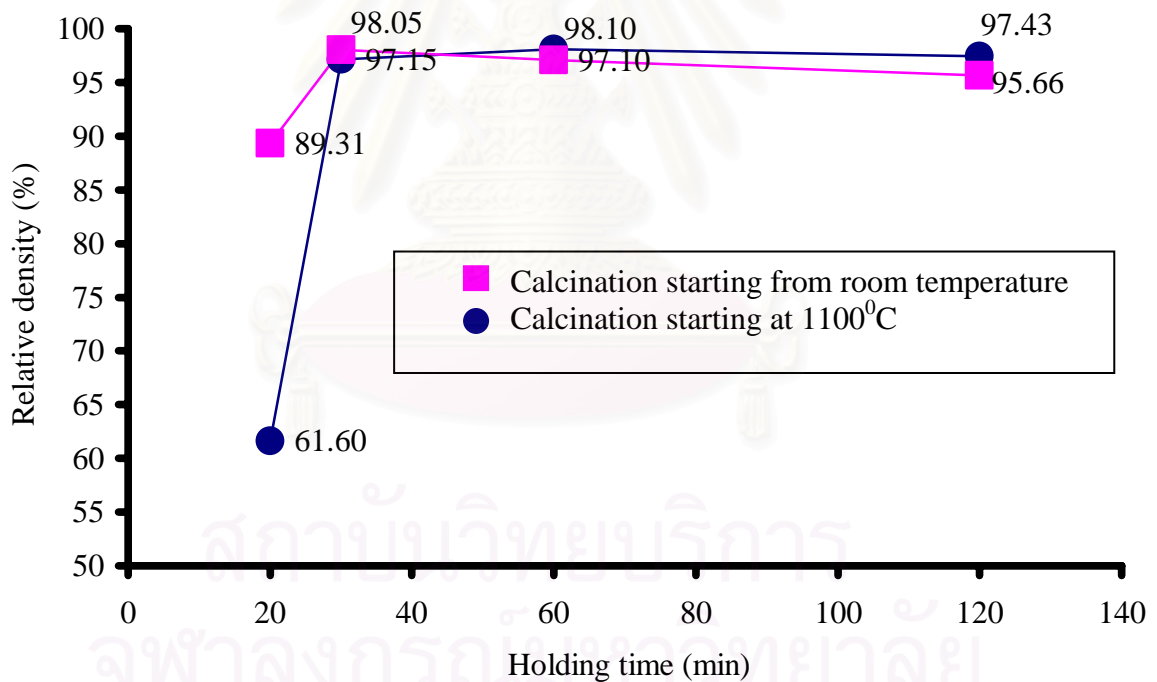


Figure 4.15 Correlation between density of specimen after sintering at 1500°C and holding time at 1200°C for AACH calcination.

In Figure 4.14 and 4.15, density of specimens after sintering at 1350°C and 1500°C, respectively, are shown. It can be seen that the green body which was at 1200 °C for only 20 minutes, has very low density. It can also be observed that the specimen, which was fabricated from the powder calcined by without temperature

ramping, would get higher density than that formed from powder calcined from room temperature, especially after low-temperature sintering. The highest density of the specimen is obtained from the powder prepared by sudden calcination and hold at 1200 °C for 1 h.

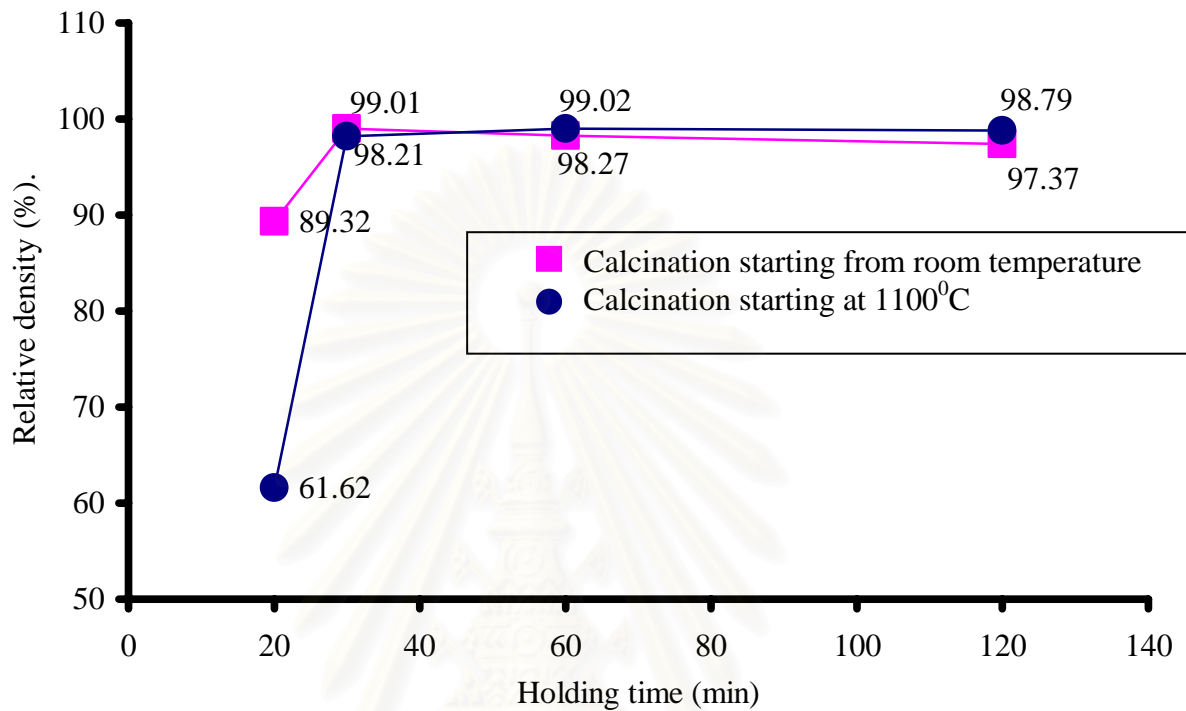


Figure 4.16 Correlation between density of specimen after HIP at 1350°C and 300 MPa for 1h and holding time at 1200°C for AACH calcination.

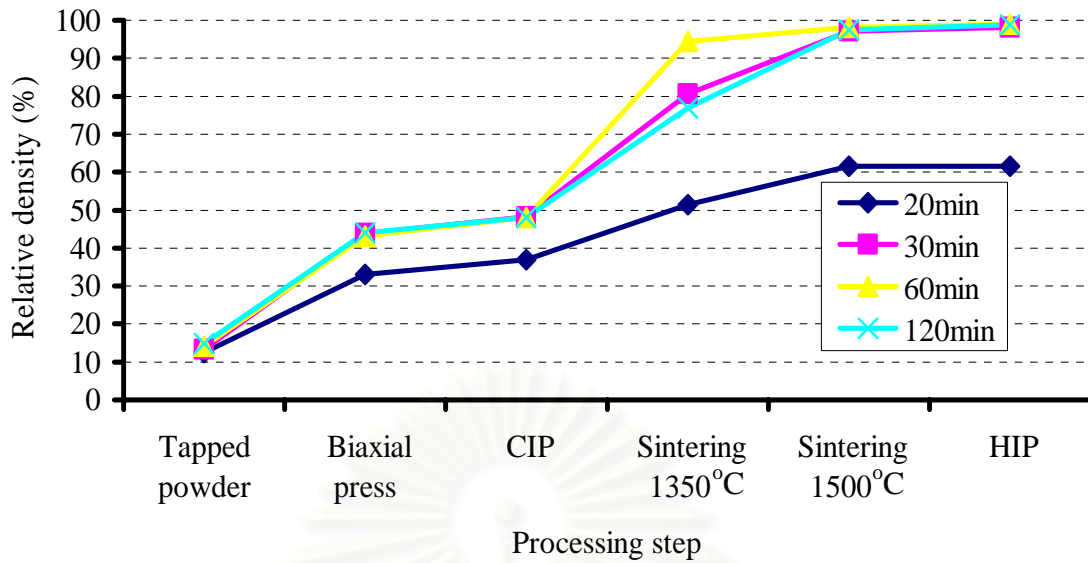


Figure 4.17 Progress of density change for specimens fabricated from powder calcined by putting AACH into the furnace at 1100°C and held at 1200°C for various periods of time.

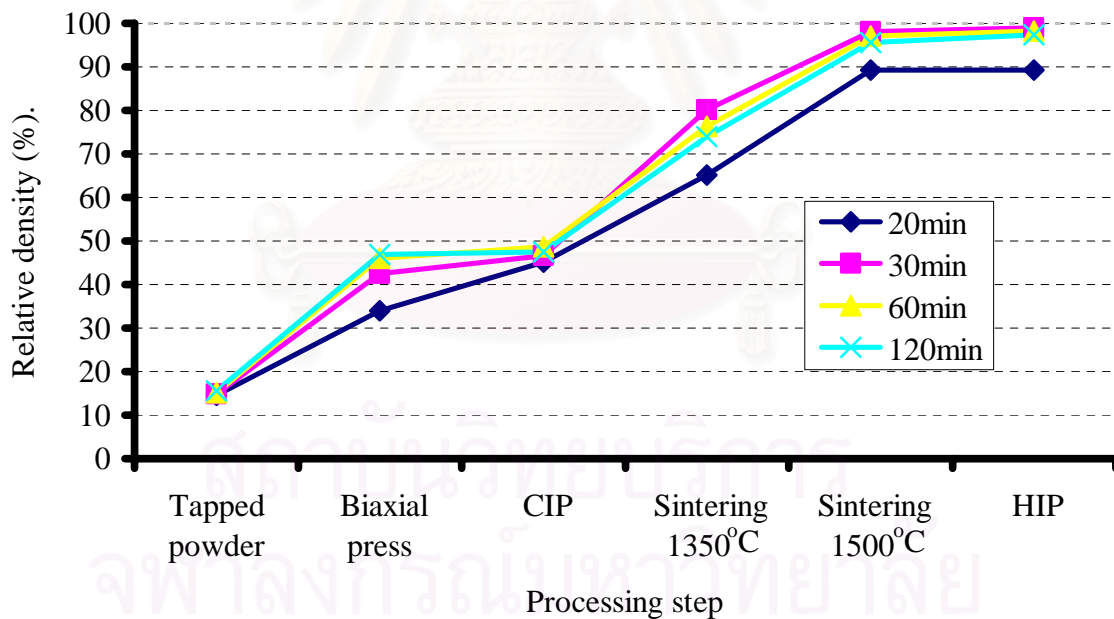


Figure 4.18 Progress of density change for specimens fabricated from powder calcined with temperature ramping up and held at 1200°C for various periods of time.

According to Figure 4.16, it is shown that HIP process can help making the specimen denser. Nevertheless, the correlation between calcination time and specimen density after HIP is similar to that shown in Figure 4.15. Summary for the change in density of the specimen along the fabrication process is given in Figure 4.17 and 4.18.

Figure 4.17 and Figure 4.18 show that density of the specimen would increase along the fabrication processes. HIP process can further increase the density of the specimens only when the relative density before HIP is higher than 95% because the specimen which has density lower than 95% would have a lot of open pores, which HIP process cannot eliminate. On the contrary the specimen with the relative density higher than 95% would have close pores, which can be eliminated by high pressure and high temperature of the HIP process (Rankin et al, 1971).

SEM images in Figure 4.19 show that the specimen, which was fabricated from α -alumina powder synthesized by no ramping temperature, has smaller grains inside the specimen (around 0.54 μm) than the specimen fabricated from α -alumina powder synthesized by ramping temperature (around 1.46 μm).

UV/Visible spectrophotometry micrographs in Figure 4.20 which compare specimen which was fabricated from α -alumina powder synthesized by difference calcination approaches and varied time. It show that specimen which was fabricated from α -alumina powder obtained from no ramping temperature and held for 1 h is highest transmittance when was compare with the specimens obtained from the other synthesized powder. Moreover, the specimen fabricated from α -alumina powder obtained from no ramping temperature would bring in higher transmittance than the specimen fabricated from α -alumina powder obtained from ramping temperature.

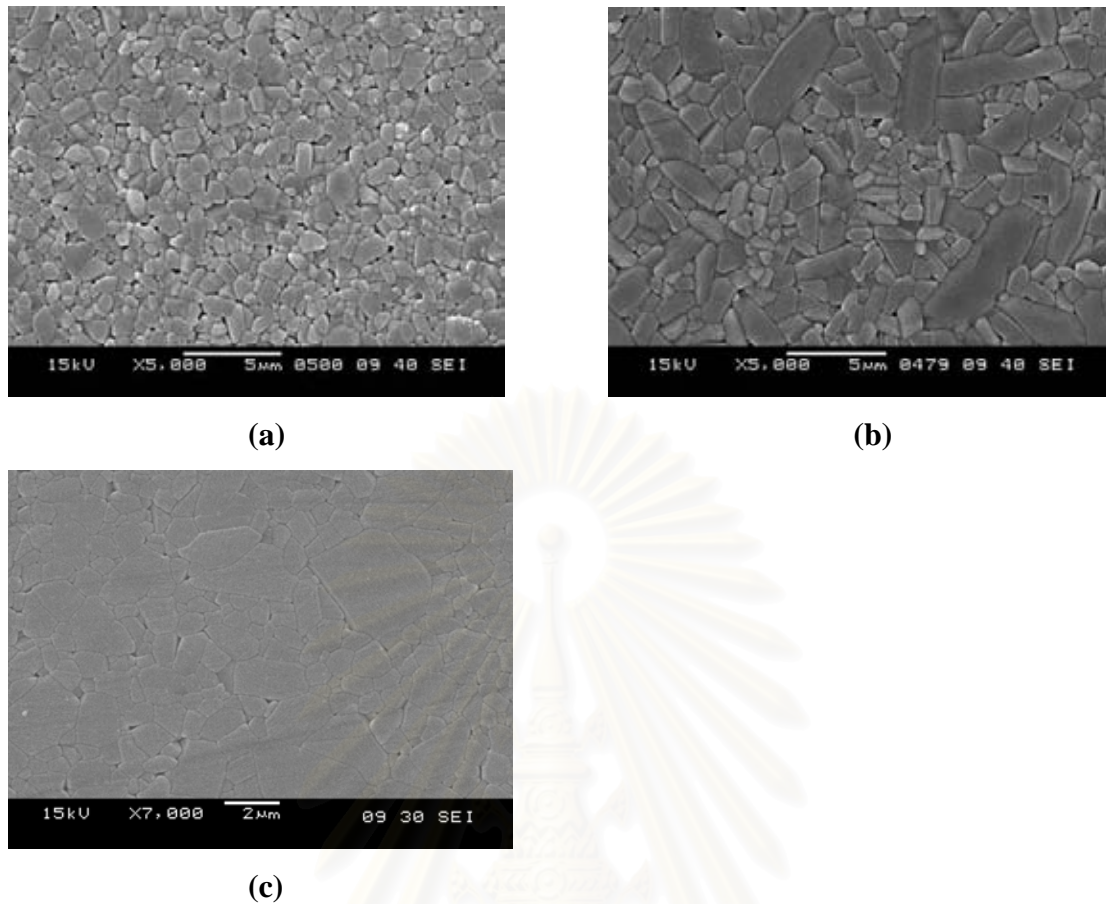


Figure 4.19 SEM micrographs of the specimen fabricated from:

- (a) No ramping & held at $1,200^{\circ}\text{C}$ for 60 min , Average grain size= $0.54\mu\text{m}$
- (b) Ramping & held at $1,200^{\circ}\text{C}$ for 30 min , Average grain size= $1.46\mu\text{m}$
- (c) Ramping & held at $1,200^{\circ}\text{C}$ for 30 min (Normal routine), Average grain size= $1.67\mu\text{m}$

สถาบันวิทยบริการ
จุฬาลงกรณ์มหาวิทยาลัย

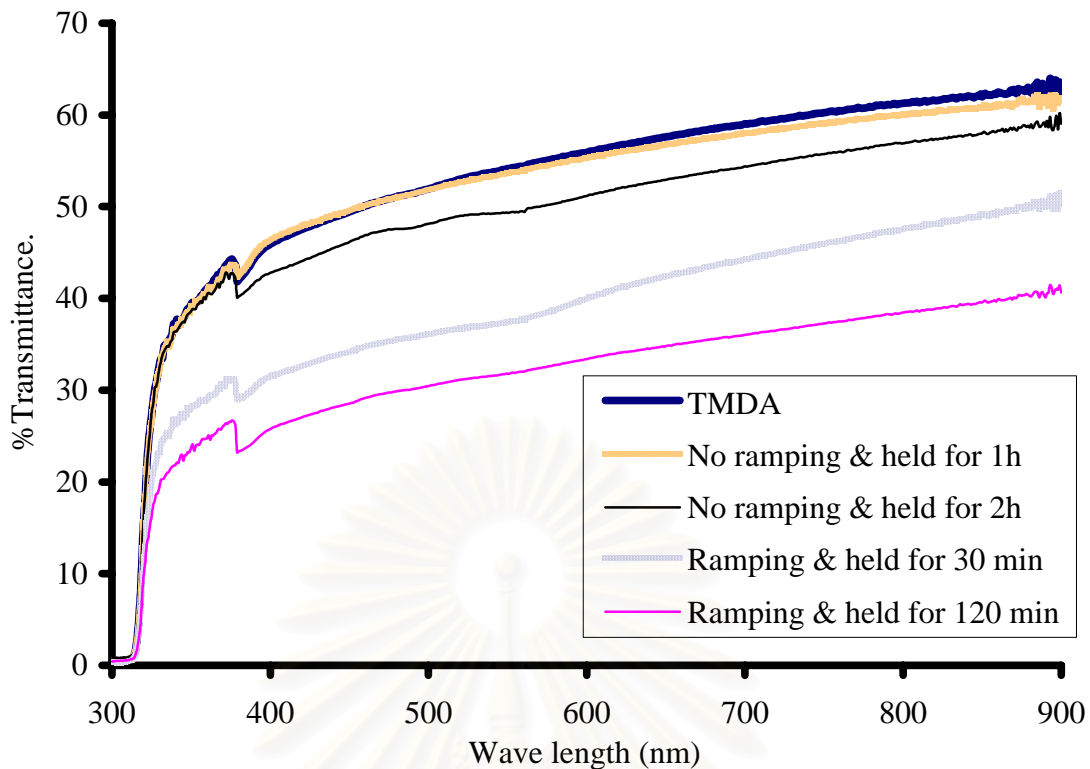
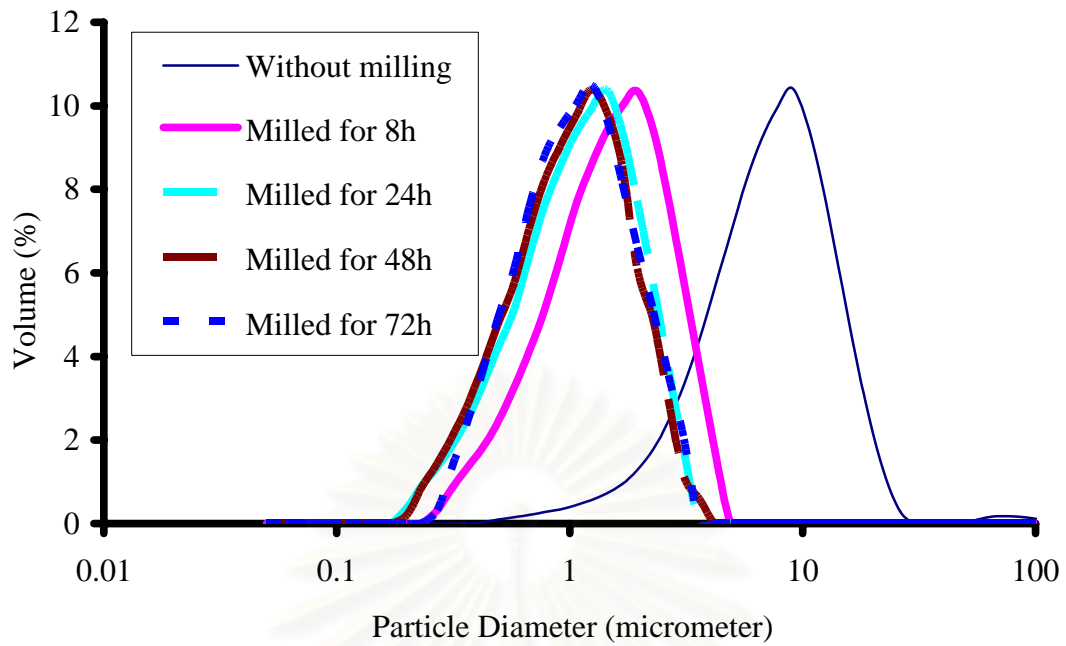


Figure 4.20 UV/Visible spectrophotometry micrographs of the specimen fabricated from: TMDA powder, α -alumina powder synthesized by normal precipitation procedure and α -alumina powder varied AACH calcination time.

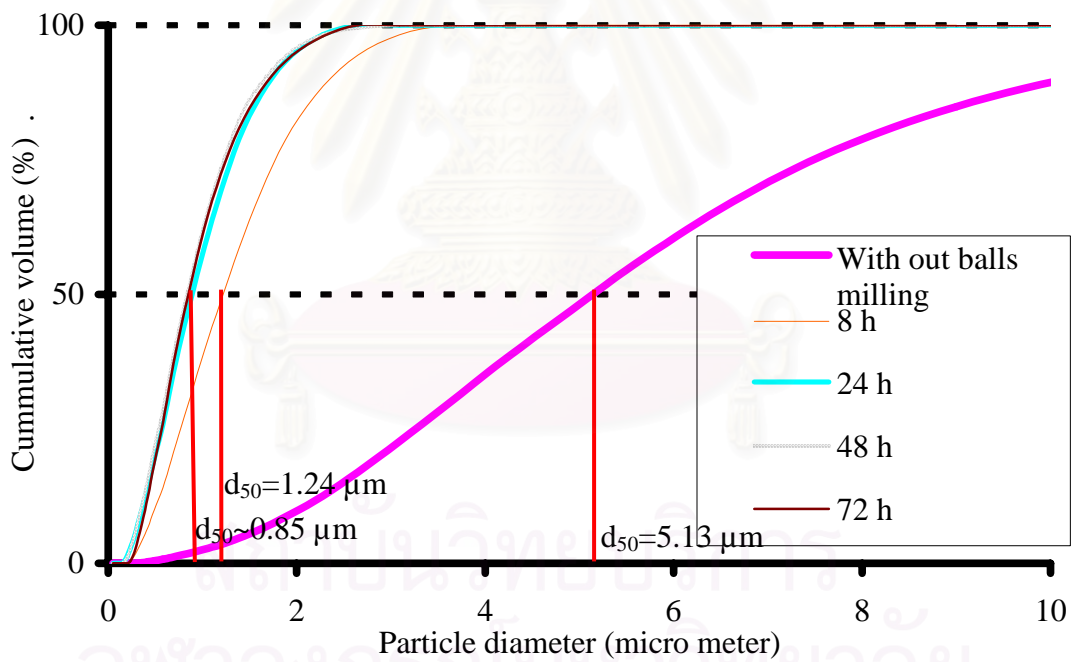
4.3) Effect of AACH Milling on Synthesized Alumina

Kyoung et al. (2000) studied preparation method of submicrometer-size α -alumina from γ -alumina. The almost-spherical and small α -alumina was obtained by milling γ -alumina with the presence of 3 wt% of alumina sol, followed by heat treatment. In this research, milling of AACH powder before calcination was concerned, since, it has been speculated that large α -alumina particles may be produced from large AACH particles.

AACH powder was milled by balls milling for 8, 24, 48 and 72 h. Particle size distribution of the obtained powder was measured in the same manner as the procedure described previously. The particle size distribution results are shown in Figure 4.21. It is shown that milling by balls mill can significantly reduce size of AACH particles, even after only 8 h of milling. Particle size of AACH powder is reduced from 5.1 μm to 0.8 μm within 24 h of milling.



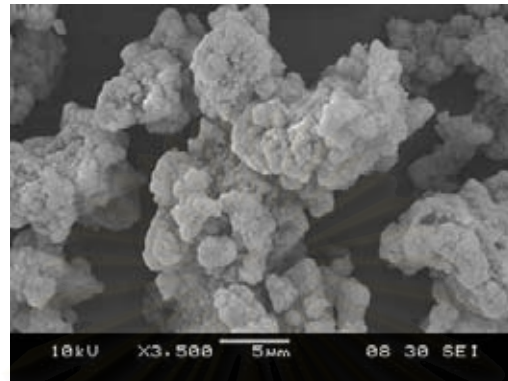
(a)



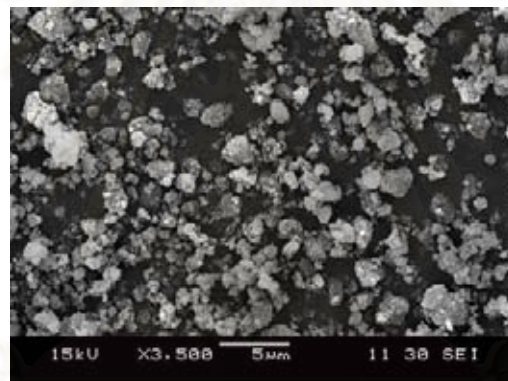
(b)

Figure 4.21 Particle size distributions of AACH powder after milling for various period of time. particle size distribution (a), cumulative particle size distribution (b).

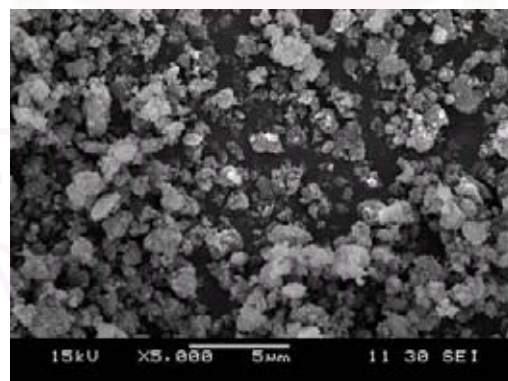
SEM images in Figure 4.22 show AACH powder after milling for various period of time. It confirms that AACH agglomerates can be broken milling and the size of AACH particles is decreased, as clearly evidenced from SEM images that AACH powder without milling is much larger than the particle after milling.



(a)



(b)



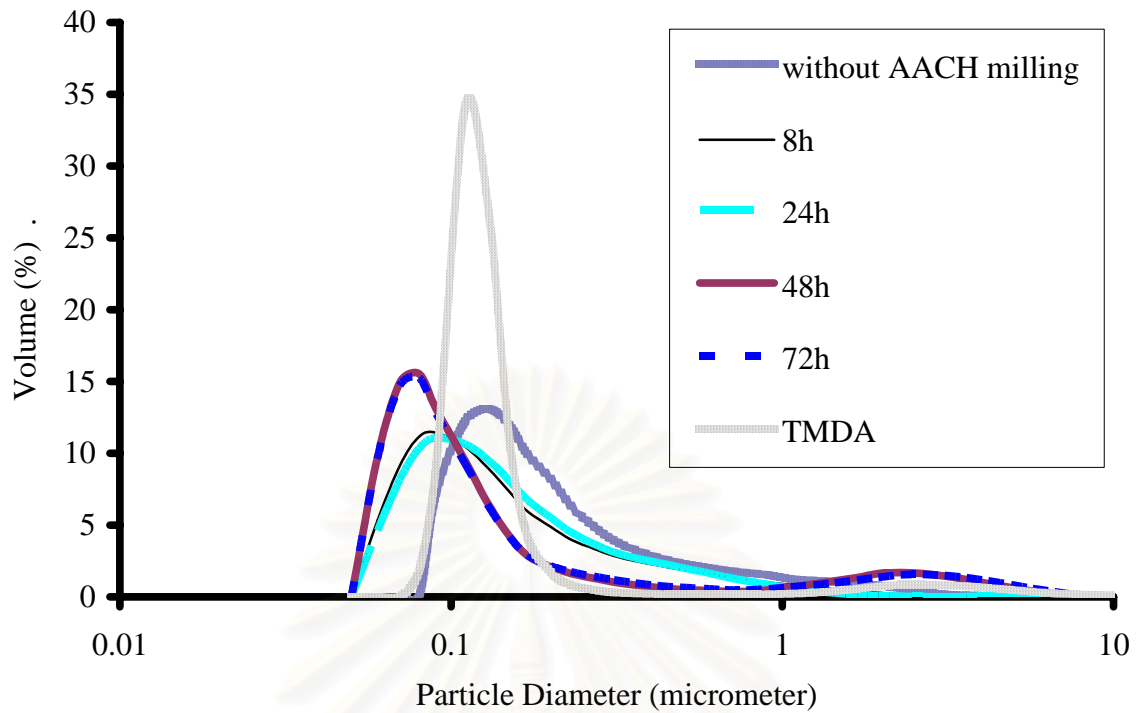
(c)

Figure 4.22 SEM image of AACH powder which varied time of milling:

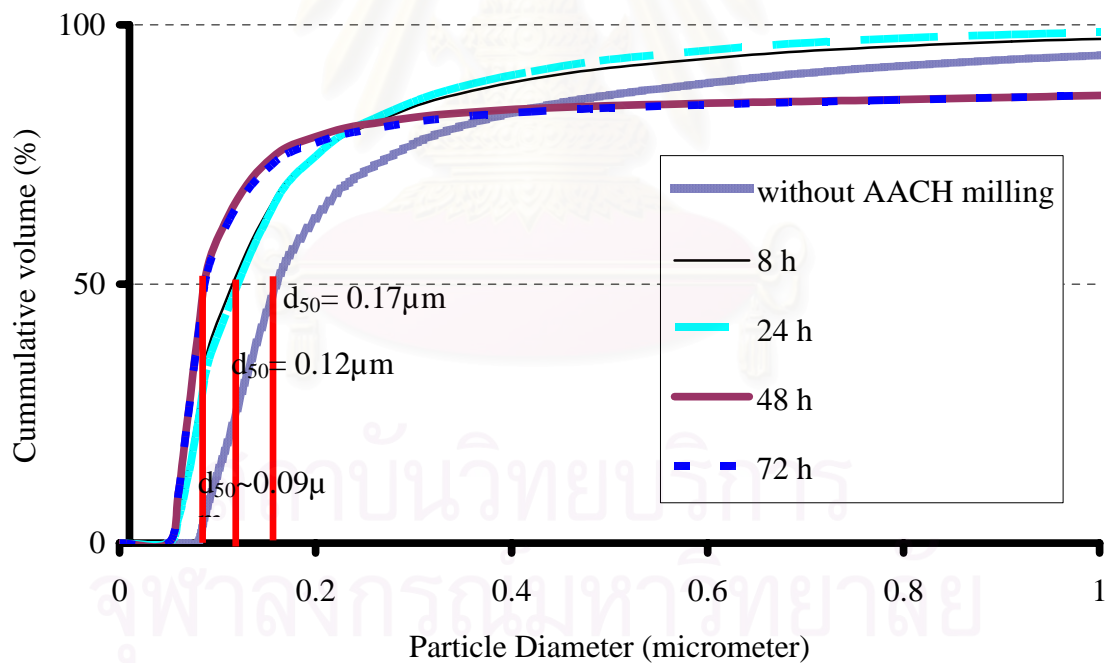
- (a) AACH with out balls milling, (b) AACH milled for 8 h and
- (c) AACH milled for 72 h

After the milling AACH was calcined in the same manner as the normal routine (i.e. calcination at 1200⁰C for 2 h, by heating the sample up from room temperature) in order to transforming to α -alumina. Particle size distribution of the obtained alumina powder was measured and compared with TMDA powder, as well as, alumina prepared without the step of AACH milling. Their size distributions are shown in the Figure 4.23. It is confirmed that the smaller AACH particles would result in smaller alumina particles. SEM images of the synthesized alumina in Figure 4.24 show that AACH milling before calcination can help decreasing agglomerates in the obtained α -alumina powder. Moreover, according to Figure 4.25 which shows tapped density of AACH before and after calcination, it is indicated that milling of AACH powder can result in an increase in tapped density of both milled AACH powder and the alumina powder obtained after calcination.





(a)

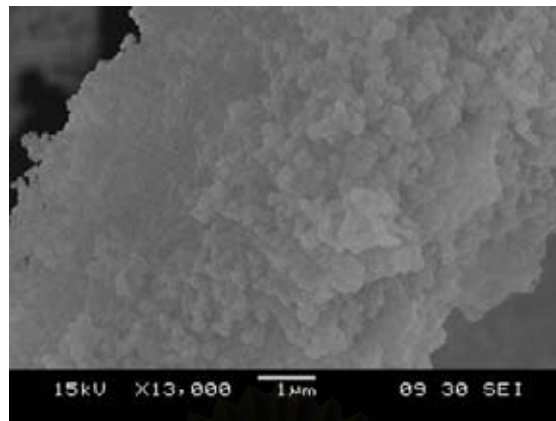


(b)

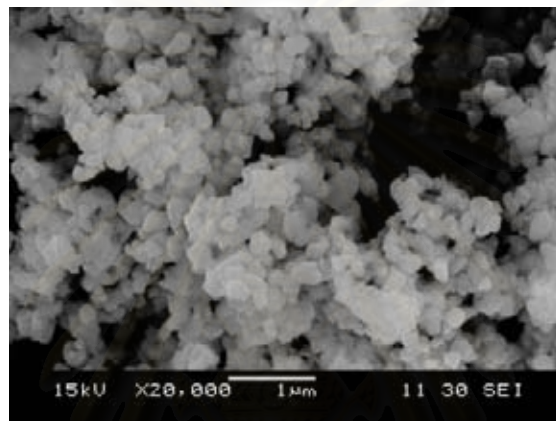
Figure 4.23 Particle size distributions of alumina powder obtained from AACH that was milled for various periods of time:

(a) particle size distribution

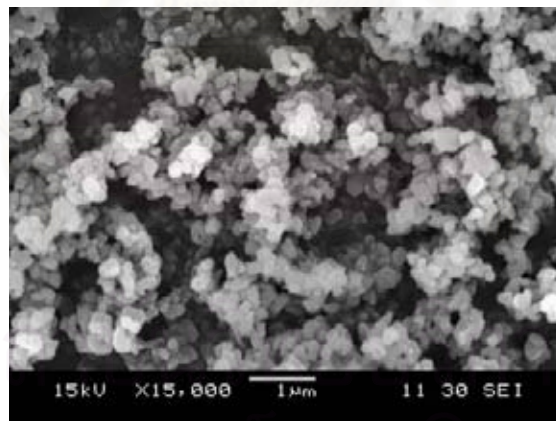
(b) cumulative particle size distribution



(a)



(b)



(c)

Figure 4.24 SEM images of alumina powder obtained from

AACH that was milled for various periods of time:

- (a) Alumina obtained from unmilled AACH
- (b) Alumina obtained from AACH milled for 8h
- (c) Alumina obtained from AACH milled for 48h

Then, the calcined powder was fabricated into alumina specimen, according to the same procedure described earlier. Density of the specimen was monitored along the procedure. These densities are shown in Figure 4.26- 4.27 which show that AACH milling would help the obtained specimen more density.

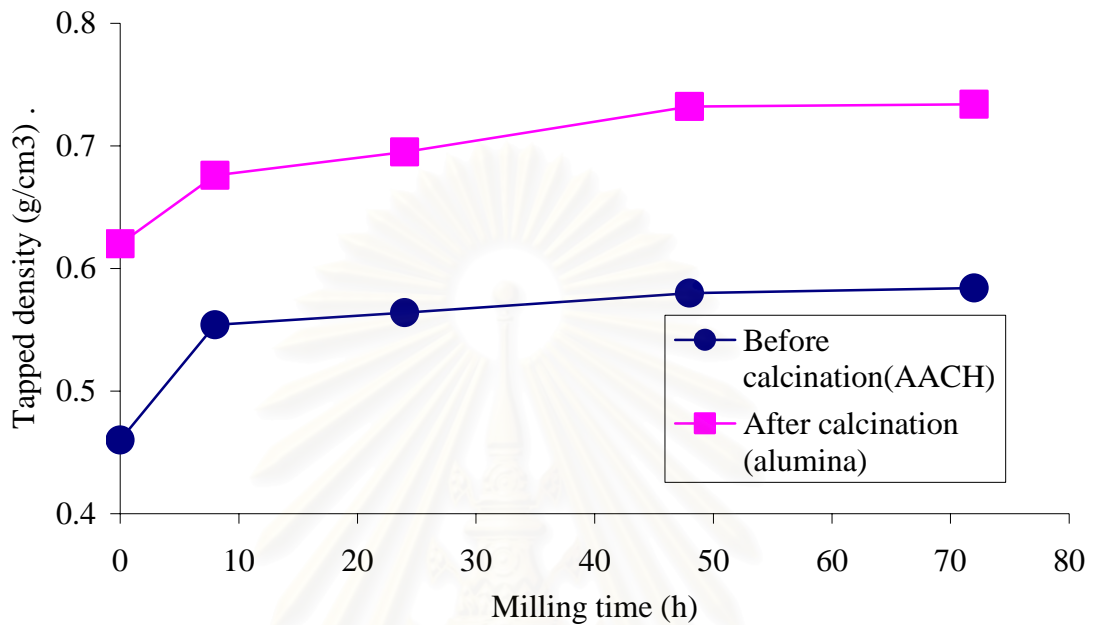


Figure 4.25 Correlation between tapped density of AACH before and after calcination, and milling time for AACH powder.

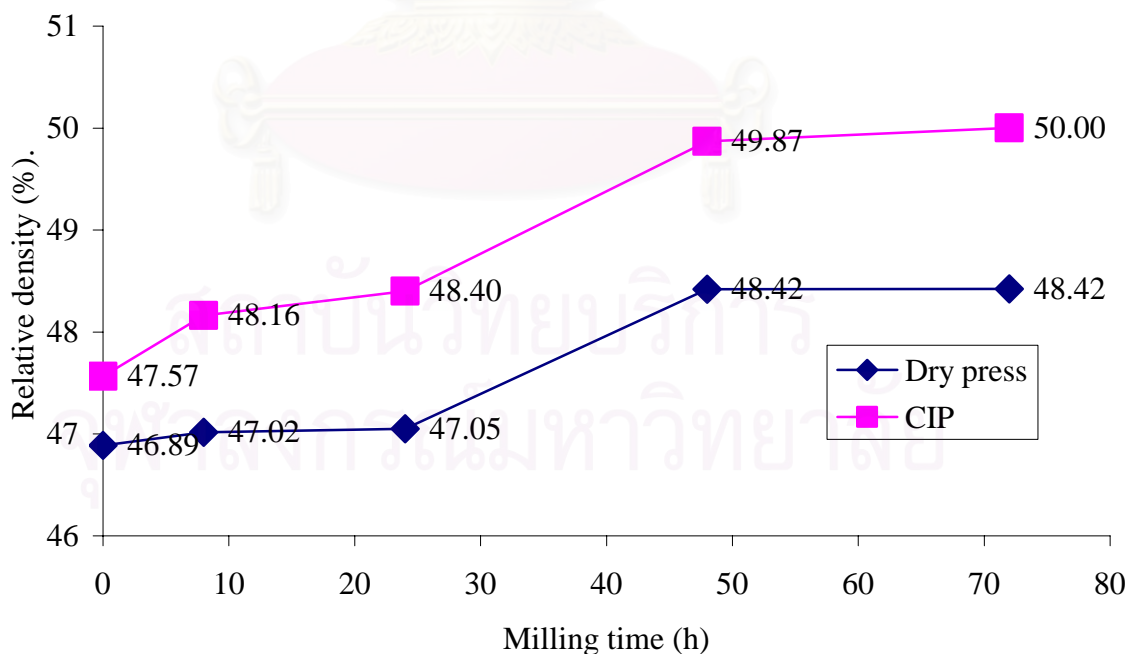


Figure 4.26 Correlation between densities of specimens after biaxial pressing and cold isostatic pressing and milling time for AACH powder.

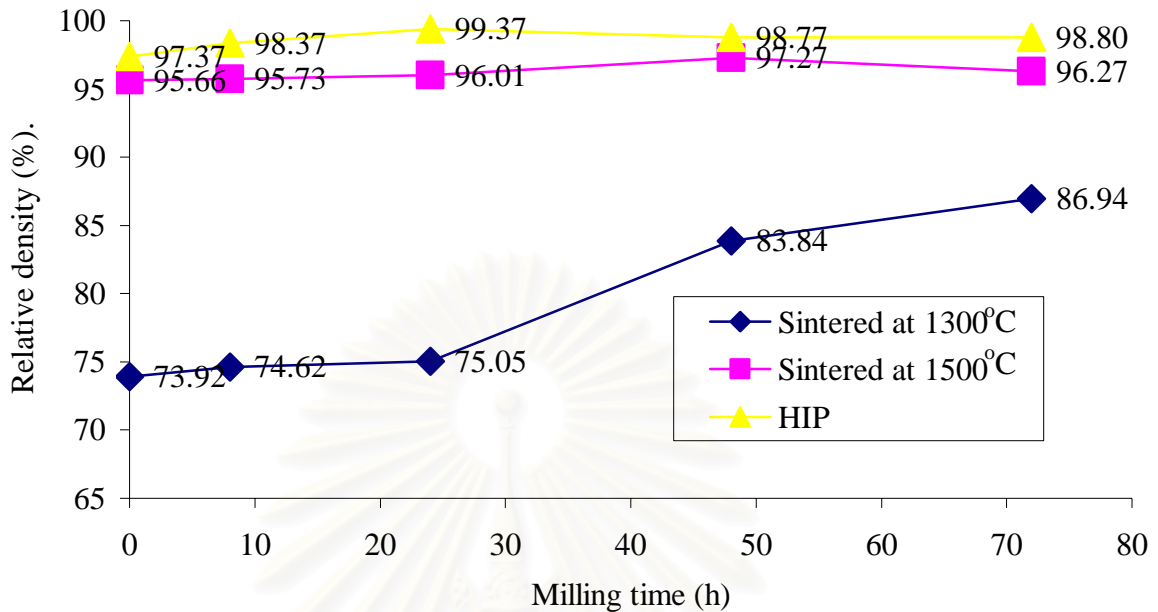


Figure 4.27 Correlation between density of specimens after sintering and hot isostatic pressing and milling time for AACH powder.

SEM images in Figure 4.28 show that the specimen, which was fabricated from α -alumina powder synthesized by no ramping temperature, has smaller grains inside the specimen (around 0.54 μm) than the specimen fabricated from α -alumina powder synthesized by ramping temperature (around 1.46 μm).

UV/Visible spectrophotometry results in Figure 4.29 which compare the specimen which was fabricated from α -alumina powder obtained from unmilled AACH with the specimen which was fabricated from α -alumina powder obtained from milled AACH. It shows that specimen which was fabricated from α -alumina powder obtained from the milled AACH has higher transmittance when was compare with the specimens obtained from the unmilled AACH.

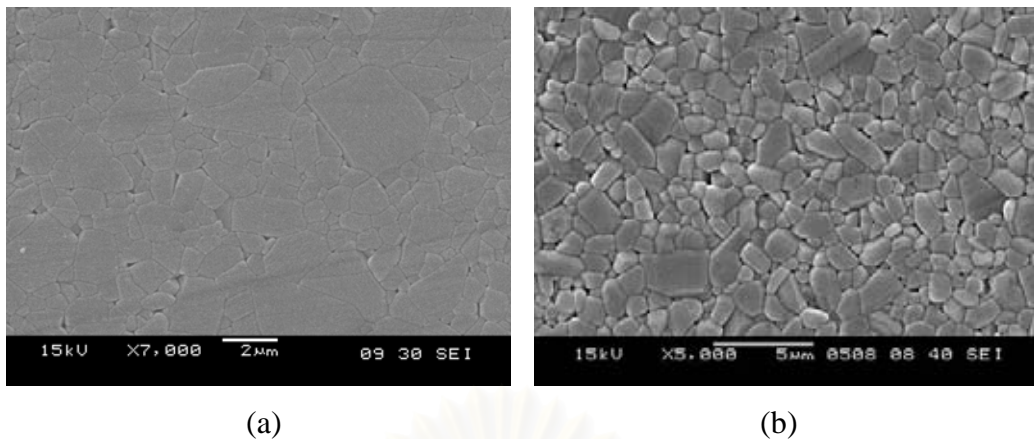


Figure 4.28 SEM micrographs of the specimen fabricated from:

- (a) Unmilled AACH (Normal routine), Average grain size= $1.67\mu\text{m}$
- (b) AACH milled for 24 h, Average grain size= $1.46\mu\text{m}$

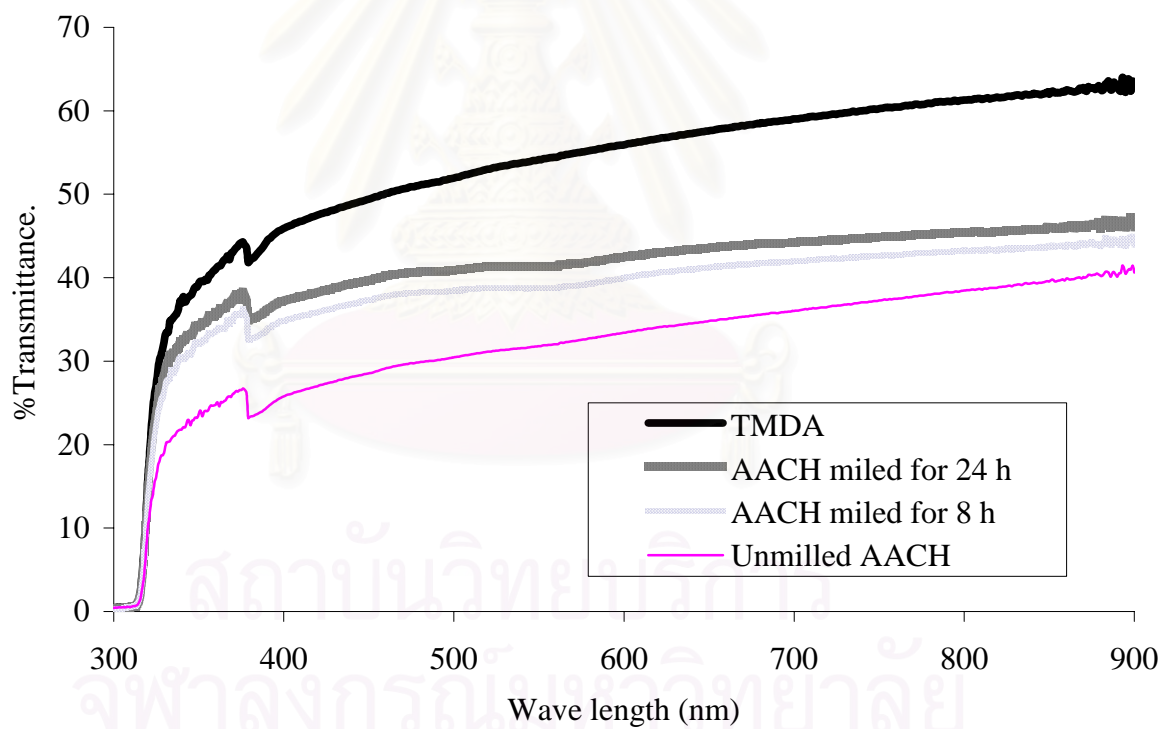


Figure 4.29 UV/Visible spectrophotometry micrographs of the specimen fabricated from: TMDA powder, α -alumina powder synthesized by normal precipitation procedure and α -alumina powder prepared from AACH milled for varying time.

4.4) AACH Surface Modification

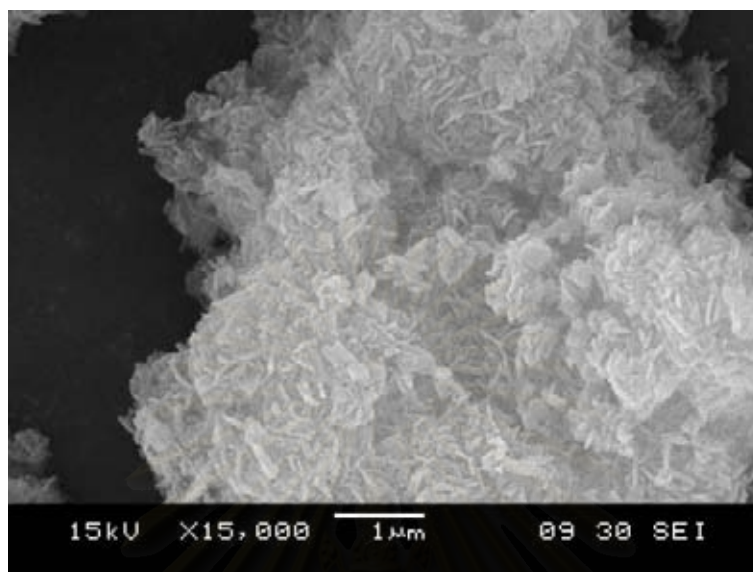
Surfactants can help the dispersion of solid metal oxide particles by means of steric hindrance and electrostatic repulsion (Esumi 2001). This idea was adapted to modify the surface of AACH before calcinations, in order to reduce the agglomeration in the obtained alumina powder. Adjusting pH in the solution is another method to disperse metal oxide particles the solution, since pH directly affects the surface charges on the surface of metal oxide particles, which consequently affects the agglomeration of the particles (Cao, 1998).

In this research, PVA (polyvinyl alcohol) was used to modify the surface while AACH, acetic acid and high molecular weight acid, i.e. oleic acid, was used to adjust pH of the solution. All of the modifying substances used are able to be removed from the alumina simply by combustion and they do not remain as impurity in the specimen.

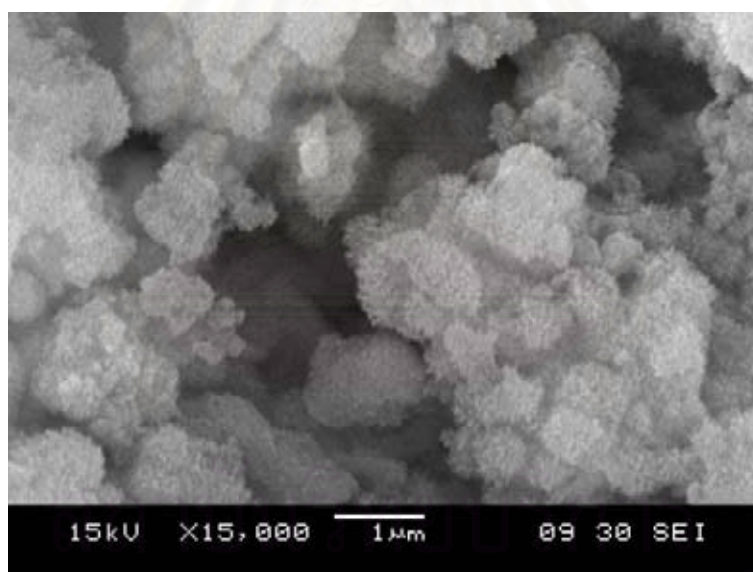
In this method, the modifying substance was added to the solution according to the procedures described in the previous chapter. The obtained AACH powder was calcined by normal procedure. Figure 4.30 shows morphology of AACH which was modified with oleic acid and PVA. It shows that the morphology of the obtained AACH was quite different from the unmodified AACH.

After the AACH was modified, it was calcined by normal procedure to get α alumina. Table 4.2 shows tapped density of the obtained α -alumina, in which it can be observed that the density is not higher than that of alumina produced without surface modification. Figure 4.31 shows morphology of the obtained alumina powder after calcination. It can be observed that the powder still has lots of hard agglomeration. Since the surface modification of AACH does not help preventing agglomerate in particles, it is expected that modifying substance has been burned out from the AACH before the sintering was occurred. Because all modifying substance would be burned out at lower temperature than sintering temperature and phase transformation temperature. Thermal gravity analysis shown in Figure 4.32 confirms that oleic acid and PVA were completely burned out before 800⁰C. This temperature is much lower

than the sintering temperature of alumina, which is around 1,100°C. (Himanshu Jain et al, 1989)

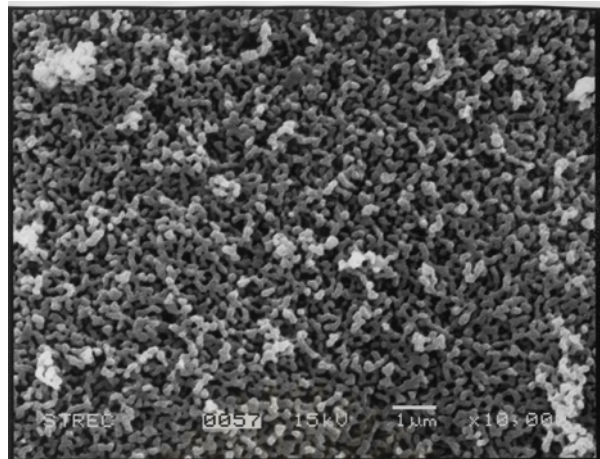


(a)

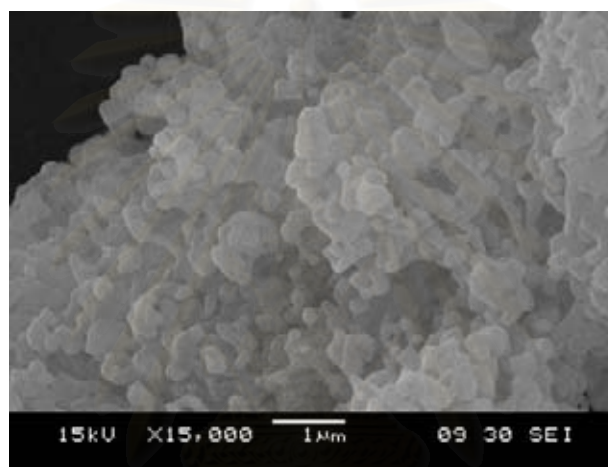


(b)

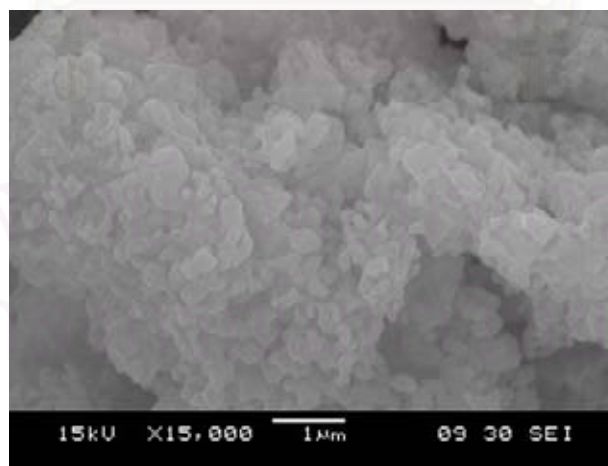
Figure 4.30 SEM micrographs of AACH modified with PVA(a) and oleic acid(b)



(a)



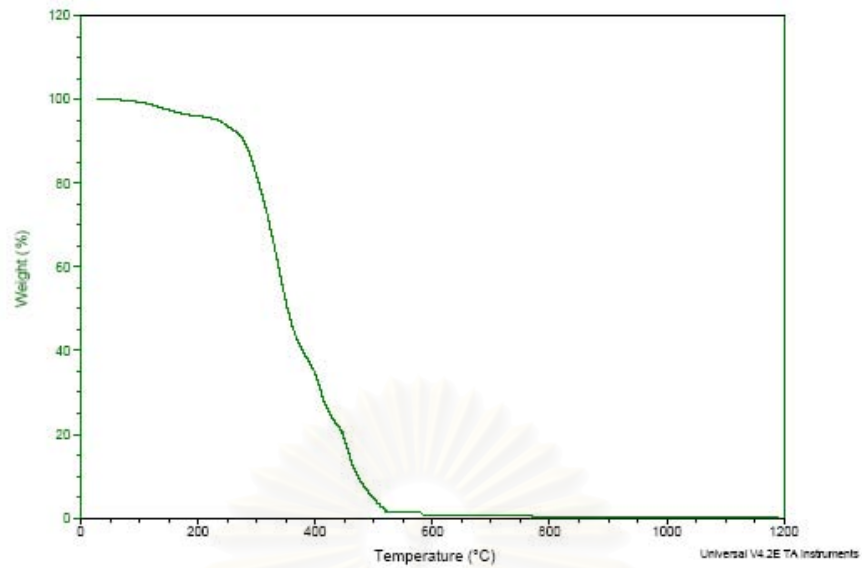
(b)



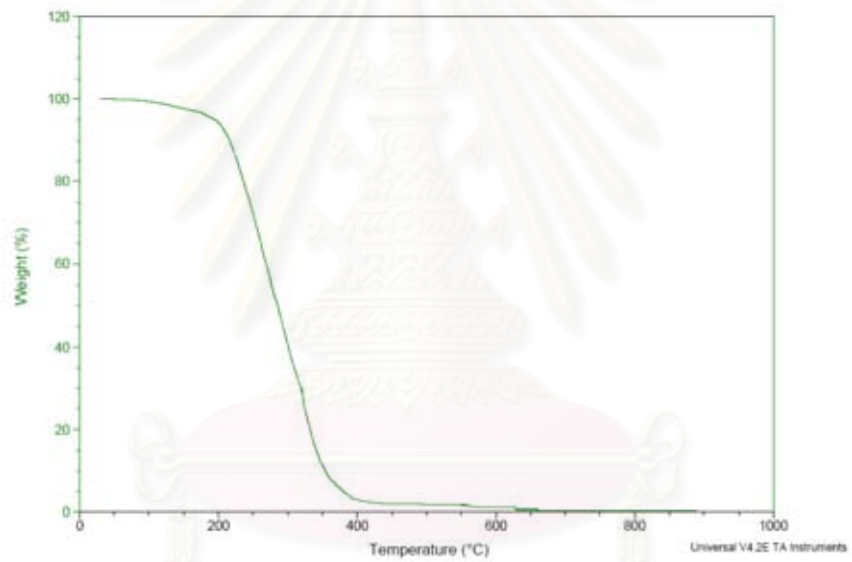
(c)

Figure 4.31 SEM micrographs of alumina powder obtained from calcination of:

- (a) PVA modified AACH.
- (b) Oleic acid modified AACH.
- (c) Acetic acid modified AACH.



(a)



(b)

Figure 4.32 TG-DTA curves of (a) PVA and (b) Oleic acid,

Although the obtained α - alumina powder dose not have good properties, regarding its morphology, it was still used to fabricate alumina specimen. Density of the specimen was observed along the fabrication step. The results are shown in Table 4.2 and compared with that of α - alumina powder obtained without surface modification. It can be observed that modifying AACH by organic substance could not bring about a high-density specimen.

Table 4.2 Density of the specimen fabricated from alumina powder synthesized with AACH surface modification.

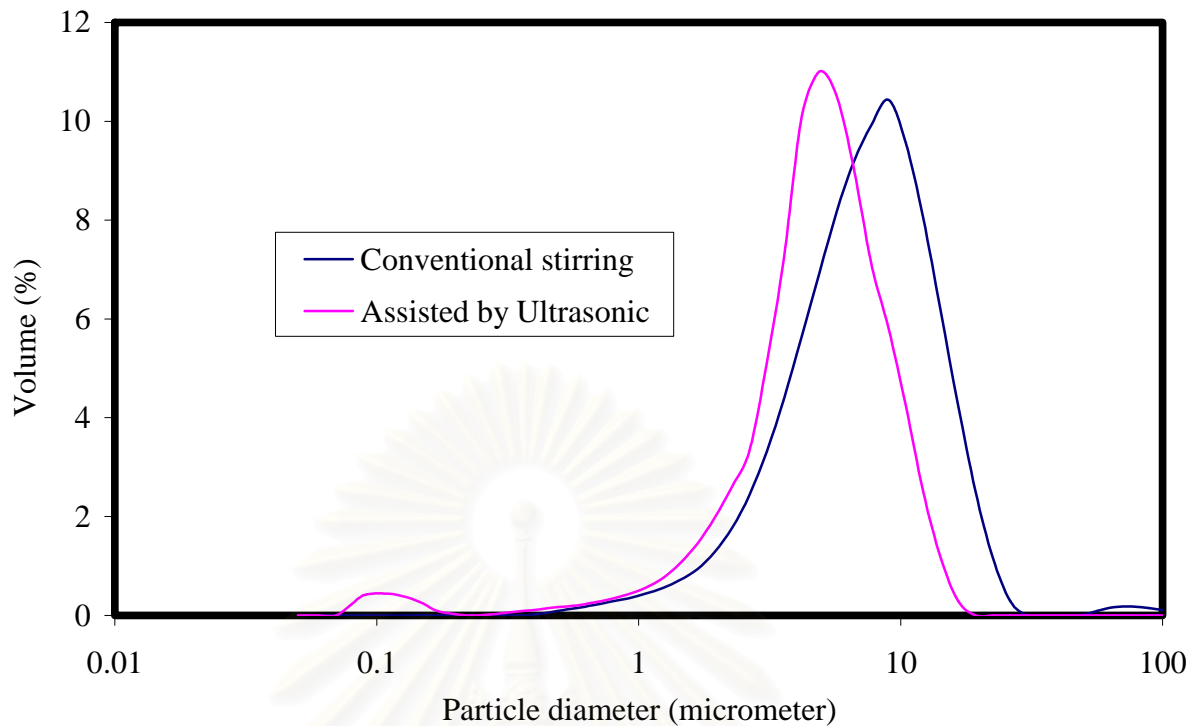
Modifying substance	Tapped density of the obtained alumina powder (g/cm ³)	Relative density of specimen after sintering at 1300°C (%)	Relative density of specimen after sintering at 1500°C (%)	Relative density of HIP specimen (%)
-	0.62	73.9	95.6	97.4
PVA	0.39	72.4	96.3	97.2
Oleic	0.62	73.1	95.8	97.0
Acetic acid	0.66	76.4	97.2	97.5

4.5) Precipitation Assisted by Ultrasonic

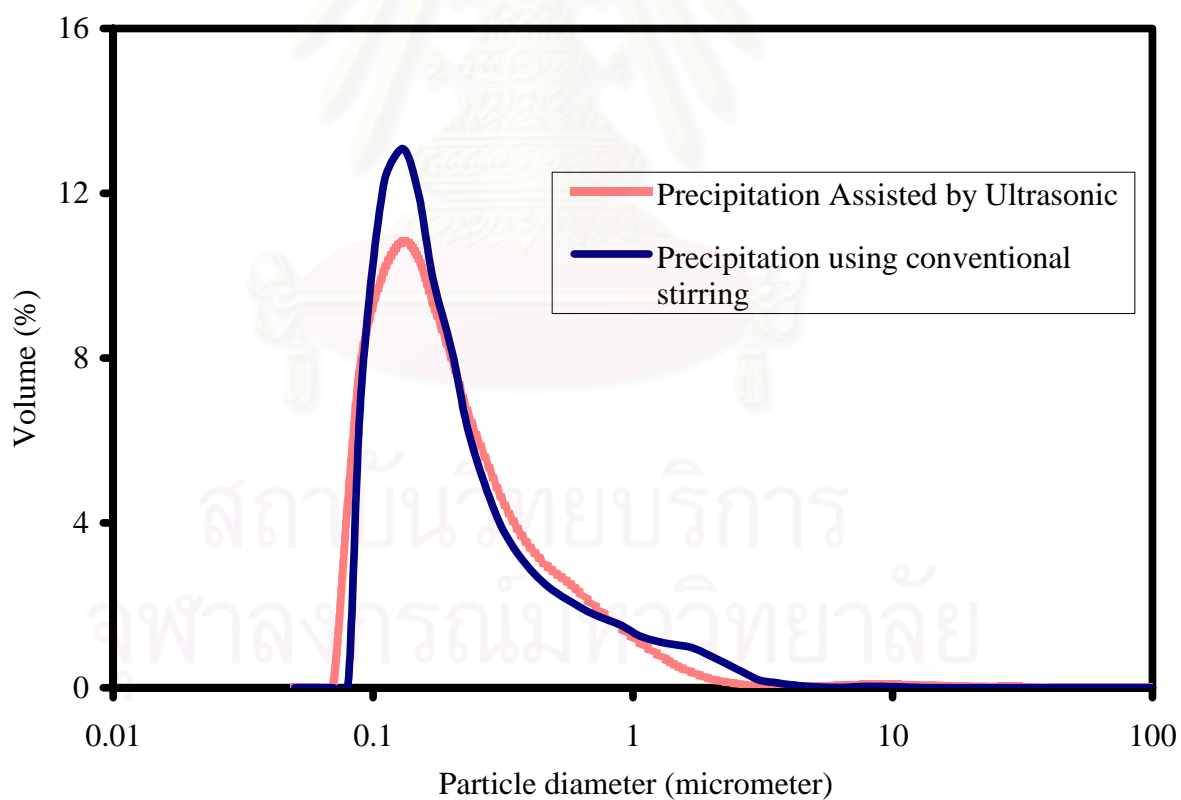
According to the results in section 4.3, the reduction in size of AACH by milling can decrease particle size of the obtained alumina powder and subsequently result in an increase in density of the obtained alumina specimen. Therefore, other means to reduce size of AACH were concerned. In this section, the use of ultrasonic wave during precipitation to agitate the system is considered. This method is almost the same procedure as the standard synthesis, except that ultrasonic bath was employed to assist the mixing, instead of magnetic stirrer.

The particle size distribution (PSD) shown in Figure 4.33(a) reveals that the median particle size of AACH synthesized with the assistance of ultrasonic is smaller than that of AACH prepared by conventional stirring.

After calcination at 1200°C for 2h, the obtained alumina powder was measured for particle size distribution (PSD) of which the results are shown in Figure 4.33(b). It can be observed that the median particle size of α -alumina obtained from AACH precipitation assisted by ultrasonic is slightly smaller than that of α -alumina obtained from standard AACH. However, the size distributions for these samples are different.



(a)



(b)

Figure 4.33 Particle size distribution comparison for AACH and α -alumina synthesized by conventional stirring(a) and by assistant of ultrasonic wave(b).

The obtained α -alumina was used to fabricate alumina specimen. Density of the specimen was measured along the fabrication step. The results are shown in Table 4.3 and compare with that of α -alumina powder obtained from standard procedure. It could be seen that density of specimens fabricated in both cases are relatively the same.

Table 4.3 Density of the specimen fabricated from alumina powder synthesized with assistance of ultrasonic wave comparing with the product fabricated by conventional method.

Precipitation method	Tapped density of the obtained alumina (g/cm^3)	Relative density of specimen after sintering at 1300°C (%)	Relative density of specimen after sintering at 1500°C (%)	Relative density of HIP specimen (%)
Conventional Stirring	0.62	73.9	95.6	97.4
Assisted by Ultrasonic	0.67	71.4	95.8	98.1

UV/Visible spectrophotometry micrographs in Figure 4.34 which compare the specimen which was fabricated from α -alumina powder obtained from synthesized by precipitation assisted by ultrasonic and specimen which was fabricated from α -alumina powder obtained from synthesized by conventional stirring. It show that the specimen which was fabricated from α -alumina powder obtained from synthesized by precipitation assisted by ultrasonic has higher transmittance than specimen which was fabricated from α -alumina powder obtained from synthesized by conventional stirring.

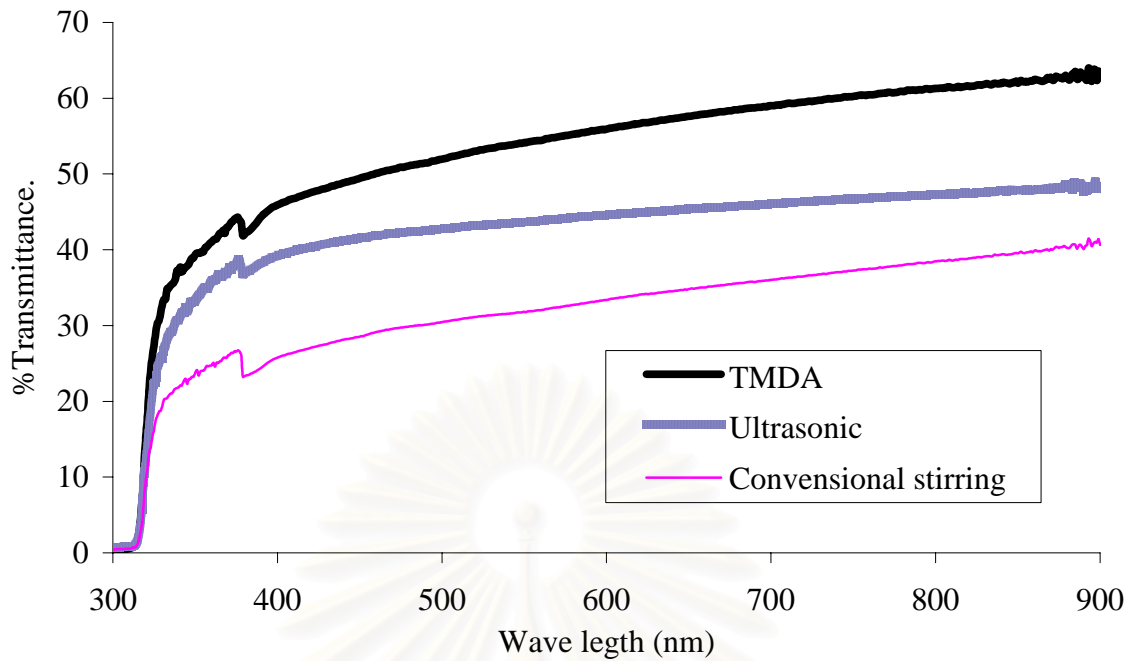


Figure 4.34 UV/Visible spectrophotometry micrographs of the specimen fabricated from: TMDA powder, α -alumina powder synthesized by precipitation assisted by ultrasonic and α -alumina powder synthesized by precipitation assisted by conventional stirring.

CHAPTER V

CONCLUSIONS AND RECOMMENDATIONS

5.1) Conclusions

In this work, alumina powder is prepared by precipitation method. Effect of calcination time and heating rate during the calcination on sintering of alumina particles and the obtained specimens, effect of AACH milling on the synthesized alumina and the obtained specimens and effect of AACH surface modification on the synthesized alumina are investigated. The conclusions of the study can be drawn as follows:

1. Too long time for calcination of AACH makes the obtained α -alumina more agglomerated by sintering and the obtained final specimen would have low density. However, using shot time for calcination would not result in complete transformation to α -alumina, which makes the obtained final specimen very low density.
2. Milling AACH before calcination by ball milling or using ultrasonic during precipitation can help reducing size of the obtained α -alumina as well as lowering agglomeration and the obtained final specimen would have higher density.
3. Modification of AACH by using organic compound before calcination could not help decreasing agglomeration because the organic compound would be burned out before reaching temperature of sintering.

5.2) Recommendations

1. In Milling of the powder by alumina balls milling, great amount of powder should be used to protect impurity from alumina balls.

REFERENCES

- Adak, A., M. Bandyopadhyay, and A. Pal. 2005. "Removal of crystal violet dye from wastewater by surfactant-modified alumina." *Separation and Purification Technology* 44:139-144.
- Apetz, R., and M. P. B. van Bruggen. 2003. "Transparent alumina: A light-scattering model." *Journal of the American Ceramic Society* 86:480-486.
- Bennett, I., and R. Stevens. 1998. "Calcination and phase changes in alumina." *British Ceramic Transactions* 97:117-125.
- Bodisova, K., P. Sajgalik, D. Galusek, and P. Svancarek. 2007. "Two-stage sintering of alumina with submicrometer grain size." *Journal of the American Ceramic Society* 90:330-332.
- Born, Max. 1975. *Principle of Optics*: The press syndicate of the university of cambridge.
- Braun, A., G. Falk, and R. Clasen. 2006. "Transparent polycrystalline alumina ceramic with sub-micrometre microstructure by means of electrophoretic deposition." *Materialwissenschaft Und Werkstofftechnik* 37:293-297.
- Chang, S., R. H. Doremus, L. S. Schadler, and R. W. Siegel. 2004. "Hot-pressing of nano-size alumina powder and the resulting mechanical properties." *International Journal of Applied Ceramic Technology* 1:172-179.
- Cho, S. J., Y. C. Lee, K. J. Yoon, J. J. Kim, J. H. Hahn, H. M. Park, and M. Yanagisawa. 2001. "Effect of coarse-powder portion on abnormal grain growth during hot pressing of commercial-purity alumina powder." *Journal of the American Ceramic Society* 84:1143-1147.
- Chou, T. C., and T. G. Nieh. 1992. "Interface-Controlled Phase-Transformation and Abnormal Grain-Growth of Alpha-Al₂O₃ in Thin Gamma-Alumina Films." *Thin Solid Films* 221:89-97.
- Deng, S. G., and Y. S. Lin. 1997. "Microwave synthesis of mesoporous and microporous alumina powders." *Journal of Materials Science Letters* 16:1291-1294.
- Echeberria, J., J. Tarazona, J. Y. He, T. Butler, and F. Castro. 2002. "Sinter-HIP of alpha-alumina powders with sub-micron grain sizes." *Journal of the European Ceramic Society* 22:1801-1809.
- Hida, M., T. Yamaguchi, T. Fujita, S. Taruta, and K. Kitajima. 2005. "Low-temperature formation of alpha-alumina from polyhydroxoaluminum-lactic acid composite gels." *Journal of the Ceramic Society of Japan* 113:226-231.
- HoneymanColvin, P., and F. F. Lange. 1996. "Infiltration of porous alumina bodies with solution precursors: Strengthening via compositional grading, grain size control, and transformation toughening." *Journal of the American Ceramic Society* 79:1810-1814.
- Krell, A., and J. Klimke. 2006. "Effects of the homogeneity of particle coordination on solid-state sintering of transparent alumina." *Journal of the American Ceramic Society* 89:1985-1992.
- Kwon, O. H., C. S. Nordahl, and G. L. Messing. 1995. "Submicrometer Transparent Alumina by Sinter Forging Seeded Gamma-Al₂O₃ Powders." *Journal of the American Ceramic Society* 78:491-494.
- Kwon, S., and G. L. Messing. 2000. "Sintering of mixtures of seeded boehmite and ultrafine alpha-alumina." *Journal of the American Ceramic Society* 83:82-88.

- Legros, C., C. Carry, P. Bowen, and H. Hofmann. 1999. "Sintering of a transition alumina: Effects of phase transformation, powder characteristics and thermal cycle." *Journal of the European Ceramic Society* 19:1967-1978.
- Levin, I., and D. Brandon. 1998. "Metastable alumina polymorphs: Crystal structures and transition sequences." *Journal of the American Ceramic Society* 81:1995-2012.
- Marchlewski, P. A., A. R. Olszyna, K. J. Kurzydowski, and B. Ralph. 1999. "Grain growth in high-purity alumina ceramics sintered from mixtures of particles of different sizes." *Ceramics International* 25:157-163.
- Michel W. Barsoum. 1997. *Fundamentals of Ceramics*: McGraw-Hill College.
- Muangsoombut, Benjaporn. 2005. "Effects of Secondary Metal Doping and Sol-Seeding on Phase Transformation of Alumina Prepared by Precipitation Method." Pp. 114 in *Chemical engineering*. Bangkok: Chulalongkorn University.
- Nordahl, C. S., and G. L. Messing. 1996. "Transformation and densification of nanocrystalline theta-alumina during sinter forging." *Journal of the American Ceramic Society* 79:3149-3154.
- Hong, J. S. Park, and D. C. Shin. 2004. "Effect of grain size on transmittance and mechanical strength of sintered alumina." *Materials Science and Engineering a-Structural Materials Properties Microstructure and Processing* 374:191-195.
- Ouyang, D. X., C. M. Mo, and L. D. Zhang. 1996. "Relationship between optical transmittance and microstructure of nanostructured alumina films." *Nanostructured Materials* 7:573-578.
- Park, H., and S. Y. Park. 2001. "Grain growth behavior of alumina during sinter-HIP process." *Journal of Materials Science Letters* 20:601-603.
- Roy, J. F., M. Descemond, C. Brodhag, and F. Thevenot. 1993. "Alumina Microstructural Behavior under Pressureless Sintering and Hot-Pressing." *Journal of the European Ceramic Society* 11:325-333.
- Sarikaya, Y., I. Sevinc, and M. Akinc. 2001. "The effect of calcination temperature on some of the adsorptive properties of fine alumina powders obtained by emulsion evaporation technique." *Powder Technology* 116:109-114.
- Tansungnoen, Soontorn. 2005. "Development of Transparent Nano-Crystalline Alumina Ceramic: Effects of Forming and Sintering Condition." Pp. 121 in *Ceramic Technology, Faculty of Science*. Bangkok: Chulalongkorn University.
- Tomaszewski, H., M. Boniecki, and H. Weglarz. 2000. "Effect of grain size on R-curve behaviour of alumina ceramics." *Journal of the European Ceramic Society* 20:2569-2574.
- Wang, C. M., H. M. Chan, and M. P. Harmer. 2004. "Effect of Nd₂O₃ doping on the densification and abnormal grain growth behavior of high-purity alumina." *Journal of the American Ceramic Society* 87:378-383.
- Wang, J. B., L. B. Wang, H. Yang, X. Y. Fu, and D. Y. Kong. 2006. "Modification of alumina bubbles with ammonium aluminum sulphate." *Ceramics International* 32:905-909.
- Yoshimura, H. N., A. C. de Camargo, E. P. Goulart, and K. Maekawa. 1999. "Translucent polycrystalline alumina: Influence of roughness and thickness on in-line transmittance." *Advanced Powder Technology* 299-3:35-43.
- Yoshizawa, Y., and F. Saito. 1997. "Reduction of transformation temperature to alpha-alumina from ammonium aluminum carbonate hydroxide by grinding." *Journal of the Ceramic Society of Japan* 105:57-61.



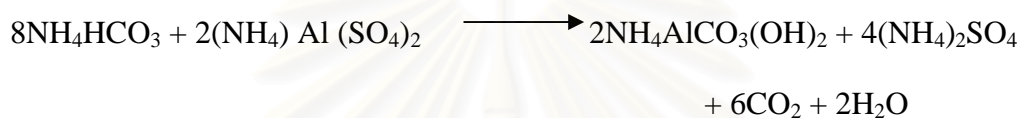
APPENDICES

สถาบันวิทยบริการ
จุฬาลงกรณ์มหาวิทยาลัย

APPENDIX A

CALCULATION OF CONCENTRATION OF BOTH REACTANTS IN PRECIPITATION METHOD

In this study, ammonium aluminum carbonate hydroxide ($\text{NH}_4\text{AlCO}_3(\text{OH})_2$) has been produced by the reaction of ammonium aluminum sulfate solution (AAS solution) and ammonium hydrogencarbonate solution (AHC solution) as following equation :



Ammonium aluminum carbonate hydroxide (AACH) was prepared with the molar ratio of AAS solution to AHC solution equal to 1:4 as the above reaction and calculation procedure is given here.

Calculation of the amount of ammonium hydrogencarbonate (AHC) and ammonium aluminum sulfate (AAS) for AACH preparation

Ammonium aluminum sulfate (AAS) and ammonium hydrogencarbonate (AHC) are used as reactants to prepare AACH.

1. Ammonium aluminum sulfate ($\text{NH}_4\text{Al}(\text{SO}_4)_2 \cdot 12\text{H}_2\text{O}$) has an molecular weight of 237.18 g/mol (not included molecule of water)
2. Ammonium hydrogencarbonate (NH_4HCO_3) has an molecular weight of 79.06 g/mol.

Example : Calculation of AACH preparation with concentration of AAS solution to AHC solution equal to 0.2 : 2.0 mol/l and molar ratio of AAS solution to AHC solution is 0.05 : 0.2 , which is equal to 1:4 as mentioned before, are as following :

1.1 AAS solution 0.05 mol consists of :

$$\text{AAS } 0.05 \times 237.18 = 11.859 \text{ g}$$

To get concentration 0.2 mol/l

$$\text{Distilled water} = 250 \text{ cm}^3$$

AHC solution 0.2 mol consists of :

$$\text{AHC } 0.2 \times 79.06 = 15.812 \text{ g}$$

To get concentration 2.0 mol/l

$$\text{Distilled water} = 100 \text{ cm}^3$$



สถาบันวิทยบริการ
จุฬาลงกรณ์มหาวิทยาลัย

CALCULATION OF THE CRYSTALLITE SIZE

Calculation of the crystallite size by Debye-Scherrer equation

The crystallite size was calculated from the half-height width of the diffraction peak of XRD pattern using the Debye-Scherrer equation.

From Scherrer equation:

$$D = \frac{K\lambda}{\beta \cos \theta} \quad (\text{C.1})$$

- where
- D = Crystallite size, Å
 - K = Crystallite-shape factor = 0.9
 - λ = X-ray wavelength, 1.5418 Å for CuK α
 - θ = Observed peak angle, degree
 - β = X-ray diffraction broadening, radian

The X-ray diffraction broadening (β) is the pure width of a powder diffraction free from all broadening due to the experimental equipment. α -Alumina is used as a standard sample to observe the instrumental broadening since its crystallite size is larger than 2000 Å. The X-ray diffraction broadening (β) can be obtained by using Warren's formula.

From Warren's formula:

$$\beta = \sqrt{B_M^2 - B_S^2} \quad (\text{C.2})$$

- Where
- B_M = The measured peak width in radians at half peak height.
 - B_S = The corresponding width of the standard material.

Example: Calculation of the crystallite size of α -alumina

$$\begin{aligned}
 \text{The half-height width of 012 diffraction peak} &= 0.25^\circ \text{ (from the figure C.1)} \\
 &= \left(\frac{2\pi}{360} \right) \cdot (0.26) \\
 &= 0.0045 \text{ radian}
 \end{aligned}$$

The corresponding half-height width of peak of α -alumina (from the B_s value at the 2θ of 25.88° in figure B.2) = 0.0038 radian

$$\begin{aligned}
 \text{The pure width, } \beta &= \sqrt{B_M^2 - B_S^2} \\
 &= \sqrt{0.0045^2 - 0.0038^2} \\
 &= 0.0024 \text{ radian}
 \end{aligned}$$

$$B = 0.0024 \text{ radian}$$

$$2\theta = 25.88^\circ$$

$$\theta = 12.94$$

$$\lambda = 1.5418 \text{ \AA}$$

$$\text{The crystallite size} = \frac{0.9 \times 1.5418}{0.0024 \cos 12.94} = 590 \text{ \AA} = 59 \text{ nm}$$

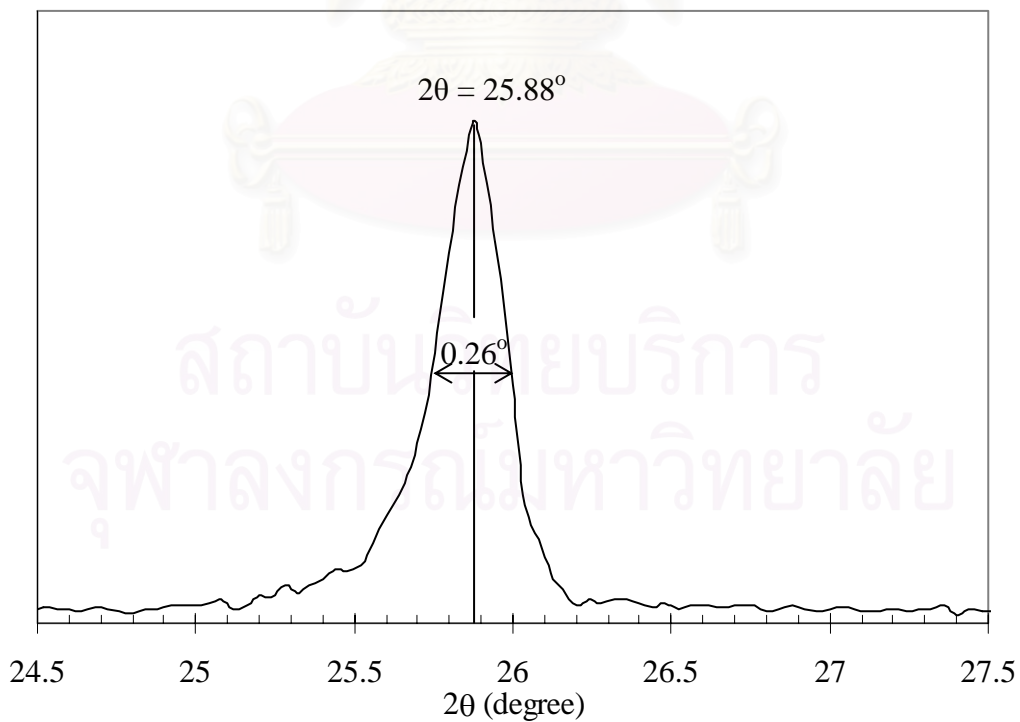


Figure B.1 The observation peak of α -alumina for calculating the crystallite size.

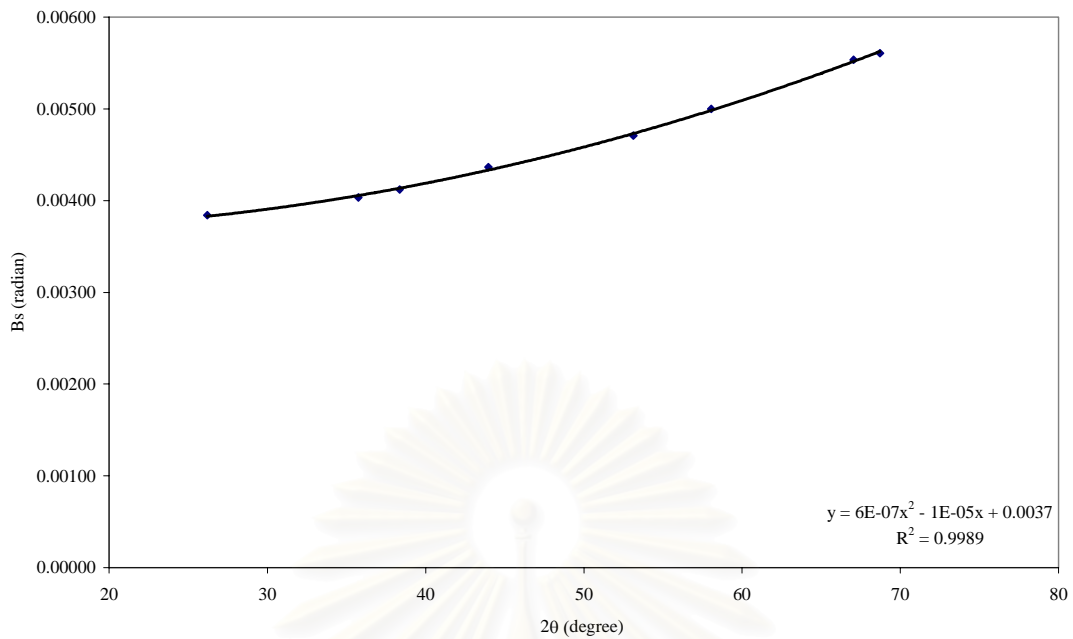


Figure B.2 The graph indicating that value of the line broadening attribute to the experimental equipment from the α -alumina standard.

สถาบันวิทยบริการ
จุฬาลงกรณ์มหาวิทยาลัย

DENSITY

- **Bulk density**

The bulk density of specimens was measured according to Archimedes' method. The air in open pores of specimen was removed by applying vacuum for 30 min and then water was poured onto specimens until submerged in water. Water was further forced into the opened pores by applying vacuum for 2 h. The dry weight W_d were measured and used to calculate the bulk density using equation (C.1) following ASTM standard (Designation : C830-93).

$$\text{Bulk density} = \frac{W_d}{W_{\text{sat}} - W_{\text{sus}}} \rho \quad (\text{C.1})$$

Where ρ is water density at the measurement temperature (0.996512 g/cm³ at 27°C)

- **Theoretical density**

The theoretical density of sintered pellets was calculated from real density using the following equation ;

$$\text{Theoretical density} = \frac{W_{\text{total}}}{W_a / \rho_a + W_b / \rho_b + \dots} \quad (\text{C.2})$$

Where W_{total} is total weight of used components.

W_a, W_b are weights of component, a and b, respectively.

ρ_a, ρ_b are real densities of component, a and b, respectively.

a, b,..... are used components.

In this experiment, the theoretical densities of pure $\text{Al}_2\text{O}_3 = 3.98 \text{ g/cm}^3$ was used for calculation.

- **Relative density**

The relative density of the sintered specimens was calculated from its bulk density and theoretical density using the following equation :

$$\text{Relative density} = \frac{\text{Bulk density}}{\text{Theoretical density}} \quad (\text{C.3})$$

$$\text{And \% of theoretical density} = \text{Relative density} \times 100$$



สถาบันวิทยบริการ
จุฬาลงกรณ์มหาวิทยาลัย

CONDITIONS FOR BALL MILL AND DISPERSION OF POWDER

Ball mill

The particles size can be reduced a by breaking some soft agglomeration of powders by using polypropylene bottle and high purity alumina balls.

Place high purity alumina ball 100 g or half of bottle, alumina powder, and ethanol solution 50 cc into the polypropylene bottle which has volume 125 cc. Mill this bottle with rotating speed 150 rpm at desired time. After milling with ball mill, filter the solution of powder and dry in the oven at 100°C for 24 h.

Dispersion of powder

Before measuring a particle size distribution of alumina powder, all powders should to be dispersed by following steps:

1. Preparation of dispersion solution with concentration 0.2 wt% by dissolving NaHMP (Sodium Hexa Methaphosphate) 0.2 g in distilled water 99.8 g.
2. Use this solution 50 cc for 0.5 g of powder, and then mix this solution with magnetic stirrer for 30 minutes.

After mixing by magnetic stirrer, pour the solution into a bottle and sealed with para-film and place it into ultrasonic apparatus for 30 minutes before measuring their particle size distribution by using Laser Particle Size Distribution Analyzer.

APPENDIX E

EFFECT OF MILLIED ALUMINA POWDER MASS ON MASS OF SPLIT ALUMINA BALL

Experimental

Put alumina powder by varying desired volume (20,10,5,0 g) , high purity alumina ball 100 g (allow a half of bottle), and ethanol solution 75 cc into the polypropylene bottle which has volume 125 cc. Mill this bottle with rotating speed 150 rpm for 24 h. After milling with ball milling method, filter the solution of powder and dry in the oven at 100°C for 24 h.

The powder was pressed into a pallet of 13 mm in diameter by biaxial hydraulic press of 20 MPa and followed by cold isostatic press under the pressure of 300 MPa. The green compact was dried in the oven at 105°C for 2 h.

The dried green bodies were sintered at 1350°C for 2 h and sintered at 1500°C repeatedly for 2 h in air under atmospheric pressure.

Characterizations

Amount of the pieces of split alumina balls can be calculated by using the following equation.

$$\text{Weight of the pieces of split alumina balls} = W_i - W_f \quad (\text{E.1})$$

Where W_i is weight of alumina balls before milling.

W_f is weight of alumina balls after milling.

Results

SEM image in Figure E.1 ;which observe the milled alumina powder, shows the extra large particle which is difference morphology on surface of particle if it was compared with synthesized alumina particle.it was expected that it is the pieces of split alumina balls and the milled alumina powder was blended with small amount of the pieces of split alumina balls.

Correlation between split alumina ball and alumina powder put in the polypropylene bottle in Figure E.2 shows and confirms that the pieces of split alumina balls would be occurred when using milling by alumina ball and the split alumina balls would be decreased when increased alumina powder put in the polypropylene bottle.

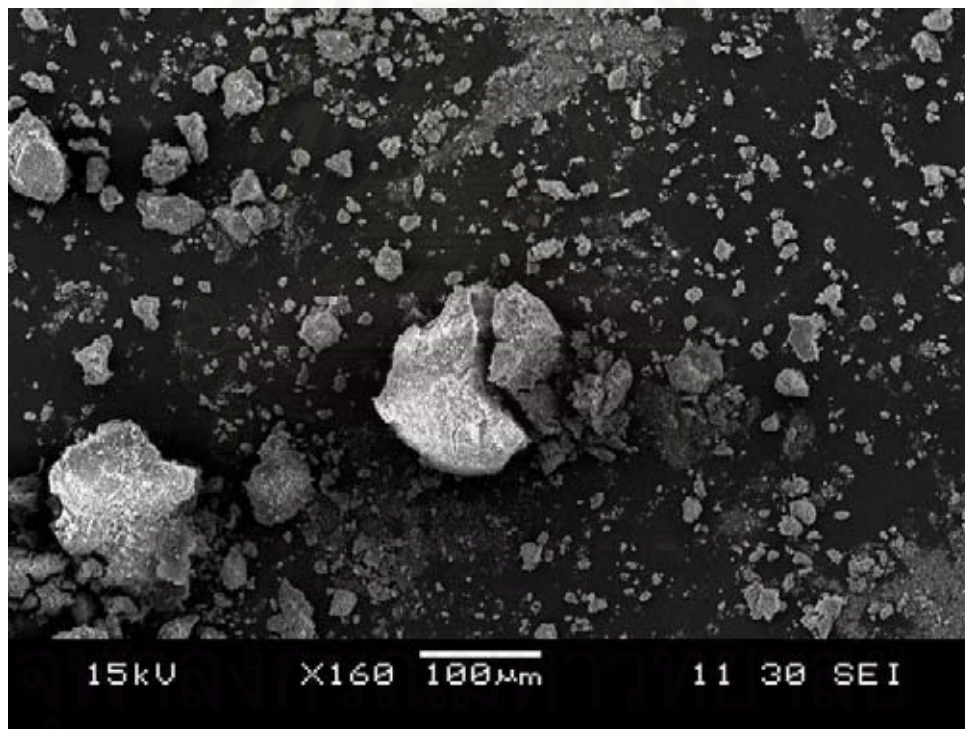


Figure E.1 SEM images of the pieces of split alumina balls was blended with alumina powder after milled by ball milling.

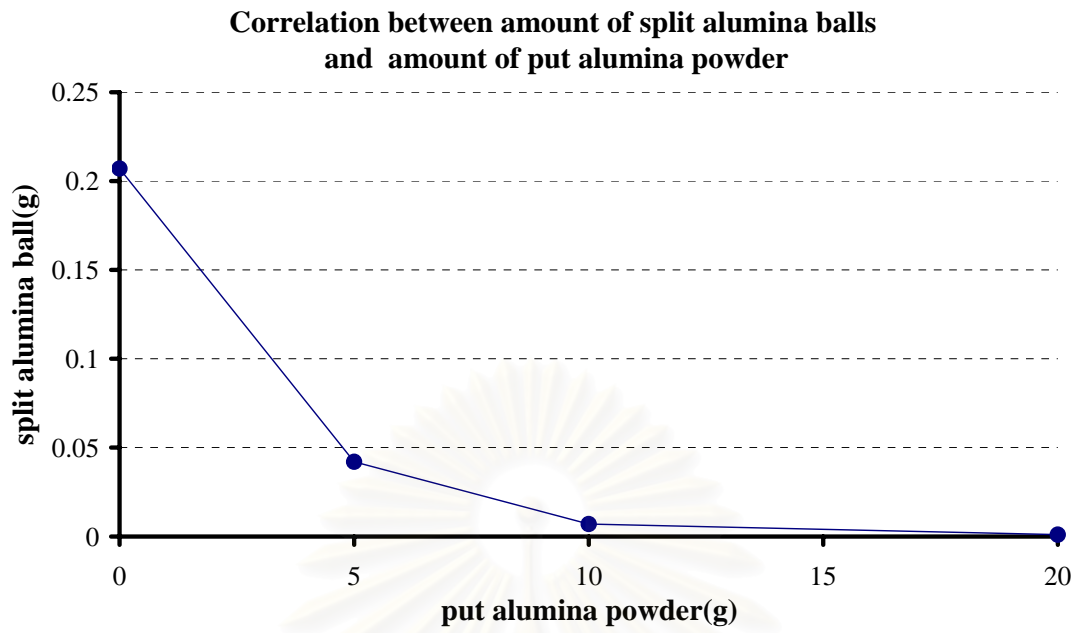


Figure E.2 Correlation between mass of the pieces of split alumina balls and mass of the put alumina powder.

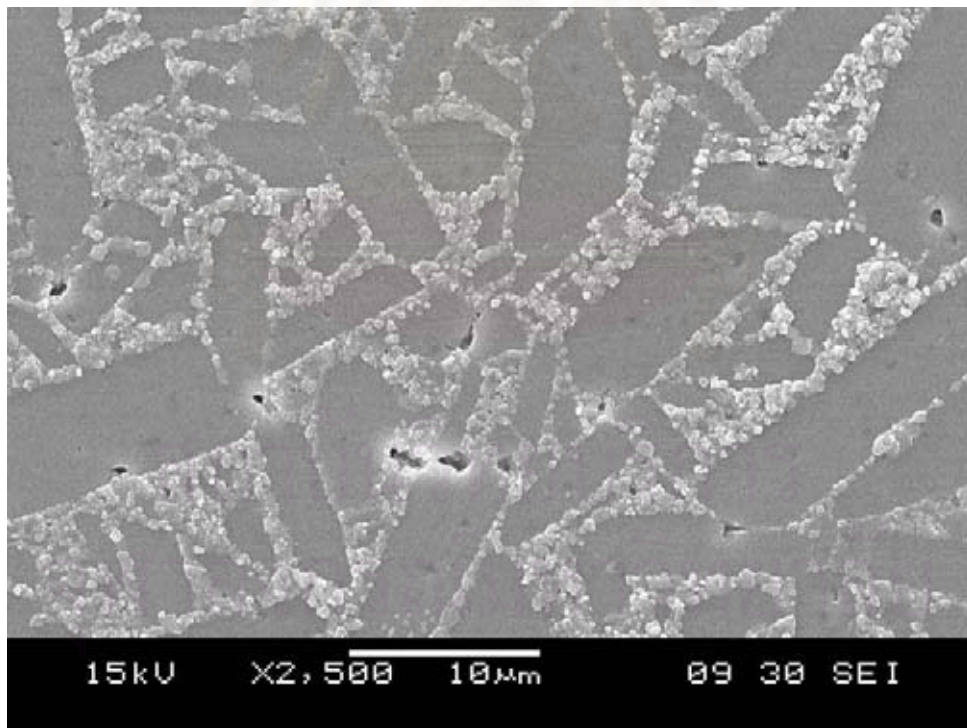


Figure E.3 SEM images of the specimen after sintering at 1500°C.

The sintered specimen; which was observe by SEM in Figure E.3, appear the abnormal grain in Al_2O_3 which was observed to occur when a small amount of impurity was present(Tae-Wook Sone,2001) due to A. Krell et al. (2003) employed commercial alumina powder (particle size about $0.2 \mu\text{m}$) doped with small amount of impurity such MgO and ZrO_2 for inhibition of abnormal grain growth.

Abnormal grain in Figure E.3 was occurred by impurity from the pieces of split alumina balls because the powder after milling was blended with the large particles which were produced from alumina balls.

Using little alumina powder for milling by ball milling method brings about not only impurity in the alumina powder, large alumina particles which were split from alumina balls but also abnormal grain in the specimen.



สถาบันวิทยบริการ
จุฬาลงกรณ์มหาวิทยาลัย

VITAE

Mr Sart Pinkaew was born in Bangkok, Thailand, on September, 1982. He received bachelor's degree in Chemical Engineering from the department of Chemical Engineering, Faculty of Engineering, Chulalongkorn University, Bangkok Thailand on May, 2004.



สถาบันวิทยบริการ
จุฬาลงกรณ์มหาวิทยาลัย